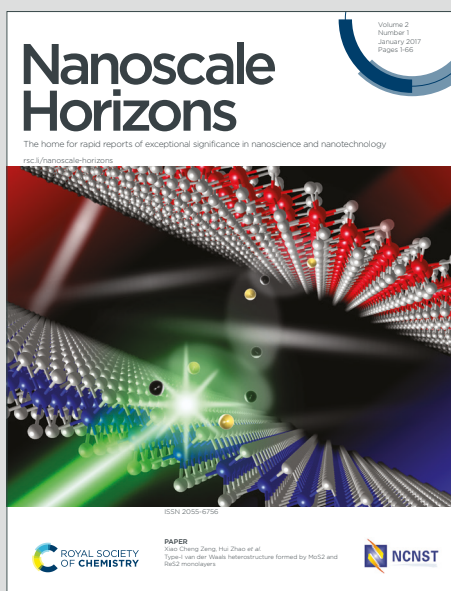


# Nanoscale Horizons

The home for rapid reports of exceptional significance in nanoscience and nanotechnology

Accepted Manuscript

This article can be cited before page numbers have been issued, to do this please use: M. Tsutsui, R. van Roij, Y. Yuan, A. Arima, M. S. Islam, R. Abe, A. Douaki, D. Garoli, I. Smalyukh and M. Dijkstra, *Nanoscale Horiz.*, 2026, DOI: 10.1039/D6NH00048G.



This is an Accepted Manuscript, which has been through the Royal Society of Chemistry peer review process and has been accepted for publication.

Accepted Manuscripts are published online shortly after acceptance, before technical editing, formatting and proof reading. Using this free service, authors can make their results available to the community, in citable form, before we publish the edited article. We will replace this Accepted Manuscript with the edited and formatted Advance Article as soon as it is available.

You can find more information about Accepted Manuscripts in the [Information for Authors](#).

Please note that technical editing may introduce minor changes to the text and/or graphics, which may alter content. The journal's standard [Terms & Conditions](#) and the [Ethical guidelines](#) still apply. In no event shall the Royal Society of Chemistry be held responsible for any errors or omissions in this Accepted Manuscript or any consequences arising from the use of any information it contains.

## 1 Nanofluidic systems for ionic intelligence

2  
3 Makusu Tsutsui,<sup>1,\*</sup> René van Roij,<sup>2</sup> Ye Yuan,<sup>3</sup> Akihide Arima,<sup>4,5</sup> Md Sifat Islam,<sup>1</sup> Ryuichiro  
4 Abe,<sup>6</sup> Ali Douaki,<sup>7</sup> Denis Garoli,<sup>7,8</sup> Ivan I. Smalyukh,<sup>3,9,10</sup> Marjolein Dijkstra<sup>11</sup>

5  
6 <sup>1</sup> SANKEN, The University of Osaka, 8-1 Mihogaoka, Ibaraki, Osaka 567-0047, Japan

7 <sup>2</sup> Institute for Theoretical Physics, Utrecht University, Princetonplein 5, 3584 CC Utrecht, The  
8 Netherlands

9 <sup>3</sup> International Institute for Sustainability with Knotted Chiral Meta Matter (WPI-SKCM2),  
10 Hiroshima University, Higashi Hiroshima, Hiroshima, Japan

11 <sup>4</sup> Research Institute for Quantum and Chemical Innovation, Institutes of Innovation for Future  
12 Society, Nagoya University

13 <sup>5</sup> Institute of Nano-Life-Systems, Institutes of Innovation for Future Society, Nagoya  
14 University, Furo-cho, Chikusa-ku, Nagoya 464-8603, Japan

15 <sup>6</sup> Research Institute for Microbial Research, The University of Osaka, 3-1 Yamadaoka, Suita,  
16 Osaka 565-0871, Japan

17 <sup>7</sup> Istituto Italiano di Tecnologia, Optoelectronics Research Line, Morego 30, I-16163 Genova,  
18 Italy

19 <sup>8</sup> Dip. di Scienze e Metodi dell'Ingegneria Università di Modena e Reggio Emilia via Amendola  
20 2, 42122 Reggio Emilia, Italy

21 <sup>9</sup> Department of Physics, University of Colorado, Boulder, Colorado, USA

22 <sup>10</sup> Renewable and Sustainable Energy Institute, National Renewable Energy Laboratory and  
23 University of Colorado, Boulder, Colorado, USA

24 <sup>11</sup> Soft Condensed Matter & Biophysics, Debye Institute for Nanomaterials Science,  
25 Utrecht University, Princetonplein 1, 3584 CC Utrecht, The Netherlands

26  
27 **Artificial intelligence is rapidly permeating modern technology, but its growth is**  
28 **increasingly constrained by the costs of delivering power and removing heat. Neural**  
29 **computation offers a striking counterpoint, for it achieves sophisticated information**  
30 **processing at exceptionally low energy by exploiting ionic flows and adaptive**  
31 **conductance. Inspired by the Hodgkin-Huxley view that function emerges from ion-**  
32 **transport dynamics, recent work has begun to implement memory and learning**  
33 **directly in fluids, where ions simultaneously carry signals and encode internal device**  
34 **state. This Review charts the emerging landscape of fluidic ionic memristors, from**  
35 **soft, bioinspired materials to manufacturable solid-state nanofluidic architectures.**  
36 **In lipid bilayers, droplet networks, tissues and ionic polymers, electrical activity is**



37 **intrinsically coupled to chemistry and mechanics, enabling plasticity across multiple**  
38 **timescales. In rigid nanopores, nanochannels and angstrom-scale slits, the softness**  
39 **is transferred from the scaffold to the ionic degrees of freedom, where electric double-**  
40 **layer dynamics, concentration polarization and confinement-driven effects produce**  
41 **history-dependent transport in robust inorganic frameworks. Hybrid approaches**  
42 **integrate gels, brushes, particles, or biomolecules within microfabricated structures**  
43 **to combine stability with rich analogue dynamics. We conclude by outlining the key**  
44 **requirements for translation from reproducibility to scalable integration towards ionic**  
45 **intelligence technologies.**  
46



## 47 1. Introduction

48 Artificial intelligence is becoming an always-present layer of the Internet, yet its  
 49 rapid expansion is now limited as much by physical constraints as by advances in  
 50 algorithms. As large language models are trained and deployed at scale, computation is  
 51 concentrated in dense accelerators and data centers, where increasing heat fluxes, cooling  
 52 burdens and the life-cycle footprint of electricity now pose major sustainability  
 53 constraints.<sup>1-3</sup> This backdrop has renewed interest in neuromorphic computing,<sup>4</sup> which  
 54 pursues brain-like learning and inference through sparse, event-driven signalling rather  
 55 than the clocked von Neumann architecture. In the Hodgkin-Huxley picture, such  
 56 computation is performed by voltage- and time-dependent ionic conductance whose  
 57 internal ionic states store history and govern dynamics, a design principle that inspires  
 58 ionic intelligence hardware in which ions, rather than electrons, carry signals and encode  
 59 memory.<sup>5-8</sup> Drawing on these biological principles, scientists have sought to create  
 60 nanofluidic memristors, artificial two-terminal devices in which ion transport under  
 61 confinement exhibits history-dependent conductance analogous to synapses.<sup>9-14</sup> Over  
 62 the past decade, this emerging class of iontronic devices has rapidly emerged as a bridge  
 63 between living neural networks and semiconductor processors, aiming to emulate brain-

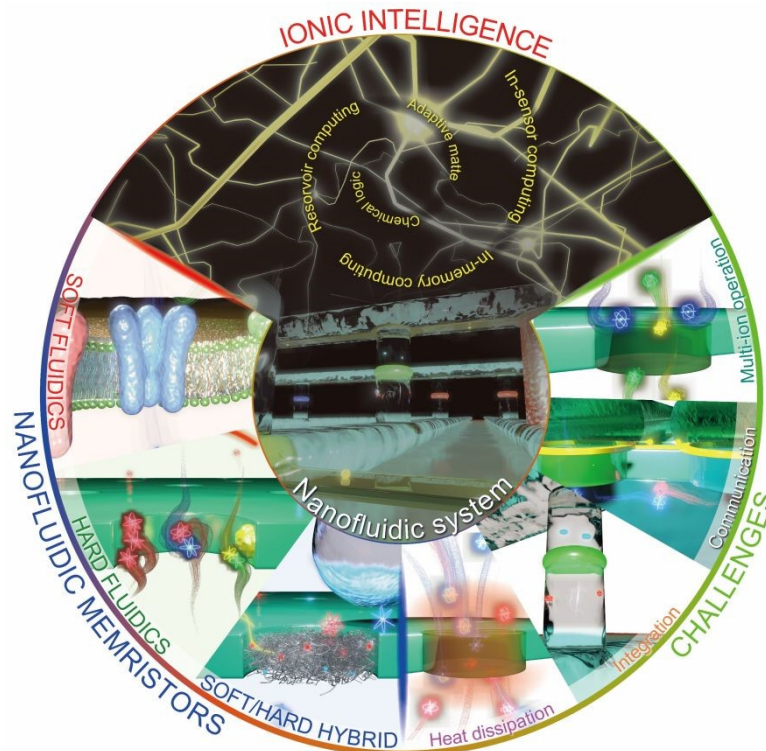


**Figure 1.** Conceptual diagram summarizing the central theme of this Review: confined ion transport can generate memory and computation when coupled to slowly evolving internal states.



64 like learning and memory with the very same carriers of information used in biology.

65 Early ionic memristors have already captured many canonical synaptic functions  
66 while operating at exceptionally low power.<sup>15</sup> Current transients in nanofluidic channels  
67 can consume only femtojoules per spike,<sup>16</sup> placing them close to the efficiency of  
68 biological synapses.<sup>16-18</sup> Fluidic memristors also share a closer physical analogy with  
69 natural synapses than conventional solid-state devices, because they function in water  
70 with mobile ions and solvent molecules as active components of transport. This  
71 chemically rich environment, together with the multispecies character of ionic carriers,  
72 their hydration shells, valence states and reversible binding, enables dynamical behaviors  
73 that are inaccessible to purely electronic systems. As a result, ion-driven memristors  
74 have begun to reproduce short-term plasticity,<sup>19</sup> long-term plasticity,<sup>20</sup> spike-timing-  
75 dependent plasticity,<sup>21</sup> and even higher-order learning-forgetting dynamics,<sup>22</sup>  
76 highlighting their distinctive potential for neuromorphic engineering.

77 Yet, substantial challenges still separate nanofluidic memristors from their full  
78 potential (Fig. 1). Reproducing the ion-selective, multi-ion operation of real neurons  
79 and glia remains a central unsolved problem. Devices capable of exploiting several  
80 ionic species in parallel, analogous to the distinct signaling roles of Na<sup>+</sup>, K<sup>+</sup> and Ca<sup>2+</sup> in  
81 biology, have yet to be realized for complex information processing. Scaling fluidic  
82 memristors into large iontronic circuits presents a further obstacle, because such systems  
83 are intrinsically more difficult to address, interconnect and control than solid-state  
84 counterparts. Even so, the field has begun to make important progress, with early  
85 demonstrations of logic operations and neural-network computation using small numbers  
86 of ionic memristors.<sup>23</sup> As attention shifts towards larger-scale hardware, hybrid  
87 architectures that combine rigid nanochannels with soft polymers or hydrogels are  
88 emerging as a promising route to unite structural robustness with adaptive ionic  
89 functionality.

90 This Review surveys the rapidly expanding landscape of nanofluidic memristors for  
91 artificial intelligence, focusing on ion transport rather than electron conduction as the  
92 basis of operation. We cover hard fluidic platforms built from solid-state nanochannels  
93 and nanopores, soft ionic media including biomembranes, droplets and polymer matrices,  
94 and hybrid architectures that combine these approaches (Fig. 2). Throughout, we  
95 emphasize how ionic dynamics, ranging from slow counterion accumulation to fast  
96 electrowetting at nanoscopic interfaces, generate memristive behaviour. We highlight key  
97 mechanisms including electric-double-layer hysteresis, ångström-scale confinement,  
98 electrohydrodynamic flow memristors, optically modulated ionic transport and chemical  
99 memory in nanopores. We then examine emerging multi-memristor circuits, including



100 ionic logic gates and synaptic networks, to show how such devices can perform  
 101 computation. Finally, we discuss the major challenges ahead, including thermal  
 102 management and scalable integration. Our aim is to provide a timely and comprehensive  
 103 perspective on nanofluidic memristors, and to clarify both the remarkable progress  
 104 towards fluid-based artificial synapses and the remaining path to fully ionic intelligent  
 105 systems that compute with brain-like efficiency and elegance.

106 To refine this conceptual framework, we move beyond a purely materials-based  
 107 soft/hard/hybrid categorization and instead organize the field around four recurring

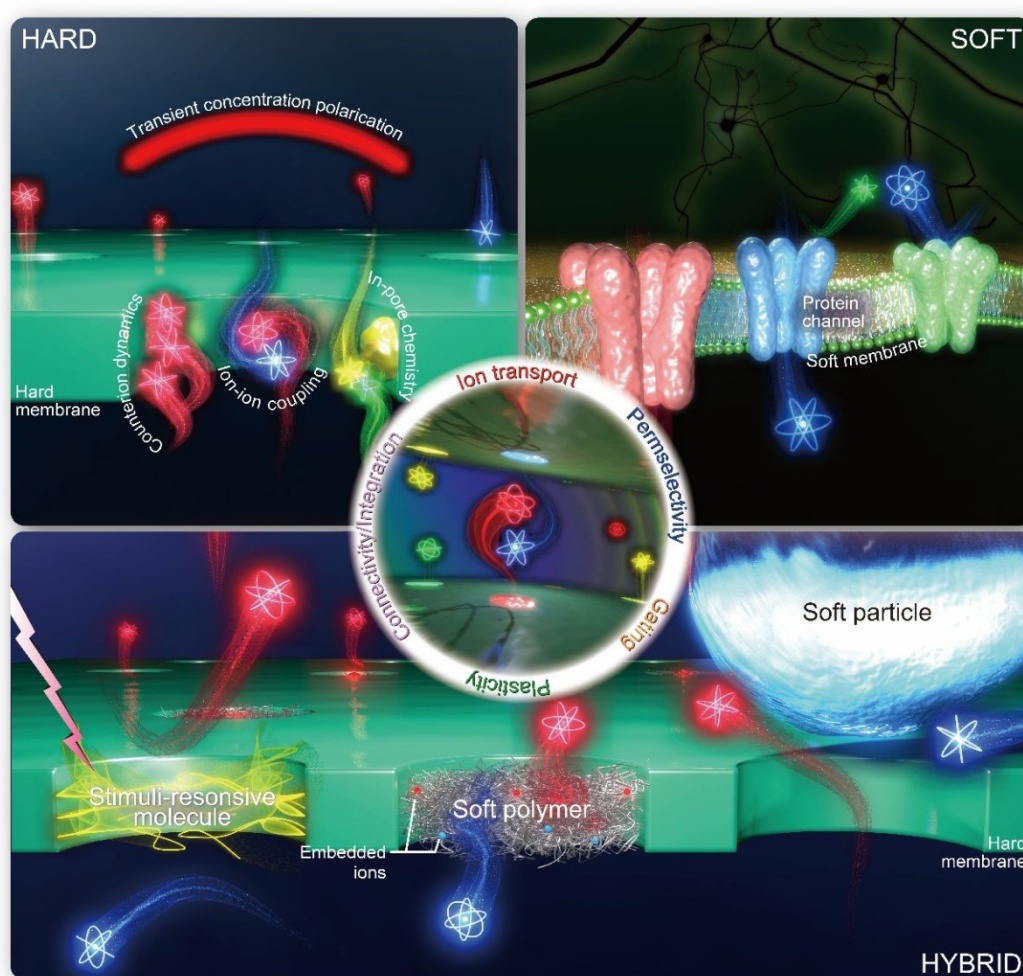


**Figure 2.** Soft, hard, and hybrid nanofluidic platforms for ionic intelligence. Conceptual map of how ionic memory and computation emerge when ion transport is confined and made state dependent. Hard systems (top left) use rigid membranes and engineered nanochannels, where history dependence arises from slow counter-ion relaxation, ion-ion correlations and in-pore chemistry, often expressed through transient concentration polarization. Soft systems (top right) rely on compliant membranes and biomolecular pores, in which ionic flux is inseparable from conformational and mechanical degrees of freedom. Hybrid systems (bottom) integrate a manufacturable hard scaffold with soft functional elements to enable reconfigurable gating and multiscale plasticity. The central inset highlights shared functional primitives in the form of an ionic circuit in an artificial nanofluidic network.



108 physical mechanisms: electric-double-layer charging and relaxation, concentration  
109 polarization and diffusive redistribution, electrochemical reactions coupled to interfacial  
110 ion adsorption, and mechano-ionic coupling arising from structural compliance. This  
111 mechanism-centered view makes it easier to compare otherwise disparate platforms on  
112 common physical grounds and to connect device physics directly to function, including  
113 short-term plasticity, long-term retention, spiking and adaptive learning. Soft lipid  
114 bilayers and hydrogels, for example, draw primarily on interfacial charging and  
115 electrochemical doping, whereas rigid nanochannels intensify diffusion, adsorption and  
116 correlation effects under extreme confinement. Hybrid systems are best understood as  
117 deliberate combinations of these mechanisms, assembled to balance programmability,  
118 robustness and scalability.

119 These platforms are therefore best viewed not as discrete categories, but as a design  
120 continuum. In soft fluidics, the state variable resides in reconfigurable matter itself,  
121 such as membranes, droplets, polymer networks and living tissues, so memory is  
122 inseparable from compliance, chemical binding and slow ionic relaxation. Hard  
123 nanofluidic systems retain the same ionic carriers and aqueous transport physics, but  
124 confine them within rigid nanopores and nanochannels, shifting plasticity from  
125 mechanical deformation to interfacial charge, hydration and reaction landscapes defined  
126 by an inorganic scaffold. Hybrid architectures occupy the intermediate regime,  
127 preserving the addressability, reproducibility and lithographic precision of hard  
128 nanofluidics while reintroducing soft internal degrees of freedom through gels, brushes,  
129 biomolecules or confined liquid phases. Conventional solid-state memristors sit  
130 adjacent to, rather than within, this fluidic continuum. They likewise encode memory  
131 through delayed internal-state evolution, but the relevant variables are typically electronic,  
132 lattice-ionic or defect-based configurations rather than a mobile aqueous ionic population.  
133 Framed in this way, the comparison highlights both the shared logic of history-dependent  
134 transport and the distinct physical substrates that each platform brings to adaptive  
135 computing.



## 136 2. Soft fluidic platform

137 We begin with soft fluidic platforms, where compliance, hydration, and molecular  
138 rearrangement are not merely structural attributes but active parts of the memory  
139 mechanism.

140 The brain is often described as a soft organ,<sup>24</sup> with an elastic modulus of only about  
141 100 Pa at 1 Hz.<sup>25</sup> This low stiffness is thought to facilitate synapse formation and robust  
142 electrical signaling during tissue development.<sup>26,27</sup> Neuronal membranes are likewise  
143 built from ductile lipid bilayers, whose softness allows embedded ion-channel proteins to  
144 undergo conformational changes that open or close their pores in response to stimuli such  
145 as voltage or neurotransmitters.<sup>28</sup> It also permits ion channels to diffuse, reorganize, and  
146 be inserted or removed over time, thereby contributing to synaptic plasticity.<sup>29</sup> At larger  
147 scales, neurons can physically remodel during learning, a process that depends on the  
148 mechanical compliance of cellular membranes and scaffolds to reshape existing  
149 connections and form new ones for long-term memory storage in neural networks.<sup>30</sup>

150 The softness of neuronal membranes plays a central part in the energetics and  
151 adaptability of neural signaling. Ion channels embedded in lipid bilayers operate  
152 between aqueous electrolytes on either side, enabling rapid ion transport through water  
153 while minimizing the energetic cost of gating. Individual channels undergo  
154 conformational transitions on energy scales comparable to  $k_B T$ , yet can regulate fluxes  
155 exceeding  $10^8$  ions per second.<sup>31,32</sup> Synaptic switching therefore consumes only  
156 femtojoules per event, giving biological neural systems an energy efficiency far beyond  
157 that of conventional electronic circuits.<sup>33</sup> By enabling both efficient biophysical  
158 signaling and structural plasticity, the mechanical softness of neural substrates contributes  
159 to the extraordinary computational capabilities of the brain.

160 Soft fluidics employs deformable, biomolecular, or entirely fluidic systems to  
161 achieve memristive behavior inspired by biology implementing intrinsically soft and wet  
162 structures of lipid membranes, ion channels, hydrogels, polymer networks, etc. In soft  
163 ionic memristors, the device components can move or reconfigure significantly during  
164 operation. They also bring biocompatibility and an ability to host biological entities  
165 directly. The interplay between mechanical compliance and ionic transport is a  
166 recurring theme, as soft systems can deform in response to ion flows. This deformation  
167 can in turn influence conduction, creating a memristive loop. In this section, we explore  
168 two major categories, those utilizing biological systems and ionic polymers (Table 1).

169  
170



**Table 1.** Representative soft nanofluidic systems exhibiting memristive ionic dynamics.

System class	Material / fluidic system	Size	Mechanism	Stimulus class	Switching speed	Retention time	Energy consump.
Bio-nanopore <sup>41</sup>	$\beta$ -barrel nanopore (FraC mutants) in KCl	Protein nanopore with hydrophobic segment of ~1.2 nm	Hydrophobic gating yielding bistable wet/dry (vapour bubble) states	Triangular voltage sweeps (150 mV, 2 s)	~2 Hz	Seconds to tens of seconds	~pJ per synaptic event
Bio-nanopore <sup>44</sup>	$\beta$ -barrel nanopores (aerolysin and MspA mutants)	nanopore with nanometre-scale lumen constriction	Field-driven counterion dissociation and local deformation	Pulse trains (110 mV, 5-10 ms)	100-200 Hz	Volatile (state depends on lipid reconfiguration)	N/A
DIB <sup>48</sup>	Droplet interface bilayer between 100 mM KCl droplets	600 nL per droplet	Voltage-driven electrocompression/electrowetting changing bilayer area/thickness	Pulse trains (0/200 mV, 0.1 s)	~2 Hz	Seconds to tens of seconds	4–8 pJ per spike
DIB <sup>49</sup>	Droplet interface bilayer between 500 mM KCl droplets	300 nL per droplet	Voltage-driven restructuring of lipid bilayer (area/thickness and headgroup dielectric loss)	Sinusoidal voltage (10-100 mHz; 80-150 mV)	N/A	Volatile (state depends on lipid reconfiguration)	N/A
DIB <sup>50</sup>	Droplet interface bilayer between 500 mM KCl droplets	200 nL per droplet	Voltage-driven restructuring of lipid bilayer (area/thickness and headgroup dielectric loss)	Pulse trains (150 mV, 1-2 ms)	~100 Hz	~tens of seconds	N/A
DIB <sup>51</sup>	Alamethicin-doped droplet interface bilayer between 500 mM KCl droplets	200 nL per droplet	Channel density/permeability changes via voltage-driven insertion of alamethicin in ion channels	Pulse trains (130 mV, 10-1500 ms)	20-50 Hz	~2 s	pW-nW
DIB <sup>53</sup>	Droplet interface bilayer formed by printed networks of aqueous droplets	~500 pL droplets	Platform work	Thermal stimulus for printing (55–60 °C) and mechanical compression tests (mHz–Hz).	N/A	N/A	N/A
Brain organoid <sup>58</sup>	Human neural organoids interfaced with microelectrode array	N/A	Stimulation-modified neural network activity/connectivity in human neural organoids	Electrical theta-burst stimulation delivered 4x with 13-min interval	Short-term effects milliseconds after stimulation.	Longer-term plasticity assessed from 60–180 min post stimulation and additional assays over hours	N/A
Brain organoid <sup>61</sup>	In vitro cortical neuron cultures on multielectrode array	mm-scale culture on chip	Cultured cortical networks adapting synaptic connectivity and firing patterns	Closed-loop electrical stimulation	Apparent learning/adaptation reported within ~5 minutes in closed-loop task	N/A	N/A
Ionic polymer <sup>71</sup>	Organic electrochemical RAM: p(g2T-TT) channel with ion-gel electrolyte	Channel ~45 $\mu$ m $\times$ 15 $\mu$ m	Electrochemical doping/de-doping	Pulse trains (1 V, 1 $\mu$ s)	~0.05 GHz	~minutes	~80 fJ per write
Ionic polymer <sup>75</sup>	All-inorganic ionic polymer memristor: Au / APP / ITO on PET	APP layer thickness ~250 nm	Voltage-driven migration/accumulation of mobile ions in ammonium polyphosphate	Pulse trains (0.1-0.4 V, 20 ns-20 $\mu$ s)	~0.05 GHz	~10,000 s retention	~nJ per write
Ionic polymer <sup>76</sup>	Proton-enabled peptide memory: Y7C peptide film coupled to IGZO synaptic transistor	Y7C film thickness ~117 nm, ~200 $\times$ 200 $\mu$ m <sup>2</sup>	Voltage-driven migration/accumulation of mobile ions in ammonium polyphosphate	Humidity+pulse trains (1 V, 0.1-1 s)	10,000-0.1 Hz	seconds to hundreds of seconds	N/A



## 2.1 Biological membrane and protein nanopores

Biological membranes, composed of lipid bilayers with embedded proteins (Figures 3a-b), have evolved to perform ionic information processing. Central to this function are ion channels, whose conductance is regulated by voltage, ligand binding and other external stimuli.<sup>34</sup> The Hodgkin-Huxley framework can itself be viewed as memristive, in that channel gating variables evolve according to voltage history and thereby produce history-dependent conductance that is essential for action-potential generation.<sup>35</sup> Although biological nanopores have been studied extensively as sensors for the detection of small molecules,<sup>36-40</sup> this same principle has also motivated the direct use of biological ion channels as building blocks for artificial synapses.

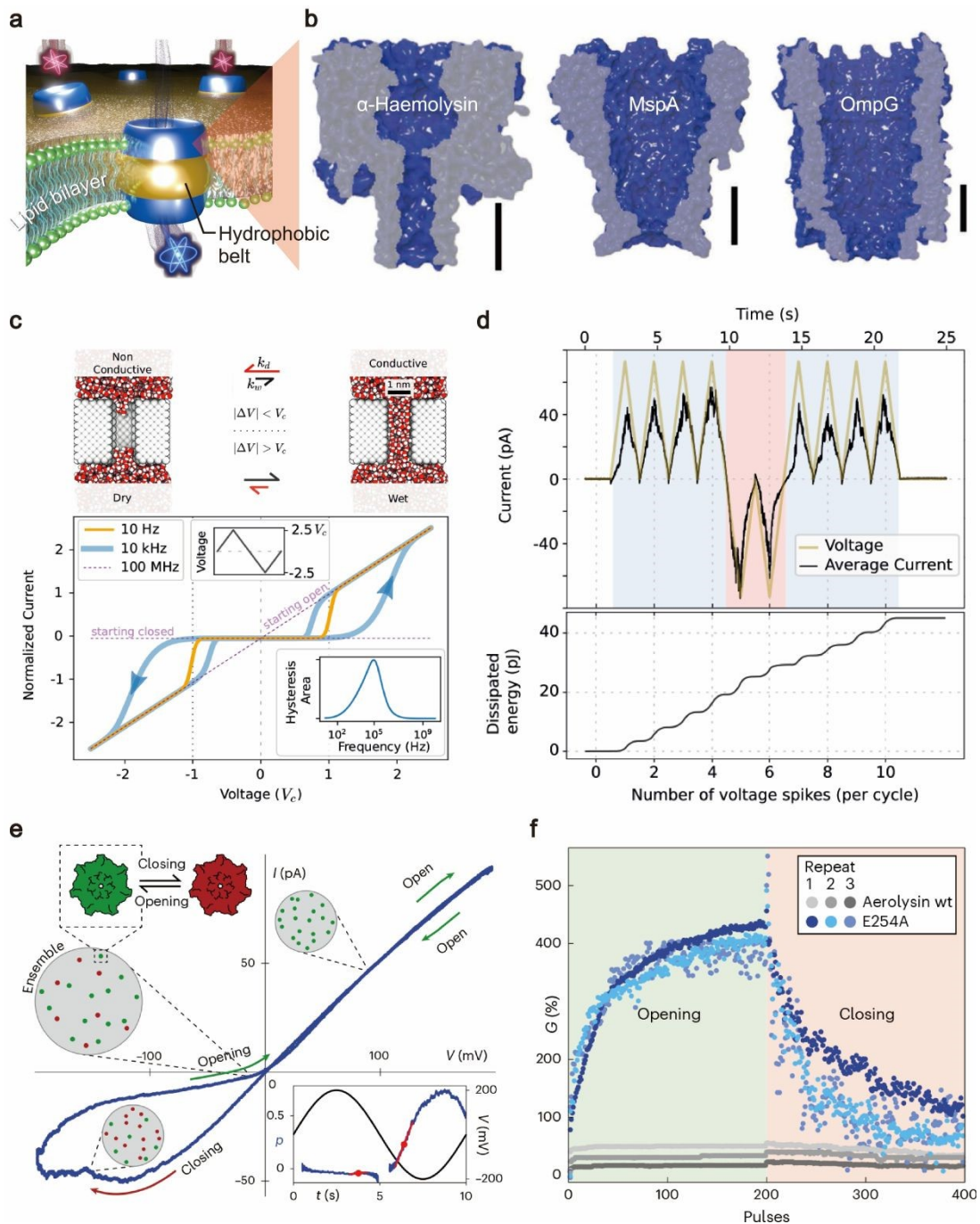
An instructive example of a bioengineered ion-channel memristor is the hydrophobically gated nanopore based on Fragaceatoxin C (FraC), a pore-forming toxin.<sup>41</sup> Here, a hydrophobic constriction undergoes voltage-driven electrowetting transitions between wet conductive and dry vapor-blocked states, generating strongly history-dependent conductance with large on/off ratios (Figure 3c). When a small number of mutant FraC pores are reconstituted in a lipid bilayer, the device displays analogue switching, stochastic state transitions and synapse-like plasticity under pulsed stimulation. This system illustrates how protein nanopores can serve as genetically encodable, structurally precise building blocks for iontronic memristors (Figure 3d).

A mechanistically distinct route to protein-based neuromorphic elements is offered by beta-barrel nanopores widely studied for sequencing applications,<sup>42,43</sup> in which lumen charge governs both open-pore rectification and voltage-driven mechanical gating (Figure 3e). A recent mutation-theory-simulation study of aerolysin showed that localized charges in the pore lumen drive ionic accumulation and depletion that set the polarity and magnitude of rectification, whereas gating emerges on slower timescales when strong electric fields dissociate counterions from lumen charges and promote local beta-barrel deformations, yielding a bistable open/closed response and memristive hysteresis. By tuning the spatial distribution of lumen charge with site-specific mutations, the authors engineered an aerolysin mutant with enhanced synaptic plasticity and demonstrated potentiation and depression by voltage pulse sequences, providing a rational design framework for programmable ionic synapses (Figure 3f).<sup>44</sup>

The advantage of genuine cell membranes, or their synthetic analogues, is that they naturally embody many of the features required for computation, including nonlinearity, time dependence and plasticity. For example, incorporating NMDA receptors into a lipid bilayer could in principle reproduce aspects of Hebbian plasticity. Although such systems remain bioengineered and experimentally complex, they illustrate how soft



208 memristors can be directly biomimetic and function in ways that closely resemble natural

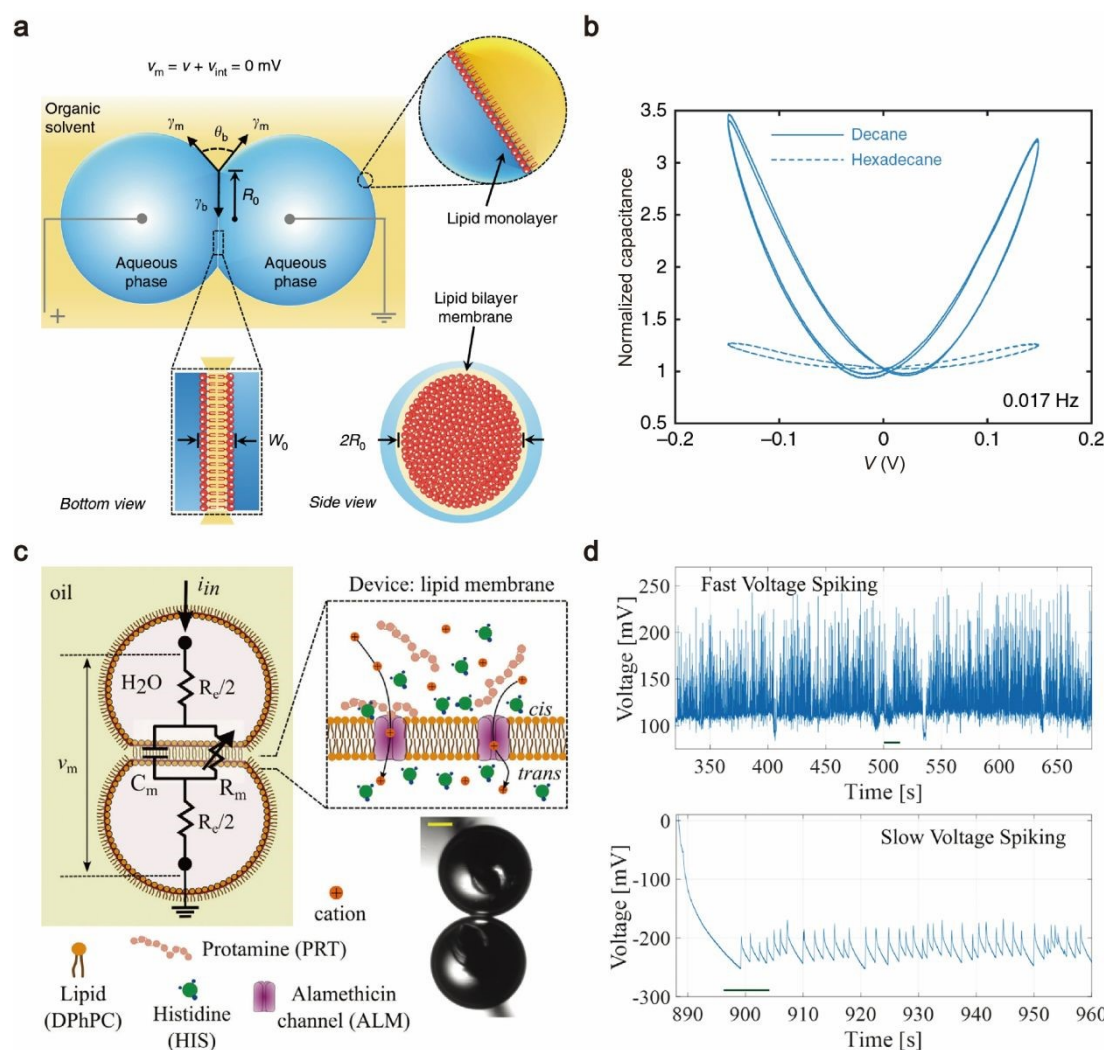


**Figure 3.** Memristive gating in biological nanopores. **a**, A sketch depicting a simplified model of protein channels inserted in a lipid bilayer. **b**, Structures of  $\alpha$ -haemolysin, MspA, and OmpG. Adapted with permission from ref. 42. Copyright 2016 Springer Nature. **c**, Electrowetting mechanism and normalized current-voltage loops showing frequency-dependent hysteresis. **d**, Spike-train operation yielding synapse-like current responses and cumulative energy dissipation. Adapted with permission from ref. 41. Copyright 2023 Creative Commons CC BY. **e**, Ensemble opening/closing produces a pinched hysteresis loop in the  $I$ - $V$  characteristics. **f**, Plasticity under repeated voltage pulses for wild-type and charge-mutant aerolysin, illustrating potentiation and depression of conductance. Adapted with permission from ref. 44. Copyright 2025 Creative Commons CC BY.



209 synapses.

210

211 **2.2 Droplet interface bilayers**212 Droplet interface bilayers (DIBs) extend the bionanopore concept from a single  
213 molecular channel to a mesoscopic, reconfigurable synaptic unit.<sup>12</sup> In these systems,

**Figure 4. Droplet-interface bilayers as voltage-responsive memcapacitors and spiking membrane neurons.**

**a**, Droplet-interface bilayer (DIB) platform in which two aqueous droplets in oil self-assemble a lipid bilayer that can host transmembrane channels; schematic (top) and optical micrograph (bottom). **b**, Voltage-driven electro-wetting and electro-compression reshape the bilayer geometry, modulating membrane thickness and radius as coupled state variables. The resulting nonlinear pinched capacitance-voltage hysteresis depends on the oil phase, demonstrating memcapacitance. Adapted with permission from ref. 50. Copyright 2019 Creative Commons CC BY. **c**, Equivalent circuit for DIB devices with electrolyte resistance in series with a membrane branch comprising a state-dependent membrane resistance in parallel with membrane capacitance; inset, reconfigurable channel networks and mobile charged modulators coupling ionic transport to membrane state. **d**, Under dc current bias, these internal dynamics can generate neural-like voltage spiking with distinct fast and slow regimes, consistent with a feedback cycle of channel insertion/opening and polyelectrolyte-mediated blocking and charge redistribution across cis/trans reservoirs. Adapted with permission from ref. 51. Copyright 2024 John Wiley and Sons.



214 two electrolyte droplets are brought into contact within oil, where opposing lipid  
215 monolayers zip together to form a bilayer patch that is electrically addressable in much  
216 the same way as a cell membrane (Fig. 3a).<sup>46,47</sup> Despite this simple geometry, DIBs can  
217 already support a surprisingly rich repertoire of synaptic functions even in the absence of  
218 ion channels, including facilitation and depression reminiscent of spike-rate-dependent  
219 plasticity, Hebbian learning, and even associative learning in a Pavlovian protocol under  
220 voltage-pulse stimulation.<sup>48</sup>

221 The origin of memory in DIBs is mechanistically distinct from protein-pore gating.  
222 Here, a voltage sweep couples ionic relaxation to interfacial mechanics (Fig. 4a): residual  
223 charge, field-driven ion adsorption within the headgroup region, and the slow recovery  
224 of membrane order together bias the conductance reached on the next cycle.<sup>49</sup> Bilayer  
225 capacitance is likewise not a passive quantity, but evolves with voltage history as  
226 membrane tension, area and dipole orientation shift. The resulting element therefore  
227 behaves as a coupled memristor–memcapacitor rather than as a purely resistive switching  
228 device (Fig. 4b).<sup>50</sup>

229 This coupling is what makes DIBs a particularly powerful extension of biological  
230 nanopore concepts for neuromorphic devices. Whereas the systems in Section 2.1  
231 derive their dynamics primarily from the conformational landscape of a specific protein  
232 channel, DIB synapses expose several tunable state variables, including electrolyte  
233 composition, droplet size, bilayer lipid chemistry and mechanical boundary conditions.  
234 The learning rule can therefore be engineered at the level of interfacial physics. Protein  
235 nanopores can nonetheless be incorporated as modular components (Fig. 4c,d).<sup>51-54</sup>  
236 Introducing channels such as alamethicin,<sup>52</sup> MscL,<sup>53</sup> or engineered mutants<sup>54</sup> adds a  
237 second layer of memory through channel population dynamics, effectively combining  
238 molecular and interfacial plasticity within a single soft element.

239 Equally important, droplets offer a route to scalability that single-bilayer protein  
240 devices struggle to match. Droplets can be generated, positioned, and connected in  
241 parallel by microfluidics, patterned into networks, or assembled as emulsions into dense  
242 soft circuits, turning the bilayer into a repeatable unit cell for wet neural architectures.<sup>55</sup>  
243 The remaining hurdles are practical-bilayer fragility and device-to-device variability,  
244 motivating polymer-stabilized membranes, partial gelation and chip-based confinement  
245 as strategies to make large droplet arrays both reproducible and long-lived.

246

### 247 **2.3 Living neural networks and organoid intelligence**

248 Brain organoids, three-dimensional neural tissue constructs grown from stem cells,  
249 are emerging as soft, living substrates for neuromorphic computing.<sup>56,57</sup> These mini-



250 brains are physically soft with stiffness on the order of only a few hundred Pascals.<sup>58</sup>  
 251 This extreme mechanical softness means organoids are predominantly fluidic systems,  
 252 composed of cells and extracellular matrices akin to soft membranes, which enables  
 253 efficient ion transport through the aqueous extracellular space and across flexible cell  
 254 membranes, much like ionic polymers in artificial devices.  
 255 Memristive behavior is intrinsically realized in organoid neural networks via

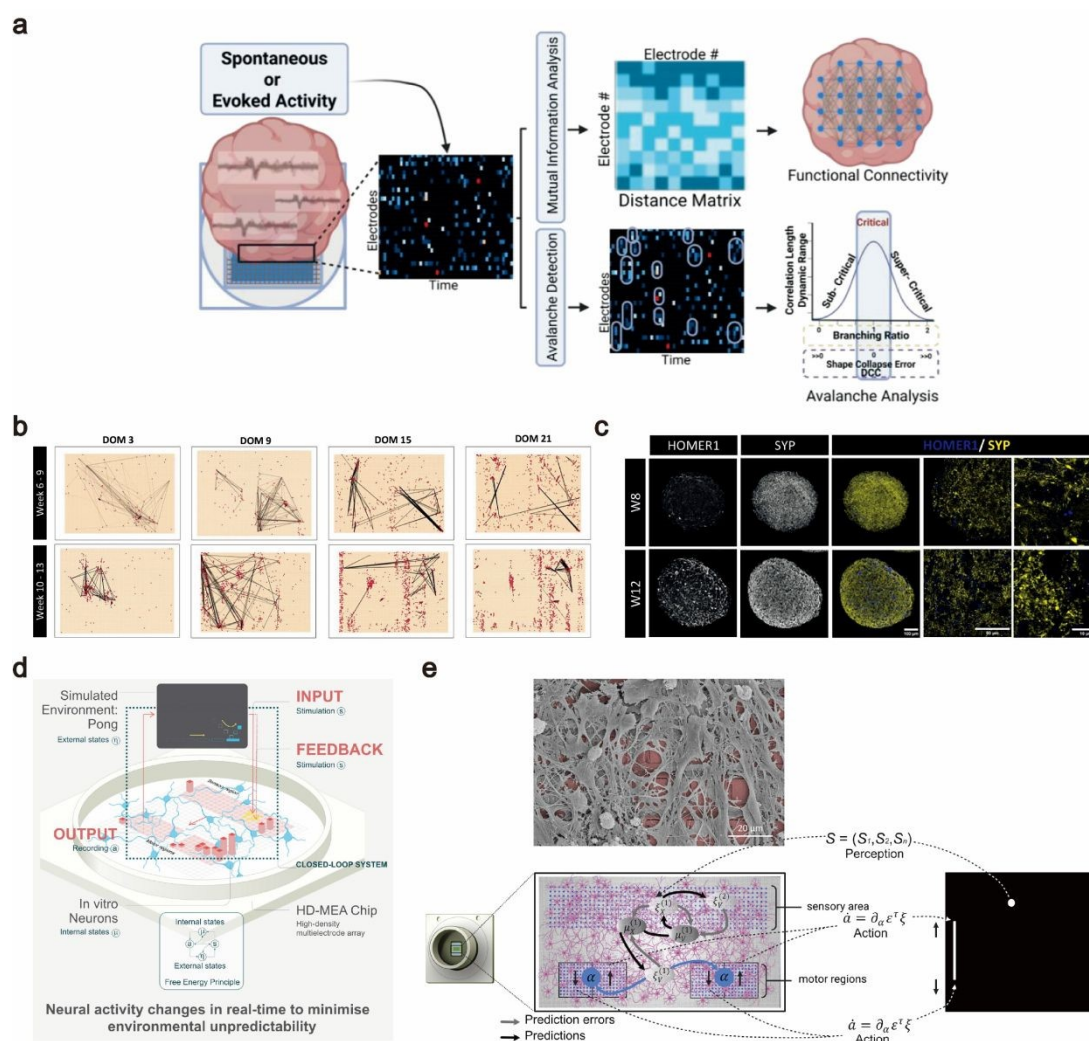


**Figure 5. Living neural networks as soft ionic substrates for computation.** **a**, High-density microelectrode array interfacing enables simultaneous recording and stimulation of cortical organoids; analysis workflows extract functional connectivity and neuronal criticality from spontaneous and evoked activity. **b**, Example functional-connectivity graphs reconstructed across development, illustrating evolving edge weights and active nodes across the electrode field. **c**, Immunostaining of pre- and postsynaptic markers in cortical organoids indicates progressive synaptogenesis that underpins emergent network dynamics. Adapted with permission from ref. 59. Copyright 2025 Springer Nature. **d**, Closed-loop DishBrain embodiment, in which cultured neurons on a microelectrode array receive sensory stimulation encoding the Pong game state and feedback to drive goal-directed adaptation. **e**, Mapping of sensory and motor channels on the array and a conceptual active-inference loop linking neuronal activity to actions and prediction errors in the virtual environment. Adapted with permission from ref. 62. Copyright 2022 Creative Commons CC BY.



256 synaptic plasticity. In these living networks, each synapse acts like a nanoscale  
257 memristor whose strength or conductivity adjusts based on prior activity. Biological  
258 synapses achieve this through ionic and molecular mechanisms. For instance, repeated  
259 stimulation causes residual  $\text{Ca}^{2+}$  buildup and receptor modifications that temporarily or  
260 permanently change synaptic efficacy. Experiments have confirmed that brain  
261 organoids exhibit both short-term and long-term synaptic potentiation and depression in  
262 response to stimulation (Figure 5a-c).<sup>59</sup> In other words, organoids can undergo short-  
263 term memory with milliseconds-to-seconds facilitation/depression of a synapse as well  
264 as long-term memory allowing persistent strengthening or weakening analogous to  
265 learning. Although these plastic changes mirror the memristive behavior engineered in  
266 ion-based artificial synapses, they emerge naturally from the underlying biochemistry of  
267 the organoids. Notably, recent high-profile work demonstrated that human neural  
268 organoids constitute the fundamental building blocks of learning. They form functional  
269 synapses with glutamatergic/GABAergic receptors and show activity-dependent gene  
270 induction accompanying synaptic potentiation.<sup>59</sup> Such findings demonstrate that a soft  
271 living organoid can perform analog memory storage through ionic synaptic modifications,  
272 effectively functioning as a memristive network without any solid-state components.

273 The link to artificial nanofluidic memristors becomes clearer when these biological  
274 processes are expressed in physicochemical terms. Residual  $\text{Ca}^{2+}$  accumulation in  
275 synapses resembles the delayed ionic relaxation that sustains electric-double-layer  
276 memory, while neurotransmitter binding and release parallel reversible adsorption and  
277 desorption processes at functionalized interfaces. These correspondences do not imply  
278 strict equivalence, but they do provide a useful design language for translating organoid-  
279 like plasticity into engineered iontronic devices.

280 By virtue of their intrinsic ionic conduction and synaptic plasticity, brain organoids  
281 are emerging as experimental platforms for neuromorphic task execution. Their  
282 distributed neuronal circuits support collective information processing reminiscent of  
283 biological brains. For example, organoids can generate organized electrical oscillations  
284 and synchronized firing patterns analogous to brain waves.<sup>59</sup> Notably, spontaneous  
285 network oscillations in a human cortical organoid have been shown to recapitulate EEG  
286 rhythms observed in the preterm infant brain, suggesting the emergence of functional  
287 connectivity and critical dynamics favorable for computation. More directly, organoids  
288 have been harnessed for computational tasks through learning-based frameworks. In a  
289 landmark study, a living brain organoid was incorporated into a reservoir-computing  
290 architecture, in which a three-dimensional neural organoid was coupled to a high-density  
291 microelectrode array for stimulus encoding and signal readout.<sup>60</sup> The organoid



292 exhibited rich nonlinear dynamics together with a fading memory of past inputs, enabling  
293 time-dependent computation. Remarkably, the system achieved unsupervised learning  
294 through network reorganization, allowing it to perform speech recognition and even  
295 predict chaotic mathematical equations in real time.<sup>60</sup> In this setting, the soft organoid  
296 functioned as a reconfigurable analogue processor whose internal synaptic weights  
297 adjusted autonomously in response to training stimuli.

298 Neuromorphic behavior in biological networks has also been illustrated by  
299 demonstrations of goal-directed learning in cultured neuronal assemblies, a line of work  
300 often grouped under the emerging concept of organoid intelligence. In 2022, a cultured  
301 layer of ~800,000 human cortical cells interfaced with electrodes, frequently described as  
302 a two-dimensional organoid or cortical network, was shown to learn to play Pong through  
303 feedback-driven training (Figure 5d-e).<sup>61,62</sup> Over time, the neuronal culture  
304 progressively reshaped its firing dynamics in response to the game environment,  
305 revealing a rudimentary form of skill acquisition and memory that sustained paddle  
306 control. The DishBrain experiment illustrates that living neural networks can acquire  
307 adaptive behavior and store memory in a manner analogous to a learning machine.  
308 Taken together with three-dimensional organoid studies, these findings offer proof-of-  
309 concept that biological soft systems can realize computational functions such as pattern  
310 recognition, control, and prediction by leveraging synaptic plasticity.<sup>59</sup> During learning,  
311 the iontronic circuits of these networks are continuously reshaped by the malleable,  
312 fluidic tissue itself, exemplifying how mechanical softness and neuromorphic function  
313 are intrinsically coupled in organoid computing.

314 Organoids derive their computing capability from a unique combination of material  
315 softness and biological architecture, standing in sharp contrast to traditional electronic  
316 hardware. They consist of living neurons, supporting glial cells and the extracellular  
317 matrix they secrete.<sup>59</sup> Within an aqueous milieu, neurons self-organize into dense three-  
318 dimensional networks interconnected by thousands of synapses. Soft phospholipid  
319 bilayer membranes act as the basic ionic capacitive and resistive elements. Owing to  
320 their nanometer-scale thickness and mechanical softness, these membranes readily  
321 undergo conformational changes in response to ion binding or voltage fluctuations,  
322 enabling electrically responsive soft-matter behavior. Protein ion channels and  
323 receptors embedded within the membranes respond to mechanical and electrical cues by  
324 opening or closing, thus dynamically regulating ion transport. This tunability enables  
325 ion transport to display rich nonlinear responses, such as channel inactivation and  
326 neurotransmitter depletion, that are essential for computation. Additionally, the  
327 nanoscale synaptic cleft forms a soft ionic domain that transiently concentrates



328 neurotransmitters and ions during activity, producing short-lived chemical gradients.  
329 Repeated signaling transiently reshapes the chemistry of the synaptic cleft, analogous to  
330 the state evolution of an active region, enabling synaptic strength to encode a short-term  
331 memory of recent activity.<sup>63</sup> At its core, the computational substrate of organoids is a  
332 network of soft, ion-conducting components from lipid bilayers and protein ion channels  
333 to neurotransmitters. Mechanical softness and flexibility are central to function at every  
334 level, with soft membranes and cytoskeletal elements enabling synaptic reorganization  
335 during learning, from the creation of new connections to synaptic growth during  
336 potentiation. This stands in contrast to rigid silicon chips, where circuit elements are  
337 fixed. In organoids, the wiring is fluid. Indeed, studies have observed organoid  
338 neurons forming new circuits and strengthening connectivity in response to stimulation,  
339 effectively rewiring their microcircuitry as learning progresses. Such plastic  
340 reconfiguration is enabled by both the biochemical machinery and the compliant physical  
341 matrix in which neurons reside.

342 The advent of brain organoids as computing units carries profound implications for  
343 bio-inspired and neuromorphic computing. First, these living systems offer a level of  
344 adaptive parallelism and energy efficiency.<sup>64</sup> Their soft iontronics approach to  
345 computation could overcome limitations of traditional rigid electronics by operating in an  
346 analog, event-driven fashion with minimal chemical energy. Intrinsic mechanical  
347 softness permits conformal biointerface integration, enabling flexible three-dimensional  
348 electrode meshes to envelop organoids without damage and opening the door to wetware  
349 co-processors that physically integrate with sensing or robotic systems. Moreover,  
350 organoid computing systems naturally embody features that hardware engineers struggle  
351 to reproduce, such as self-organization and fault-tolerance. Through memristive  
352 synapses, these systems achieve on-chip learning and memory without explicit  
353 programming, and even when partially damaged, the remaining tissue can reorganize to  
354 restore function, echoing recovery mechanisms in the brain. This mortal yet  
355 regenerative substrate thus defines a new computational paradigm, in which hardware  
356 itself can grow, adapt, decay, and be renewed. Despite their promise, organoids pose  
357 major challenges for reliable computing, including biological variability, finite lifespans,  
358 and ethical issues inherent to human-derived neural systems. Nonetheless, recent  
359 studies have validated the core concept that soft living neural networks can perform  
360 meaningful computations. As research progresses, it is conceivable that hybrid  
361 approaches integrating organoid-based processors with conventional electronic systems  
362 could be explored, potentially harnessing the complementary strengths of biological  
363 adaptability and electronic precision.

## 364 2.4 Ionic polymers and soft iontronics

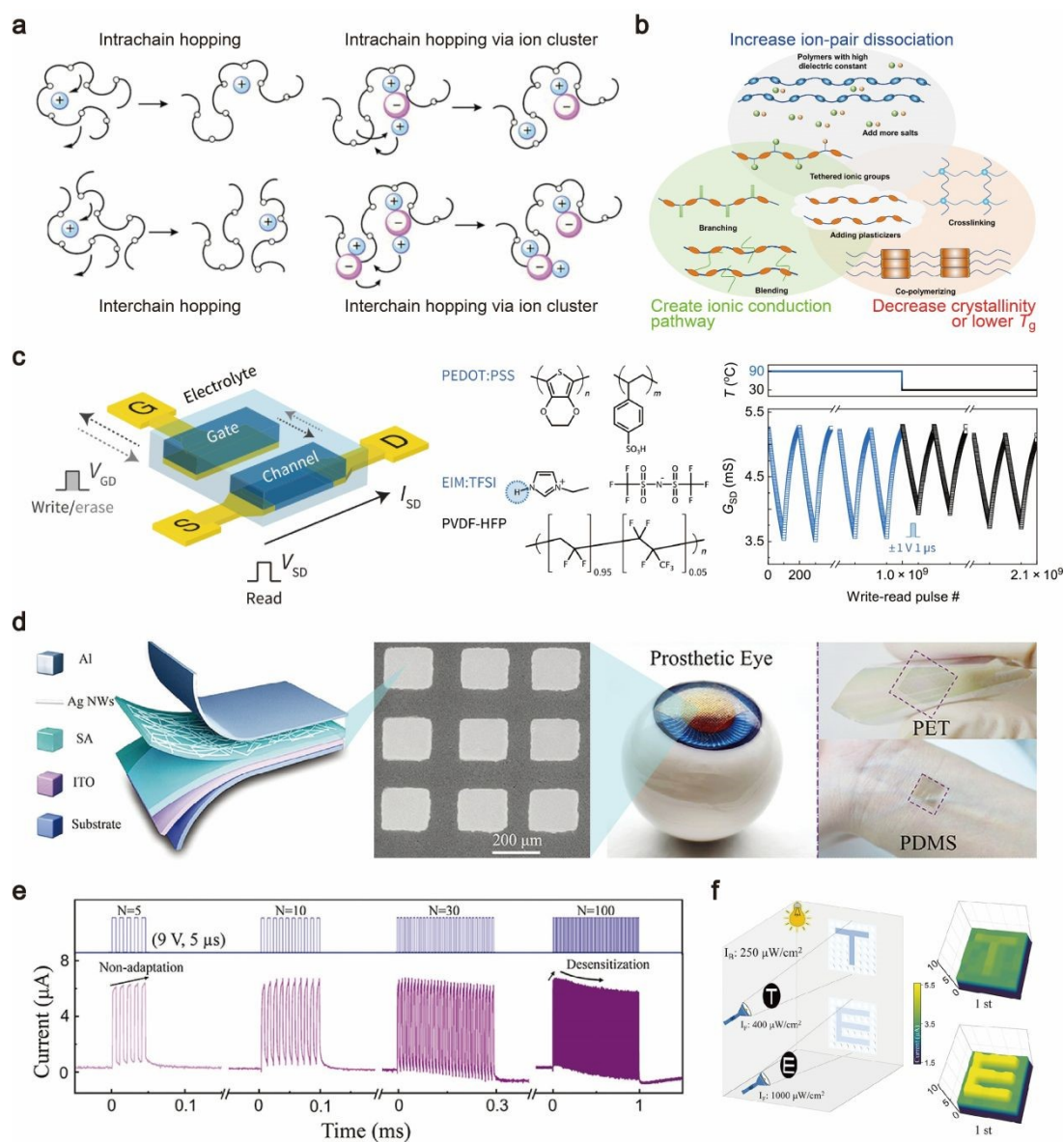


**Figure 6. Soft polymer iontronics as a bridge from transport physics to adaptive sensing.** **a**, Schematic view of ion motion in polymer electrolytes, highlighting intra-chain and inter-chain hopping that set the intrinsic relaxation times governing ionic conductivity. **b**, Materials-level design levers for raising conductivity. Adapted with permission from ref. 66. Copyright 2023 Creative Commons CC BY. **c**, Solid-state organic electrochemical random-access memory in which an ion-gel gate modulates the doping state of a conjugated-polymer channel, enabling low-voltage analog weight updates and temperature-resilient operation with sub-microsecond programming and  $>10^9$  write-read endurance. Adapted with permission from ref. 72. Copyright 2020 The American Association for the Advancement of Science. **d**, Flexible sodium-alginate complementary memristor architecture and array-level integration, illustrating conformable form factors for prosthetic and wearable platforms. **e**, Pulse-train responses in the alginate device that transition from non-adaptation to desensitization as stimulus number increases, implementing a hardware analogue of sensory gain control. **f**, A neuromorphic vision concept in which adaptive preprocessing improves pattern recognition across changing background intensity, linking ionic memory directly to perception-level tasks. Adapted with permission from ref. 73. Copyright 2024 John Wiley and Sons.



365 Rather than borrowing the molecular machinery of biology, ionic polymers offer a  
366 synthetic, processable medium in which memory is written into ion distributions and soft-  
367 matter relaxation, enabling devices that are flexible, scalable, and compatible with large-  
368 area manufacturing.<sup>65-68</sup> They span electrolyte-swollen hydrogels, ionomers such as  
369 Nafion, and polyelectrolyte networks built from biopolymers. Their defining feature is  
370 that the conductor is not a fixed pore but a dynamic matrix of charged segments binding  
371 and releasing counterions, polymer domains swelling or densifying, and nanoscale  
372 morphology evolving under bias (Figure 6a-b). These slow internal degrees of freedom  
373 provide the state variable for memristive behavior, while the macroscopic form can be  
374 cast as films, patterned over centimeters and integrated on soft substrates.<sup>69,70</sup>

375 The mechanism contrasts with the biological motifs. In protein nanopores,  
376 memory is encoded in conformational landscapes of a channel. In droplet bilayers, it  
377 emerges from coupled ionic relaxation and interfacial mechanics. In organoids, it is  
378 distributed across synapses and gene programs. Polymer synapses, by comparison, store  
379 their state in the physics of ion binding, diffusion, and viscoelasticity within a single  
380 material layer, trading biological richness for device-level simplicity and  
381 manufacturability.<sup>71</sup>

382 A common architecture is the ionic gel, in which an electrolyte is immobilized within  
383 a polymer scaffold. Because ions move through a crowded network rather than a free  
384 solution, relaxation is slowed and conductance lags the applied field.<sup>72</sup> Fixed charges  
385 add a further source of history dependence by transiently trapping counterions and  
386 altering local osmotic pressure, while the same redistribution of ions can couple to  
387 electromechanical strain so that swelling and conductivity evolve together. The  
388 resulting behavior appears as electrical hysteresis, often in the form of a pinched current-  
389 voltage loop and, in some materials, a persistent deformation that in turn feeds back on  
390 transport (Fig. 6c).<sup>72</sup>

391 Natural polyelectrolytes provide a clear example of how chemistry and mechanics  
392 can become memory.<sup>73</sup> In alginate gels, crosslinking is mediated by divalent cations  
393 such as  $\text{Ca}^{2+}$ , so an applied field can drive ion exchange and create spatially  
394 heterogeneous crosslink densities (Fig. 6d-f). Because both the ionic profile and the  
395 polymer network relax only slowly, regions with distinct mechanical and ionic properties  
396 can persist after stimulation, leaving a structural memory that is later read out through  
397 changes in ionic conductance. More generally, polysaccharide gels with path-dependent  
398 hydration or ionic crosslinking offer a route to purely ionic memory without invoking  
399 metallic filaments or electronic charge storage.

400 Denser ionomers provide a complementary pathway in a solid membrane. In



401 Nafion, protons drift through nanometer-scale ionic domains lined with sulfonate groups,  
402 and a fraction becomes transiently trapped or stabilized by local hydrogen-bond  
403 networks.<sup>74,75</sup> Slow rearrangement of these ionic clusters makes resistance evolve with  
404 voltage history, yielding memristive transport at low bias. Bipolar ion-exchange  
405 membranes extend this concept by adding interfacial reaction dynamics: forward bias  
406 promotes water dissociation at the junction, whereas recombination proceeds with  
407 different kinetics, so the interfacial ionic state carries memory.<sup>74,75</sup>

408 A major application space in which ionic polymers excel is flexible and wearable  
409 electronics. Using gels and polymer electrolytes, researchers have developed iontronic  
410 capacitive touch sensors and synaptic transistors for human-machine interfaces, naturally  
411 extending to flexible memristive artificial synapses. For example, Zhao *et al.*<sup>76</sup> reported  
412 a flexible all-inorganic ionic polymer-based memristor that exhibited stable synaptic  
413 behavior. Although the detailed operating mechanism of this device lies beyond the  
414 scope of this discussion, it likely relies on ionically driven internal reconfiguration within  
415 an inorganic polymeric matrix to achieve low-voltage, non-volatile resistance modulation.  
416 More broadly, such results demonstrate how ionic conduction coupled to slow structural  
417 or chemical rearrangements in polymeric systems can support memory effects suitable  
418 for neuromorphic functionality.

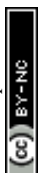
419 Ionic polymers also allow computation to be coupled to the environment.  
420 Humidity-responsive peptide films, for example, gate proton conduction through water  
421 uptake, so resistance depends on both electrical history and ambient chemistry.<sup>77,78</sup> This  
422 multifunctionality suggests polymer synapses that sense and learn within the same  
423 material, an ability that is difficult to achieve with isolated protein pores or fragile bilayer  
424 droplets.

425 In practice, polymer iontronics is defined by a useful compromise. These devices  
426 typically operate at low voltage and can retain memory for minutes to hours because ionic  
427 and structural relaxation is slow, although switching speeds are often limited by diffusion  
428 and viscoelasticity. Their decisive advantage is integration by processing rather than by  
429 assembly, in terms of the fact that films can be cast, coated, or printed into dense arrays,  
430 positioning ionic polymers as a pragmatic counterpart to the biological systems.

431

### 432 **3. Solid-state nanofluidic platforms**

433 Having established the role of softness, we next turn to solid-state nanofluidic  
434 platforms. Unlike biological synapses or ionic polymer systems, solid-state nanopores  
435 and nanochannels are mechanically rigid. Their defining feature is not ductility or  
436 deformability, but geometric and chemical stability during operation. At first glance,



437 this rigidity may seem disadvantageous compared with the adaptive softness of neurons

**Table 2.** Hard nanofluidic systems with memristive ionic dynamics.

System class	Material / fluidic system	Size	Mechanism	Stimulus class	Switching speed	Retention time	Energy consump.
Counterion dynamics <sup>86</sup>	Track-etched PET double conical nanopores, KCl concentration gradients	Tip diameter ~5–20 nm	Broken symmetry from divalent-ion screening and pH-driven deprotonation	Pulse trains (10 V, 1.0–1.5 s)	~1 Hz	~20 min	NA
Counterion dynamics <sup>87</sup>	Conical polyimide nanopores, 0.1 M KCl	Tip diameter ~20–50 nm	Voltage-derived transient ion concentration polarization	Pulse trains (2 V, 2–1,000 ms)	1–50 Hz	~40 s	NA
Counterion dynamics <sup>94</sup>	Tapered microfluidic channel, 10 mM KCl	Channel tip 5 $\mu$ m, base 200 $\mu$ m, length 150 $\mu$ m	Voltage-derived transient ion concentration polarization	Pulse trains (2.5–5 V, 0.75 s)	~1 Hz	~1 s	~1–10 $\mu$ J
Space confinement <sup>102</sup>	Angstrom-scale slit nanochannels (theory)	Slit height ~0.7–1.4 nm	Electric-field-induced ion clustering in Å-scale slits	AC voltage (0.1 V, 100 Hz)	~100 Hz	N/A	N/A
Space confinement <sup>103</sup>	Active carbon 2D channel, 1 mM CaCl <sub>2</sub>	Channel height ~5 nm	Surface adsorption/desorption-mediated ion transport	Pulse trains (1 V, 10 s)	~0.1 Hz	~hours	N/A
Space confinement <sup>104</sup>	MoS <sub>2</sub> and hBN 2D nanochannel, KCl, CaCl <sub>2</sub> , AlCl <sub>3</sub>	Channel height 0.7–2 nm	Transient concentration polarization and ion–ion/surface-charge interactions	Write pulses ~20–60 s	~0.1 Hz	Short (<100 s) and long term (> 3days) memory	N/A
EOF <sup>105</sup>	Immiscible liquid–liquid interface in nanochannels	PDMS nanochannel, 200 nm x 63 nm x 10 $\mu$ m	Electroosmosis-derived motion of liquid–liquid interface confined in nanochannels	Pulse trains (4–10 V, 0.5 s)	2 Hz	> 20 min	N/A
Optical <sup>107</sup>	Graphene–MoS <sub>2</sub> heterojunction nanopore, 1 M KCl	Heterojunction nanopore size ~2–20 nm	Light-induced electron–hole separation in a p–n heterojunction nanopore inducing photovoltage-driven ion pumping	Light pulses (365–1050 nm, 0.2–5 Hz)	Response time 50 ms	N/A	16.3 mW/cm <sup>2</sup> per light pulse
Optical <sup>109</sup>	Layered graphene oxide nanochannel	Lamellar graphene oxide nanochannel, spacing ~0.42 nm; length mm-scale	Light illumination driven Na <sup>+</sup> migration/ion redistribution in nanochannels	Light pulses (532 nm, 6 mW, 0.2 s)	5 Hz	N/A	~1.2 mJ per light pulse
Optical <sup>110</sup>	B <sub>3</sub> N subnanometer pores, mixed electrolyte (1.0 M KCl + 0.1 M NaCl) (MD simulation)	Subnanometer pores; 16 pores in ~7 nm x 7 nm membrane patch (hBN monolayer)	Light illumination driven Na <sup>+</sup> migration/ion redistribution in nanochannels	Pulse trains (0.5 V, 3 ns)	~0.1 GHz	~ $\mu$ s	0.1–100 aJ per pulse
In-pore chemistry <sup>117</sup>	Conical PET nanopore in PBS+KCl+CoCl <sub>2</sub>	Nanopore tip size 2–7 nm	Voltage-driven nanoprecipitation/dissolution inside a conical nanopore modulating aperture/selectivity	Pulse trains (2 V, 15 s)	Seconds-scale switching	N/A	N/A
In-pore chemistry <sup>118</sup>	SiN <sub>x</sub> nanopore interfacing MnCl <sub>2</sub> and PBS	Nanopore size 100–300 nm	Voltage-driven nanoprecipitation/dissolution inside a conical nanopore modulating aperture/selectivity	Pulse trains (0.2–0.8 V, 50 ms)	~20 Hz	>100 s	~0.1 nJ per pulse
EOF <sup>119</sup>	SiN <sub>x</sub> nanopore membrane decorated with Pd and covered by graphite, 1 M KCl	Nanopore size 100 nm	Voltage-driven mechano-ionic blistering changing atomically thin pore/nanocavity geometry	Pulse trains (1.2 V, 2 s)	>10 Hz	N/A	N/A



438 or ionic polymers. Yet solid-state nanofluidic systems compensate for the absence of  
439 mechanical compliance by exploiting field-driven ionic reconfiguration, electrochemical  
440 memory, and interfacial phenomena under confinement. Advances in nanofabrication  
441 now allow pores to be engineered at dimensions approaching those of biological ion  
442 channels, opening transport regimes shaped by ion dehydration, Coulomb blockade and,  
443 in some cases, even quantum effects.<sup>79–82</sup> More importantly, rigidity brings precise  
444 fabrication, reproducibility and compatibility with large-scale integration,<sup>83,84</sup> making  
445 solid-state nanofluidics the most realistic route towards mass-produced ionic  
446 neuromorphic hardware. Whereas neurons rely on mechanical softness to realize  
447 plasticity, solid-state nanofluidic memristors instead harness the electrochemical softness  
448 of ionic states. In both cases, memory arises from the delayed relaxation of internal  
449 degrees of freedom. In neurons, these include protein conformations and biochemical  
450 cascades; in rigid nanopores, they are primarily ionic distributions, hydration states and  
451 interfacial configurations. Solid-state nanofluidic memristors can therefore be viewed  
452 as rigid scaffolds for wet intelligence: architectures in which ions compute, remember  
453 and adapt within mechanically stable confinement.

### 454 3.1 Counterion dynamics in micro- and nanochannels

455 A central source of memristive behavior in rigid nanochannels is the electric double  
456 layer. When a voltage is applied across a permselective nanochannel or nanopore, ions  
457 begin to redistribute, creating regions of enriched or depleted ionic concentration (Figure  
458 7a).<sup>85,86</sup> If the voltage is changed before complete equilibration, residual ionic gradients  
459 and space-charge distributions from the prior state can persist and modulate subsequent  
460 transport, endowing the channel with a memory of its bias history (Figure 7b). Indeed,  
461 this mechanism underlies some of the earliest demonstrations of memristive behavior in  
462 ionic systems, where slow counterion dynamics in nanopore electric double layers give  
463 rise to hysteretic current-voltage responses.<sup>87</sup> In its simplest form, a fixed-charge  
464 conical nanopore rectifies ionic current, and when the bias is swept faster than ionic  
465 relaxation, residual depletion and accumulation persist at opposite ends of the pore,  
466 producing the pinched  $I$ - $V$  hysteresis with inherently frequency dependence, wherein  
467 slow voltage sweeps allow ions to equilibrate and eliminate memory, intermediate sweep  
468 rates produce strong hysteresis, and extremely fast sweeps yield an almost ohmic  
469 response as ionic motion becomes effectively frozen,<sup>88,89</sup> reflecting the fundamental  
470 timescales of ion migration and capacitive charging in nanoscale channels.

471 The same mechanism extends beyond nanometer confinement. Single channels  
472 with asymmetric geometry, surface charge or salinity can exhibit ionic rectification<sup>90,91</sup>



474 and, in some cases, negative differential resistance,<sup>92,93</sup> because the applied field  
475 establishes longitudinal depletion and accumulation regions. Strikingly, memristive

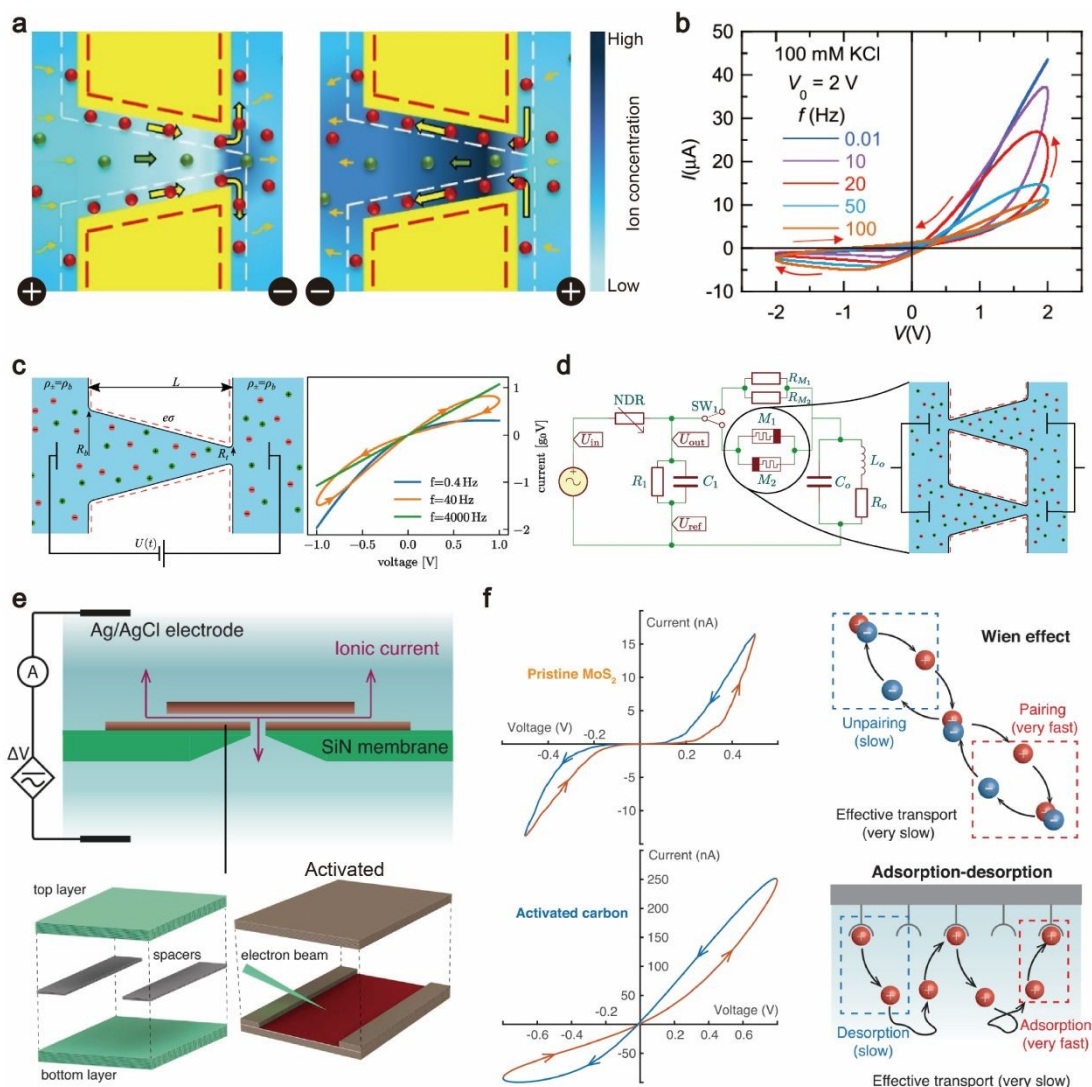


**Figure 7. Counterion dynamics- and deep confinement-derived ionic memristors.** **a**, Ionic concentration polarization at an asymmetric constriction, where bias-driven enrichment and depletion create a non-equilibrium ionic landscape that relaxes only slowly, imprinting history dependence on the conductance. Adapted with permission from ref. 86. Copyright 2024 American Chemical Society. **b**, Pinched hysteresis loops in the current-voltage characteristics of a multipore conical nanopore membrane under sinusoidal driving, showing the frequency-dependent opening and closing of the memristive window as the drive period approaches the ionic relaxation time. Adapted with permission from ref. 19. Copyright 2023 American Chemical Society. **c**, Minimal conical-pore model highlighting the role of access resistances and permselective enrichment/depletion zones in shaping rectification and hysteresis. **d**, Circuit-level abstraction in which ionic memristors are treated as dynamical elements that can be embedded into neuromorphic signal-processing architectures. Adapted with permission from ref. 94. Copyright 2025 Creative Commons CC BY-NC 3.0. **e**, Two-dimensional nanofluidic channels assembled from layered materials and locally activated to define angstrom-scale transport pathways. **f**, Representative hysteresis in pristine MoS<sub>2</sub> and activated-carbon channels together with proposed microscopic origins of long-lived state variables, including field-enhanced ion-pair dissociation (Wien effect) and adsorption-desorption kinetics under strong confinement. Adapted with permission from ref. 105. Copyright 2023 The American Association for the Advancement of Science.



476 behavior persists even for micrometer-wide channels, where history dependence can be  
477 traced to incomplete depletion and delayed re-equilibration of ions within extended  
478 space-charge layers upon field reversal.<sup>94</sup>

479 The underlying ion dynamics is set by a diffusion-controlled timescale that can be  
480 engineered through geometry. Starting from the coupled Poisson-Nernst-Planck-Stokes  
481 equations, the relaxation time is predicted to scale as  $\tau \approx L^2/(12D)$  for a channel of length  
482  $L$  and ionic diffusivity  $D$  (Figure 7c).<sup>95</sup> The quadratic dependence on  $L$  provides a  
483 simple design handle: doubling the channel length increases  $\tau$  by roughly a factor of four,  
484 prolonging the lifetime of ionic memory. Channel taper and wall charge further reshape  
485 the concentration polarization field<sup>96-100</sup> and tune the prefactor, offering additional control  
486 (Figure 7d). Analytical reductions and finite-element calculations consistently support  
487 this diffusive scaling and its sensitivity to geometric and interfacial parameters.<sup>95</sup>

488 This geometric programmability allows to adjust the temporal structure for a target  
489 computation. In colloid-filled tapered microchannels that embed a conducting  
490 nanochannel network, transient salt concentration polarization yields stable volatile  
491 memristors whose retention time can be selected by channel length.<sup>101</sup> Exploiting this  
492 tunability, individual channels have been used as synaptic elements for reservoir  
493 computing, where their nonlinear, history-dependent conductance transforms temporal  
494 voltage pulse trains into separable states. In a benchmarking task, time-series encodings  
495 of handwritten digits were classified with a simple readout layer, achieving performance  
496 comparable to solid-state dynamic memristor reservoirs.<sup>101</sup>

497 Together, even structurally rigid channels can display memristive ion transport  
498 because counterions and co-ions relax on finite timescales after the electric field is  
499 changed. In these purely electrostatic devices, memory is encoded in the slow build-up  
500 and decay of space charge, producing pinched current. Such systems have provided a  
501 clean starting point for ionic memory and have already been assembled into simple  
502 networks that execute logic and computing functions. The next step is to move beyond  
503 volatile, single-mechanism behavior towards non-volatile switching and multilevel states,  
504 while retaining manufacturable, parallel integration. Counterion dynamics in hard  
505 nanochannels, therefore, remains a foundational route to nanofluidic memristors as a  
506 direct analogue of early electronic memristor concepts, but governed by mobile ions and  
507 the physics of the electric double layer.

508 From a design perspective, channel geometry, ion concentration and electric field  
509 strength are best treated not as independent parameters but as coupled variables.  
510 Shrinking a channel does more than shorten the transport path: it increases the surface-  
511 to-volume ratio, strengthens interfacial charging, and amplifies the effects of adsorption



512 and depletion. Increasing electrolyte concentration, meanwhile, reduces the Debye  
513 length and can suppress hysteresis, yet under sufficiently strong driving it can also  
514 intensify concentration polarization and thereby prolong non-equilibrium ionic states.  
515 Device optimization therefore requires the co-design of geometry, electrolyte  
516 environment and electrical protocol, because retention, switching amplitude and volatility  
517 emerge from their combined action.

### 518 **3.2 Ångström confinement and correlated ion states**

519 As nanofluidic channels approach molecular dimensions down to Ångström-scale  
520 slits only a few water molecules thick, ion transport can no longer be described as a  
521 weakly perturbed continuum.<sup>102</sup> Strong ion-surface interactions, partial dehydration,  
522 and enhanced ion-ion correlations create metastable ionic configurations whose  
523 rearrangement can be slow. As a result, conductance can depend on stimulus timing and  
524 bias history, yielding memory effects even in mechanically rigid, crystalline channels.

525 A first clear route to such memory was articulated through theory and molecular  
526 simulations of monolayer electrolytes confined in sub-nanometer slits.<sup>103,104</sup> In this  
527 regime, an applied electric field promotes the formation of correlated ionic clusters, while  
528 reversing the field then requires these structures to dissolve and reform, producing  
529 hysteretic, history-dependent conduction in an otherwise static channel. In silico,  
530 pairing such elements could even yield neuronal-like excitability and spontaneous voltage  
531 spiking, illustrating how confinement-enhanced correlations can be promoted from  
532 molecular self-assembly to dynamical primitives for computing.<sup>104</sup>

533 Building on this conceptual framework, experiments pushed Ångström-scale  
534 confinement toward device-level programmability by exploiting the same two-  
535 dimensional slit geometry with different wall chemistries (Figure 7e). In pristine MoS<sub>2</sub>  
536 channels, conductance could be potentiated by one voltage polarity and depressed by the  
537 opposite, yielding bipolar memristive updates reminiscent of bidirectional synaptic  
538 weight changes.<sup>104,105</sup> Activated-carbon channels, by contrast, more often showed  
539 unipolar and volatile memory, relaxing back toward a baseline after the stimulus is  
540 removed. Both the loop polarity and the memory lifetime could be tuned by  
541 confinement and electrochemistry, including channel height (sub-10 nm), salt conditions,  
542 and pH. A compact scaling argument relates the characteristic memory time to the  
543 diffusive transport time multiplied by a Dukhin-number factor that captures the strength  
544 of surface adsorption, making geometry a direct knob for programming ionic timescales  
545 (Figure 7f).<sup>105</sup>

546 Most recently, the same platform has been shown to access the full range of  
547



548 nanofluidic memristor loop styles.<sup>106</sup> By varying electrolyte composition, pH, driving  
 549 frequency, channel material and channel height, it was demonstrated that all four  
 550 canonical memristor types can emerge in two-dimensional nanochannels, including two  
 551 loop styles that had not previously been observed experimentally. A minimal model that  
 552 combines ion-ion interactions with surface charge and entrance depletion reproduced  
 553 these transitions and clarified how the same device family can be steered between volatile  
 554 and non-volatile regimes. In this programmable setting, synapse-inspired dynamics  
 555 such as short-term depression with recovery arise as a direct consequence of controlled

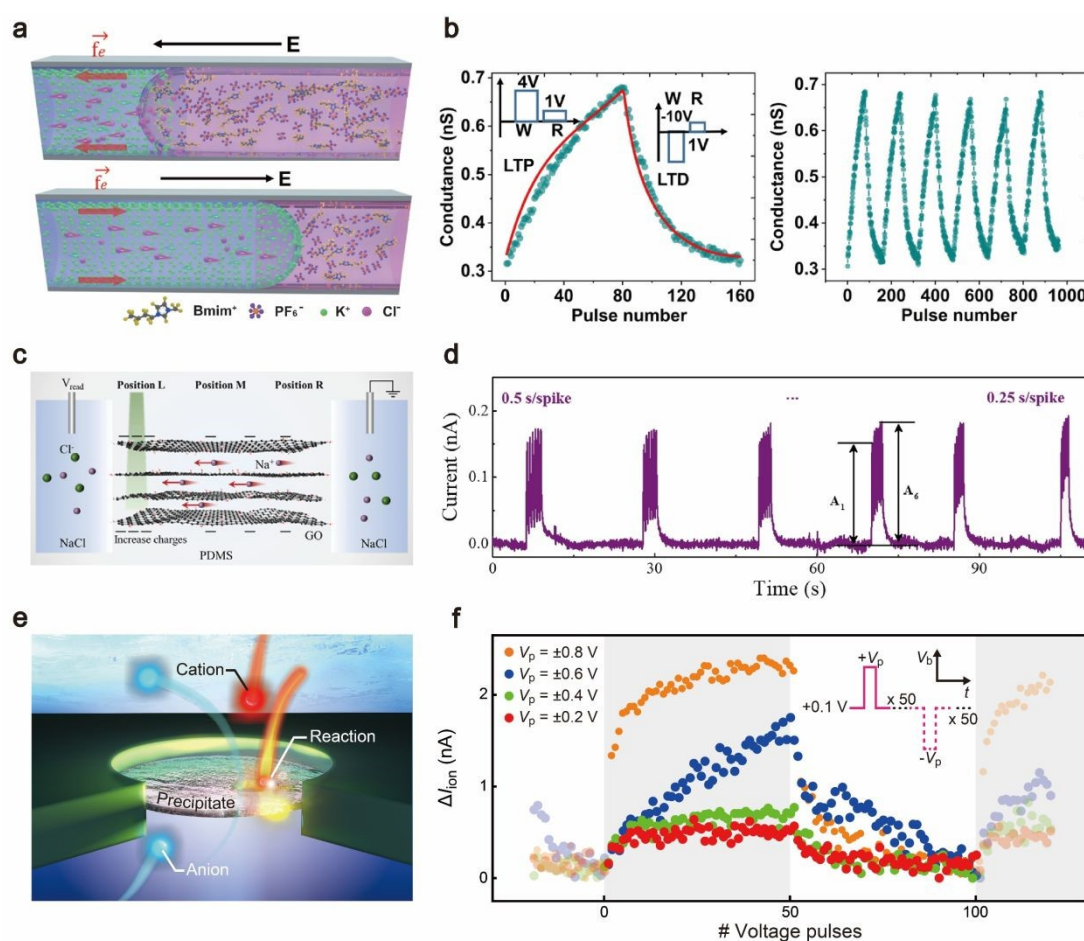


**Figure 8.** Stimulus modalities for programming hard nanochannels. **a-b**, An interfacial memristor formed by a nanochannel that bridges an aqueous KCl phase and an immiscible room-temperature ionic liquid (BmimPF6), where voltage-driven displacement of the liquid-liquid interface tunes ionic transport and supports analogue conductance updates. Adapted with permission from ref. 107. Copyright 2019 American Chemical Society. **c-d**, Optogenetics-inspired nanofluidic artificial dendrite based on PDMS-coated layered graphene oxide. Localized light illumination generates an internal potential difference that drives  $\text{Na}^+$  migration along lamellar nanochannels, producing position-addressable response currents and reconfigurable spiking. Adapted with permission from ref. 111. Copyright 2025 John Wiley and Sons. **e-f**, Chemically gated pores in which transmembrane bias controls in-pore precipitation/dissolution chemistry, enabling pulse-programmable conductance states. Adapted with permission from ref. 120. Copyright 2025 Creative Commons CC-BY-NC-ND.



556 ionic relaxation.<sup>106</sup>

557 These advances recast Ångström-scale slits as a chemically programmable substrate  
558 for ionic memory, where the internal state is encoded in correlated ion organization and  
559 interfacial kinetics rather than in simple double-layer charging. The ability to co-design  
560 polarity, volatility, and relaxation time through geometry and electrolyte chemistry  
561 provides a direct route from nanoscale physics to neuromorphic function, and suggests  
562 that arrays of atomic channels could serve as ultralow-power analogue elements for  
563 adaptive information processing.

564

### 565 **3.3 Electrohydrodynamic memristors in confined channels**

566 Another distinct mechanism for ionic memristors in hard nanofluidic systems  
567 involves fluid flow and moving interfaces. In these devices, memory resides not only  
568 in the ionic distribution but also in the physical position of a fluid boundary or meniscus  
569 that shifts under electrical bias. The operating principle typically relies on  
570 electroosmotic flow or electrowetting, whereby an applied voltage drives liquid to  
571 advance or recede within a channel, thereby modulating the conductive pathway.  
572 Hysteresis emerges when the interface position depends on the history of the applied  
573 voltage. For instance, a higher bias may displace the interface further, while upon  
574 voltage reduction or reversal, the interface may not immediately return to its initial  
575 position because of capillary forces or viscous dissipation. The resulting memristive  
576 response is governed by the fraction of the channel occupied by the conductive fluid  
577 relative to a nonconductive phase, which acts as the internal state variable.

578 A seminal example is the nanofluidic memristor based on an electrolyte-ionic liquid  
579 interface.<sup>107,108</sup> The device consisted of a nanochannel in PDMS connecting two  
580 reservoirs, with one filled with a KCl solution and the other with a hydrophobic ionic  
581 liquid immiscible with water (Figure 8a). At equilibrium, the two fluids meet at the  
582 center of the channel, forming a well-defined meniscus. Applying a voltage induces  
583 competition between electroosmotic flow and interfacial tension, with one polarity  
584 advancing the aqueous-ionic liquid interface and the opposite polarity retracting it. The  
585 large contrast in ionic conductivity between the ionic liquid and the aqueous phase causes  
586 the channel conductance to depend on their relative occupancy. At intermediate states,  
587 the channel behaves as a variable resistor composed of a high-conductivity electrolyte  
588 segment in series with a low-conductivity ionic liquid segment. The interface motion  
589 was hysteretic, with viscous drag and meniscus energy barriers, including contact-angle  
590 hysteresis at the walls, preventing immediate relaxation after voltage removal or reversal.  
591 Accordingly, voltage sweeps exhibited pinched hysteresis loops, and the device could be



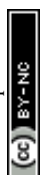
592 programmed into multiple conductance states using voltage pulses of different  
593 magnitudes (Figure 8b). The memristor showed excellent endurance and retention, as  
594 the negligible vapor pressure of the ionic liquid prevented drying or significant interfacial  
595 drift over time. In effect, the system behaves like a nanoscale electrical piston that  
596 drives a fluid boundary back and forth, with the piston position serving as the memory  
597 state.<sup>107,108</sup>

598 The hydrodynamic approach is appealing in that it leverages the inherently analog,  
599 continuum behavior of fluids. In principle, the meniscus position, and thus the device  
600 conductance, can assume a continuous range of values, enabling multilevel memory and  
601 gradual weight updates for neuromorphic computing. The approach embodies a trade-  
602 off between speed and retention: slow, inertial fluid motion limits switching speeds but  
603 enables nonvolatile memory by pinning the interface without power. This nonvolatility  
604 arises because, once displaced, the ionic liquid-aqueous interface remains pinned by  
605 capillary forces until a sufficiently large reverse bias is applied to overcome the pinning  
606 barrier. This is analogous to a mercury droplet in a capillary, which moves under  
607 pressure but remains pinned by surface tension until an opposing threshold is exceeded.  
608 Although fluid motion and interfacial deformation can dissipate energy, operation is often  
609 quasi-static, allowing the energy per switching event to remain low when distributed over  
610 time. Hydrodynamic memristors therefore occupy a unique regime in which mechanical  
611 and ionic degrees of freedom intersect.

### 613 3.4 Optical programming and readout

614 Light offers a particularly clean handle for programming nanofluidic memristors.  
615 Unlike electrical gating, which requires dedicated wiring and electrodes for each element,  
616 optical stimuli can be delivered remotely, patterned in space and multiplexed in time. In  
617 optically gated devices, photons act as write pulses that reshape the ionic state though  
618 generating photovoltages, redistributing surface charge, or imposing local  
619 thermal/chemical gradients, while the resulting ion current provides an immediate read.  
620 This sensory-computing coupling echoes optogenetics in biology, although the state  
621 variable is not a protein conformation but the evolving distribution of ions and hydration  
622 shells within nanometer confinement.

623 Niu et al.<sup>109</sup> demonstrated a minimalist route to optical control by embedding a  
624 semiconductor heterojunction into a single nanopore. Upon illumination, the junction  
625 generated an additional photovoltage (tens of millivolts under their conditions),  
626 effectively turning the nanopore into a self-biased ionic pump. Under steady electrical  
627 bias, the ion current increased under light and tracked optical on-off modulation with a



628 response time of about 50 ms, consistent with photocarriers creating an internal field that  
629 adds to, or subtracts from, the applied bias and therefore shifts the concentration-  
630 polarization state in and around the nanopore.<sup>109</sup>

631 Wang and colleagues<sup>110</sup> built an optically modulated nanofluidic ionic transistor  
632 using a metal-organic framework membrane grown within a porous anodic alumina  
633 template. The framework is intrinsically negatively charged, and illumination generates  
634 electron-hole pairs that transiently increase the negative surface charge of the MOF  
635 crystallites, drawing additional cations into the tortuous pores. This photoinduced ion  
636 accumulation produces excitatory post-synaptic current-like transients, paired-pulse  
637 facilitation, and a pulse-history-dependent transition from short-term to longer-lived  
638 plasticity, as the relaxation time for cation release competes with the optical pulse interval.  
639 By using trains and patterns of light spikes to tune synaptic weight, the device reproduced  
640 higher-level behaviors such as learning-experience, Pavlovian associative learning, and  
641 optical Morse-code encoding/decoding, illustrating how optical addressability can be  
642 pushed beyond switching toward information processing within a single ionic element.<sup>110</sup>

643 An optogenetics-inspired design pushed optical addressability from a single pore to  
644 a dendrite-like nanofluidic element by embedding layered graphene oxide (GO)  
645 nanochannels in an elastomer (Figure 8c).<sup>111</sup> Here, light creates an electric potential  
646 difference between illuminated and dark regions of the GO, driving directional Na<sup>+</sup>  
647 migration and producing pronounced ionic photocurrents. Because the optical input can  
648 be applied at different positions and in multiple spots, the device naturally supports  
649 distributed integration. It reproduced spatial summation with both sublinear and  
650 superlinear regimes, and it expressed temporal plasticity under trains of light spikes,  
651 including paired-pulse facilitation as well as spike-duration- and spike-rate-dependent  
652 conductance modulation. By combining spatiotemporal optical stimuli with ionic  
653 readout, the authors further demonstrated neuromorphic perception and a reflex-like  
654 output in a soft robotic actuator, emphasizing that optical control can move nanofluidic  
655 memristors beyond two-terminal switching toward computation within a single fluidic  
656 element (Figure 8d).<sup>111</sup>

657 Mechanistic insight from atomically thin membranes provides a complementary  
658 perspective on how optical write operations might be converted into durable ionic  
659 memory. Molecular dynamics simulations of a subnanoporous two-dimensional  
660 membrane showed that synaptic-like plasticity can arise from competitive bicationic  
661 transport, where strongly adsorbed Na<sup>+</sup> transiently blocked permeation pathways that  
662 otherwise conducted K<sup>+</sup>, and voltage spikes desorbed Na<sup>+</sup> to potentiate permeability.<sup>111</sup>  
663 Because adsorption and desorption introduce distinct time constants, the same structure



664 can, in principle, interpolate between volatile and longer-lived states by tuning ion species,  
665 concentration, and stimulus waveform. Notably, the estimated energy cost per  
666 conductance update was in the attojoule range, highlighting why optical actuation,  
667 capable of delivering localized write pulses without parasitic leakage, may be especially  
668 attractive for scaling to large arrays. These studies suggest a general design rule for  
669 optical nanofluidic memristors: use light to impose a controllable internal photoelectric  
670 bias or a local thermal perturbation<sup>113</sup> that steers ion occupancy in confined junctions, and  
671 exploit the ensuing relaxation dynamics to encode computation in the ionic state.

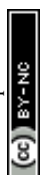
672

### 673 **3.5 In-pore chemistry and reaction-driven memory**

674 In-pore chemistry offers a direct route to ionic memory, where the internal state is  
675 encoded in the local chemical composition and phase within the confined pore volume.  
676 Under transmembrane bias, electromigration and concentration polarization bring  
677 reactants into contact and drive reversible transformations, most prominently  
678 precipitation and dissolution, that open or obstruct the conduction pathway. Because  
679 the state evolves through reaction-diffusion kinetics rather than instantaneous  
680 electrostatics, the characteristic response time and retention can be tuned over orders of  
681 magnitude by pH, reactant concentration, multivalency, temperature, the stimulus  
682 waveform, and the confinement geometry. In practice, these levers allow the same  
683 physical platform to be pushed towards volatile short-term plasticity or long-lived, quasi-  
684 nonvolatile memory.

685 The origins of this concept can be traced to early observations of current instabilities  
686 caused by nanoconfined reactions. When two solutions mix within a nanopore, a  
687 transient precipitate was shown to repeatedly form and clear, producing oscillatory ionic  
688 currents.<sup>113</sup> The resulting nanoprecipitation in a nanopipette tip was demonstrated to be  
689 actively created and eliminated by switching the voltage polarity, enabling controlled  
690 blockage and recovery.<sup>115</sup> The earliest stages of nucleation and crystal growth through  
691 transient current blockades were tracked using a nanopipette platform.<sup>116</sup> Similar  
692 features were also observed from slow Ca<sup>2+</sup> binding to charged pore walls.<sup>117</sup> These  
693 studies established that field-driven transport creates a reactive mixing zone whose  
694 evolving chemistry becomes the memory variable.

695 Liu et al.<sup>118</sup> demonstrated a complementary regime in conical nanopores, where  
696 reversible CaHPO<sub>4</sub> nanoprecipitation at the pore tip generates pronounced pinched  
697 hysteresis loops. Here, the memristive characteristics are set by precipitation and  
698 dissolution kinetics and can be tuned by CaHPO<sub>4</sub> concentration, voltage amplitude, and  
699 scan rate. Under pulsed stimulation, the conductance relaxes back once the stimulus is



700 removed, yet remains robustly resettable, resembling short-term plasticity in biological  
701 synapses. This chemistry-driven volatility is attractive for temporal filtering and  
702 adaptive gain control, where forgetting is a feature rather than a limitation.<sup>118</sup>

703 Cho et al.<sup>118</sup> moved beyond hysteresis in the time-averaged conductance by encoding  
704 memory in the frequency of ion-current oscillations. In their conical nanopore, dynamic  
705 formation and removal of nanoprecipitates produce stochastic switching between high-  
706 and low-conductance states. The oscillation statistics depend on the direction of the  
707 voltage scan and on prior stimuli, appearing as a history-dependent open-state probability.  
708 Under programmed pulse trains, the device exhibits synaptic-like long-term potentiation  
709 and depression, consistent with delayed precipitate formation and clearing, together with  
710 slower drift in the effective space charge. A reduced description in which precipitation  
711 is limited by the cation arrival rate captures the emergence of oscillations and their bias-  
712 history dependence.<sup>119</sup>

713 A distinct solid-state implementation that spatially separates anionic and cationic  
714 reactants across the membrane.<sup>120-122</sup> One reservoir contains phosphate-buffered saline,  
715 whereas the opposite side supplies mobile cations from chloride salts (Figure 8e). The  
716 applied voltage drives these cations into the nanopore, where they encounter phosphate  
717 and reversibly form metal-phosphate precipitates that close the pore under one polarity  
718 and dissolve under the other. This voltage-gated in-pore chemistry yields extreme  
719 rectification and enables memristive switching at sub-nanowatt power (Figure 8f).  
720 Because the gate is a reaction product, the dynamic response is, in principle, engineerable:  
721 pH controls phosphate speciation and solubility, reactant concentrations set  
722 supersaturation and nucleation rates, and the cation identity and temperature tune  
723 dissolution kinetics. These parameters offer a practical route to tune the balance  
724 between rapid, volatile switching and slowly relaxing states with extended retention.<sup>45,119</sup>

725 In-pore chemistry memristors expand nanofluidic memory beyond purely  
726 electrostatic hysteresis. By co-designing confinement with reaction kinetics, they  
727 provide a chemically programmable memory kernel whose volatility, retention and  
728 learning dynamics can be tuned using standard chemical control parameters.

729

#### 730 **4. Hybrid architectures: rigid scaffolds with soft ionic states**

731 We now turn to hybrid architectures, in which rigid microfabricated scaffolds are  
732 deliberately paired with soft ionic elements. Their appeal is a clear functional split: the  
733 hard framework delivers geometric precision and addressability, while the soft phase  
734 introduces slow internal state variables, chemical selectivity and analogue adaptability.

735 Soft-hard hybrid nanofluidic systems combine rigid nanostructures, such as solid-



736 state nanopores or nanochannels, with soft ionic components including polymers, gels,  
737 biomolecules, and fluids. Such hybrid architectures are designed to balance scalability,  
738 reproducibility, and integration offered by hard materials with the adaptive, history-  
739 dependent ionic dynamics characteristic of soft matter. From a neuromorphic  
740 standpoint, hybrid systems are especially attractive as they reflect the multiscale  
741 architecture of biological neural systems, where rigid structural elements coexist with soft,  
742 dynamically reconfigurable components. In artificial systems, this division of labor  
743 enables a fixed, manufacturable geometry while preserving fluid, reconfigurable degrees  
744 of freedom that underpin learning and memory.

745 In hybrid nanofluidic memristors, a solid-state scaffold fixes the transport geometry,  
746 providing well-defined channel dimensions, alignment, and connectivity. Such  
747 scaffolds can be fabricated using top-down nanofabrication methods compatible with  
748 wafer-scale processing, enabling high device uniformity and large-area array integration.  
749 Within this rigid framework, soft ionic components like ionic gels and biomolecules  
750 introduce internal state variables that evolve in response to electrical, mechanical, or  
751 chemical stimulation. Examples include polymer brushes grafted inside nanopores,  
752 ionic gels filling nanochannels, or biomolecules tethered to pore walls. These soft  
753 components modulate the ionic pathway through swelling, ion binding, conformational  
754 changes, or phase transitions while preserving their macroscopic geometries. As a result,  
755 device conductance becomes history-dependent not through permanent changes in  
756 channel geometry, but rather through memory encoded in the ionic microenvironment.

757 Soft-hard hybrid systems offer a key advantage by decoupling mechanical stability  
758 from functional plasticity. In purely soft systems, memory formation is often  
759 inseparable from mechanical deformation, which can lead to drift, fatigue, and limited  
760 reproducibility over extended operation. By contrast, purely hard systems typically rely  
761 on ionic redistribution or chemical transformations to achieve plasticity, which can  
762 restrict the diversity and adaptability of functional responses. Hybrid architectures  
763 circumvent both limitations. The rigid scaffold absorbs mechanical stress and preserves  
764 long-term structural integrity, while the soft component remains free to reorganize  
765 internally and encode memory. From a neuromorphic perspective, this feature can be  
766 similar to that in biology, where relatively stable axonal and dendritic scaffolds coexist  
767 with synapses whose efficacy is continually re-tuned by molecular reorganization. Such  
768 decoupling is particularly advantageous for long-term operation and training stability in  
769 neuromorphic hardware, as the learning element can undergo repeated adaptation without  
770 degrading the underlying device architecture.

771 Hybrid systems also naturally exhibit multiple memory timescales, a defining



772 feature of biological cognition. Rapid ionic redistribution within the liquid phase gives  
773 rise to short-term plasticity, whereas slower processes, including ion binding, polymer  
774 relaxation, and reversible chemical reactions, govern long-term memory retention.  
775 Because these processes occur within a confined geometry defined by the solid scaffold,  
776 they can be precisely tuned through design parameters such as pore diameter, pore length,  
777 polymer density, grafting length, or electrolyte composition. This tunability potentially  
778 enables hybrid devices to emulate a broad spectrum of synaptic behaviors, ranging from  
779 volatile, stimulus-dependent responses to stable, non-volatile memory states. In  
780 neuromorphic computing, such multiscale plasticity is essential for implementing  
781 learning rules that require both transient adaptation and persistent weight updates,  
782 analogous to short-term facilitation and long-term potentiation in biological synapses.

783 In this section, we examine several representative classes of soft-hard hybrid  
784 nanofluidic systems, including ionic gel-filled nanopores, polymer brush-functionalized  
785 nanochannels, and other hybrid combinations. We emphasize how the interplay  
786 between mechanical rigidity and softness gives rise to memristive functionality, and how  
787 such designs address key challenges such as device stability, reproducibility, and  
788 integration density.



789

**Table 3.** Soft/hard hybrid systems with ionic memory.

System class	Material / fluidic system	Size	Mechanism	Stimulus class	Switching speed	Retention time	Energy consump.
Droplet/ microchannel <sup>54</sup>	Liquid-liquid interface microdroplet memristor in a microfluidic chip	1.5 mm long droplet	Voltage-driven droplet penetration into a microwell blocking/unblocking ion transport	Spike trains (10 V, 0.1 s); temperature used to modulate phase behavior	0.025–2.5 Hz	~200 s	N/A
Ionic gel/ microchannel <sup>124</sup>	PDMS microchannels hosting bipolar polyelectrolyte gels, 10 mM KCl	Microchannel ~2 mm x ~500 $\mu$ m; P- and N-gel lengths ~1 mm each	Voltage-derived changes in depletion/accumulation zones of bipolar polyelectrolyte gels	Pulse trains (1 V, 4 s)	~0.01 Hz	200–4,000 s	N/A
Polymer blush/ nanopore <sup>130</sup>	Conical polyimide nanopore with dual-responsive PNIPAAm-co-AAc polymer brushes, 0.1 M KCl	Tip size ~25 nm; base opening ~1.2–1.5 $\mu$ m	Stimuli-responsive conformation/charge state modulation of polymer brushes in channel	Environmental pH (3.6–9.4) and temperature; electrical I–V probing ( $\pm$ 500 mV)	pH-induced rectification changes typically in minutes	N/A	N/A
Polymer brush/ nanopipette <sup>135</sup>	Glass nanopipette modified with polyimidazolium brush; 10 mM NaCl	Tip size ~150 nm	Polyelectrolyte-confined ions undergoing strong ion-polymer interactions and slow reorganization	Environmental pH (3.6–9.4) and temperature; electrical I–V probing ( $\pm$ 500 mV)	pH-induced rectification changes typically in minutes	~500 ms	~1 pJ per pulse
Ionic liquid/ micropipette <sup>136</sup>	PimB-modified glass micropipette interfacing $K_3Fe(CN)_6$ and KCl	Tip size ~3 $\mu$ m	Adsorption/desorption of ferricyanide switching surface charge and ionic selectivity/EOF in nanochannels	DC voltage 3 V	Oscillatory spiking: period ~4.02 s (~0.31 Hz); frequency tunable up to ~18.7 Hz	Volatile/self-reset	N/A
Liposome/ nanopore <sup>141</sup>	$SiN_x$ solid-state nanopore gated by nanoparticles/liposomes	Nanopore size 115 nm, liposome size hundreds nm	Nanoparticle trapping/release inside a nanopore changing effective aperture/resistance	Opening response ~1.2 ms; closing response down to ~0.3 s	N/A	~10 nJ	N/A



## 790 4.1 Gel-filled nanopores and ionogels

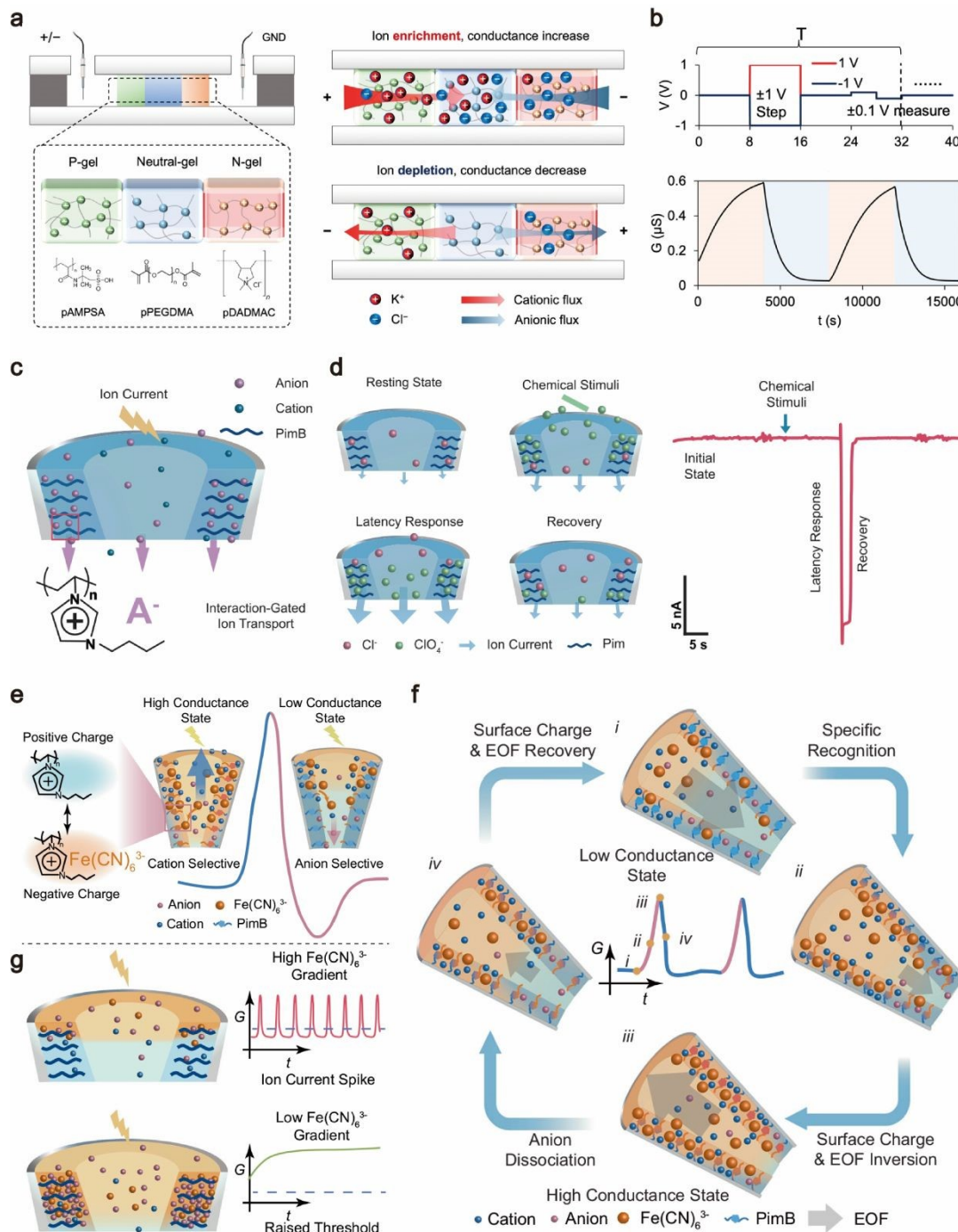
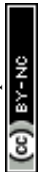


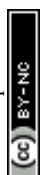
**Figure 9.** Soft/hard hybrid fluidic systems carrying ionic memory into device-scale functions. **a**, Architecture of an iontronic memristor in which a three-layer bipolar polyelectrolyte-gel stack. **b**, Volatile-to-stable conductance dynamics under step programming and low-amplitude readout. Adapted with permission from ref. 124. Copyright 2024 Creative Commons CC-BY 4.0. **c-d**, A polyelectrolyte-confined fluidic memristor converting molecular/ionic interactions into a history-dependent ionic conductance. Adapted with permission from ref. 135. Copyright 2023 American Association for the Advancement of Science. **e-f**, Mechanistic cycle for autonomous spiking in a nanofluidic oscillating neuron. **g**, Representative ion-current spike trains controlled by chemical gradients, showing repetitive firing and threshold modulation. Adapted with permission from ref. 136. Copyright 2025 Creative Commons CC-BY-NC.



791 One straightforward hybrid strategy involves filling or coating a solid-state nanopore  
792 or nanochannel with an ionic gel, such as a crosslinked polyelectrolyte or polymer  
793 electrolyte. In this configuration, the solid substrate, typically silicon, glass, or a  
794 mechanically robust polymer such as polyethylene terephthalate (PET), defines the  
795 channel geometry and ensures mechanical integrity, while the embedded ionic gel  
796 provides a continuous, non-volatile ionic medium whose internal dynamics can encode  
797 memory. The gels can be patterned at nanometer length scales, for instance, through  
798 localized photopolymerization within confined cavities, making them compatible with  
799 dense integration. They also mitigate practical issues associated with liquid electrolytes,  
800 including evaporation, nanobubble formation, and fluid displacement. In effect, the gel  
801 functions as a soft, adaptive core confined within a rigid nanofluidic shell, combining  
802 structural stability with dynamic ionic functionality.

803 A representative example is a track-etched PET membrane containing a conical  
804 nanopore that is filled with a salt-doped polyacrylamide hydrogel. In this hybrid structure,  
805 the conical nanopore provides a rigid, well-defined transport geometry, while the  
806 hydrogel introduces a soft, ionically active medium within the pore. Early work  
807 demonstrated that ionic current rectification in such conical nanopores is preserved after  
808 gel filling and that the gel can actively modulate the ionic response.<sup>123</sup> Extending this  
809 concept to memristive behavior becomes possible when the gel is made stimulus-  
810 responsive. For instance, if the gel contains charged functional groups, a strong electric  
811 field can locally deplete counterions and drive electro-osmotic water transport, leading to  
812 partial gel contraction. Upon reduction or reversal of the field, the gel does not  
813 instantaneously re-swell because of its viscoelastic relaxation, leaving the pore transiently  
814 more open or more obstructed than its initial state. This delayed swelling-deswelling  
815 cycle introduces a history dependence in the conductance, giving rise to hysteresis in the  
816 current-voltage characteristics. In this way, the internal relaxation dynamics in the soft  
817 matrix act as the memory variable, while the rigid nanopore confines and stabilizes the  
818 overall device geometry.

819 A more sophisticated realization of this concept is embodied in cascade hetero-gated  
820 gel systems for ionic modulation (Figure 9a).<sup>123</sup> This approach envisions stacking or  
821 patterning multiple gels with distinct ionic properties within a single nanofluidic channel.  
822 Each gel layer functions as a history-dependent ionic gate, whose conductance evolves  
823 according to its own internal dynamics. For example, one layer may slowly accumulate  
824 protons and become more conductive under repeated stimulation, whereas another unit  
825 may preferentially expel ions or undergo partial deswelling, thereby reducing  
826 conductance. Arranged in series, therefore, these layers offer dynamically coupled



827 barriers to ion transport, giving rise to complex hysteresis and rich temporal responses  
828 (Figure 9b).<sup>124</sup> By confining the gels within a rigid channel, the overall geometry  
829 remains fixed, so that gel reconfiguration affects ionic pathways rather than deformation.  
830 From a neuromorphic perspective, such cascade architectures resemble multilayer  
831 synapses, in which distinct molecular processes operating on different time constants  
832 jointly regulate signal transmission and plasticity.

833 Ionic compositions can be engineered to tailor the dynamic ion transport  
834 characteristics. In this context, polyelectrolyte gels confined within nanopores have  
835 been explicitly highlighted as a promising platform for ionic memristors.<sup>125</sup> Their  
836 intrinsic nonlinearity, arising from ion-polymer interactions and swelling dynamics,  
837 naturally lends itself to memristive behavior. Furthermore, because the gels can host  
838 high concentrations of mobile charge, they enable relatively large ionic currents at low  
839 bias, easing impedance matching with electronic circuits compared with highly dilute  
840 liquid electrolytes. Experimental support for this concept comes from work<sup>124</sup>  
841 demonstrating that filling a micropipette tip with a fixed-charge polyelectrolyte gel  
842 produced inverted ionic current rectification and could mimic synaptic neurotransmitter  
843 release. Although this system was initially explored as a chemical delivery probe, the  
844 underlying mechanism could be extended to memristive operation. In particular, if the  
845 gel were engineered to retain ionic composition or charge distribution after stimulation,  
846 for example, through multicomponent ion doping or slow relaxation kinetics, the same  
847 architecture could encode memory in its transport response.<sup>126</sup>

848 Filling nanofluidic channels with gels also offers clear advantages for scalable  
849 integration. Arrays of nanopores can be fabricated on a single chip and subsequently  
850 filled in a single step by spin-coating or vacuum infiltration of a pre-gel solution, followed  
851 by curing. This approach is substantially simpler than individually addressing each pore  
852 with microfluidic plumbing and effectively solidifies the fluidic architecture into a  
853 mechanically robust device. The principal trade-off is a reduction in ionic mobility,  
854 since diffusion coefficients in gels are typically one to several orders of magnitude lower  
855 than in free solution, depending on polymer density and crosslinking.<sup>127</sup> However, for  
856 many neuromorphic computing tasks, where integration, memory retention, and analog  
857 weight evolution are more critical, such moderate operating speeds would be  
858 acceptable.<sup>128</sup>

859 Ionic gel-filled nanopores represent a compromise between the functional richness  
860 of liquid-based systems and the reliability of solid-state devices. They can reproduce  
861 key behaviors of purely fluidic architectures, such as threshold ion depletion and  
862 interfacial wetting transitions, while offering substantially improved mechanical stability



863 and compatibility with large-scale integration. Challenges remain, including achieving  
864 homogeneous gel filling in ultrasmall pores, avoiding bubbles or void formation, and  
865 precisely controlling gel chemistry at the nanoscale. Nonetheless, continued advances  
866 in nanofabrication, polymer synthesis, and in situ curing strategies are likely to mitigate  
867 these limitations.

868

## 869 **4.2 Polymer-brush nanochannels**

870 A particularly elegant hybrid approach involves incorporating polymer brushes,  
871 consisting of densely tethered polymer chains, on channel walls. Instead of filling the  
872 entire space, a polymer brush coating on the surface enables dynamic tuning of the  
873 effective size, charge, and ionic selectivity.<sup>129,130</sup> Furthermore, polymer brushes are  
874 known to undergo conformational changes depending on the ionic environment, solvent  
875 quality, and pH.<sup>131</sup> They can also trap and release counterions in a hysteretic manner,  
876 for example when the brush contains multiple charge states or segments with differing  
877 ionic affinities.<sup>132,133</sup>

878 A notable example is the polyelectrolyte brush-confined ionic memristor,<sup>134,135</sup>  
879 consisting of a grafted layer of polyimidazolium chains inside a glass nanopipette (Figure  
880 9c). These brushes carry positive charges along their backbone, attracting anions.  
881 When a voltage was applied, the brush region could load up with anions, creating a high  
882 conductance state. Upon bias reversal, delayed anion release from the brush preserved  
883 elevated conductance, resulting in memristive hysteresis. In addition to synaptic  
884 functions, the device uniquely enabled chemical-electrical signal transduction, potentially  
885 allowing an artificial chemosensitive synapse for converting a chemical input into an  
886 electrical memristive signal (Figure 9d-g). This example highlights a broader strength  
887 of brush-filled nanochannels through their rich chemical tunability. Polymer brushes  
888 can be engineered with functional groups that selectively respond to specific  
889 biomolecules or neurotransmitters.<sup>136</sup> For example, boronic acid-functionalized  
890 brushes can reversibly bind glucose, with transient concentration changes modulating  
891 conductance and imprinting a temporary chemical memory. Such chemically induced  
892 plasticity opens a route to devices that adapt in response to chemical signals or rewards,  
893 analogous to neuromodulation in biological neural systems, where neurotransmitters such  
894 as dopamine dynamically regulate synaptic strength.<sup>135,137</sup>

895 Another advantage of polymer brushes is their ability to respond across multiple  
896 timescales. At the molecular level, brushes can polarize extremely rapidly under local  
897 electric fields, as ions redistribute around individual polymer chains on nanosecond  
898 timescales. Concurrently, collective processes such as brush collapse or swelling unfold



899 much more slowly, often over seconds. As a result, a brush-filled nanopore can exhibit  
900 both fast, transient changes in ionic current and slower, adaptive drifts in conductance.  
901 This intrinsic separation of timescales allows a single device to capture features of both  
902 short-term and long-term plasticity, integrating rapid responsiveness with persistent  
903 memory within the same physical element.<sup>137</sup>

904 In such hybrid architectures, the inorganic scaffold provides a mechanically robust  
905 framework with well-defined geometry, enabling a degree of device-to-device uniformity,  
906 while the polymer brush supplies the nonlinear ionic dynamics responsible for memory.  
907 Because the brushes are covalently tethered to the surface, they remain spatially confined  
908 and do not migrate or leach as free polymers might, leading to improved cycling  
909 stability.<sup>133</sup>

910 Polymer brush-filled nanochannels represent a rational hybrid design that merges  
911 the predictability of engineered surfaces with the adaptability of soft matter. They have  
912 enabled key advances, including chemical-to-electrical synaptic transduction, linking  
913 ionic memristors to chemical neuromodulation. By tuning brush chemistry and  
914 architecture such as charge type, grafting density, and chain length, the timescale and  
915 analog range of memristive behavior can be precisely controlled, with trade-offs between  
916 retention and response speed. At the nanoscale, polymer brushes serve as ionically  
917 active layers that endow rigid channels with memory and selectivity, where the solid  
918 scaffold provides mechanical stability and electrical interfacing, while the soft brush  
919 supplies ionic plasticity and chemical functionality essential for neuromorphic devices.

920

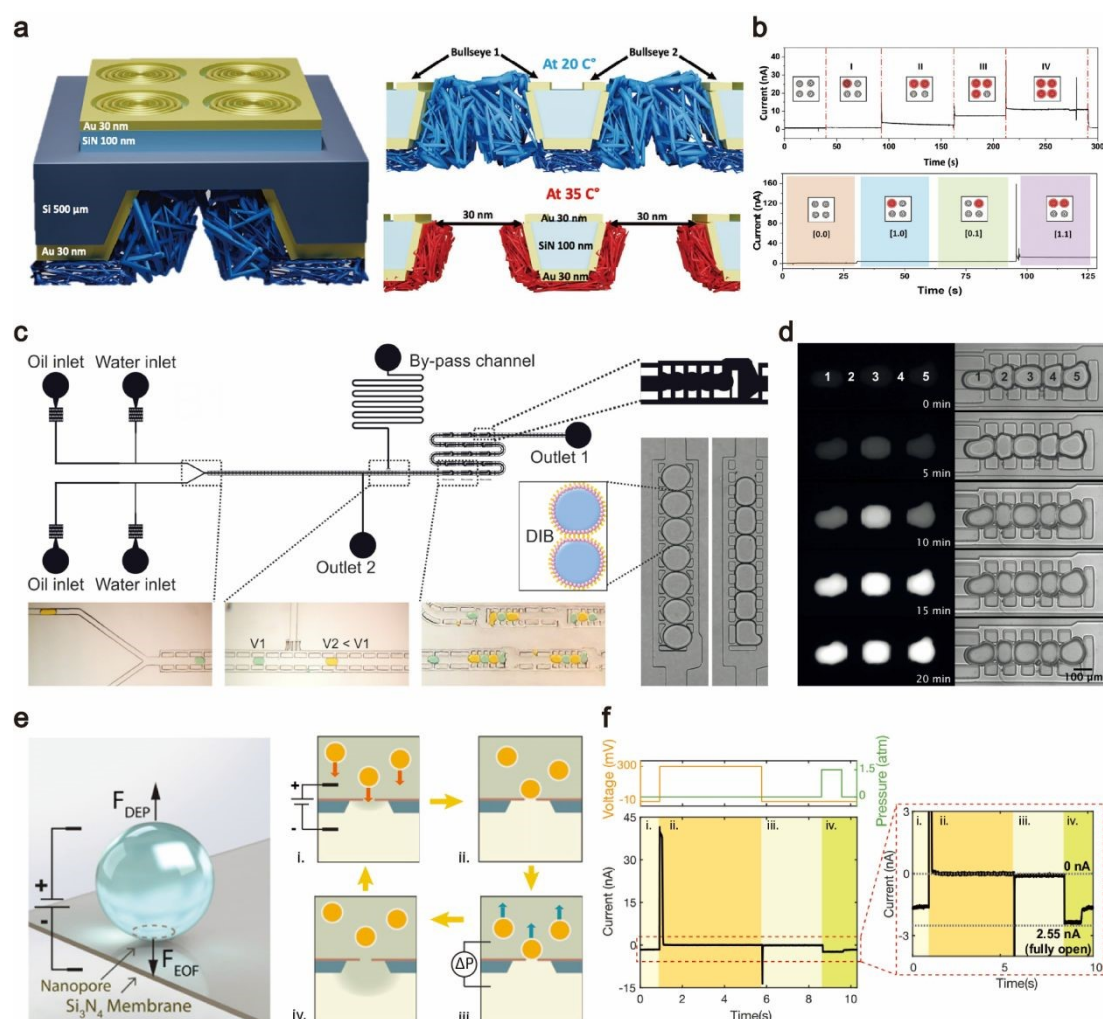
### 921 **4.3 Stimuli-responsive polymer-filled nanopores**

922 In general, the more manufacturable and dense the scaffold becomes, the harder it is  
923 to deliver a stimulus with the spatial precision and speed needed for truly addressable  
924 switching. A neat way around this is to move the active degree of freedom into a  
925 polymer inside the channel and trigger it remotely. In a recent thermoplasmonic  
926 design,<sup>113</sup> poly(N-isopropylacrylamide) brushes on the backside of a solid-state nanopore  
927 act as a temperature-responsive gate, swollen below the critical solution temperature to  
928 block ion passage, but collapsing when local heating pushes the pore above the transition,  
929 reopening the channel (Figure 10a). What makes the approach feel distinctly nano-  
930 engineered is how the stimulus is delivered: a gold bullseye resonator concentrates the  
931 light illumination onto the nanopore aperture, producing rapid, reproducible temperature  
932 excursions and, in turn, robust ionic switching with On/Off ratios up to around 60 over  
933 repeated cycles. Beyond proving the principle, the kinetics and addressability start to  
934 look device-relevant, where rise/fall times of a few milliseconds were achieved,



935 approaching the kilohertz regime of the conductance switching operation. Because the  
936 laser spot can be diffraction-limited to below  $1\ \mu\text{m}$ , individual pores in an array can be  
937 selected and orchestrated into simple current-based logic (Figure 10b), turning a polymer-  
938 filled nanochannel from a single switch into an optically programmable ionic circuit  
939 element.<sup>113</sup>

940

941 **4.4 Droplet-on-chip systems**

**Figure 10. Programmable gating at the soft-hard interface.** **a**, Thermoplasmonic optical gating of polymer-functionalized nanopores. A gold bullseye concentrates light illumination to locally heat PNIPAM above its critical solution temperature, selectively switching pores within an array with micrometer-scale addressability. Adapted with permission from ref. 113. Copyright 2025 Creative Commons CCBY-NC-ND 4.0. **b**, A passive microfluidic shift-register architecture positions and stores trains of lipid-stabilized water-in-oil droplets. Adapted with permission from ref. 138. Copyright 2015 Creative Commons CC BY 4.0. Droplet contact self-assembles droplet-interface bilayers, enabling automated arrays for multiplexed assays. **c**, Nanoparticle-blockage-mediated nanopore gating: rigid or soft nanoparticles are driven to a silicon nitride nanopore entrance to reversibly close the conduit in a ball-and-chain-like manner; small voltage or pressure stimuli yield millisecond response and complete closing. Adapted with permission from ref. 141. Copyright 2022 Creative Commons CC BY-NC-ND.



942 Another hybrid strategy integrates droplet interface bilayers into solid microfluidic or  
943 electronic frameworks (Figure 10c-d). In this approach, aqueous droplets are positioned  
944 in microfabricated wells on a chip, where lipid bilayers form reproducibly between  
945 adjacent droplets.<sup>138</sup> The solid substrate supplies electrodes, fluidic confinement, and  
946 addressing infrastructure, while the soft bilayers host the ionic processes responsible for  
947 computation.<sup>55</sup> By arranging multiple droplet pairs into patterned networks, it becomes  
948 possible to construct hybrid wet neural circuits that remain physically robust and  
949 electrically addressable. Early demonstrations have used techniques such as  
950 microdroplet printing to generate arrays of droplet interface bilayers with reasonable  
951 reproducibility.<sup>139</sup> A central challenge remains long-term stability, as bilayers are prone  
952 to rupture or drift over time, including partial gelation of droplets or polymer  
953 encapsulation have shown promise in mitigating these issues. If such stabilization can  
954 be achieved reliably, this architecture could enable large-scale arrays of memristive  
955 synapses on a single chip, with each droplet pair functioning as an individual, addressable  
956 synaptic element.

#### 957 958 **4.5 Nanoparticle-trapped nanopores**

959 Another hybrid strategy involves embedding nanoparticles or nanoscale inclusions  
960 within fluidic channels to introduce field-responsive internal degrees of freedom. For  
961 instance, in a conical nanopore, a confined nanoparticle or soft inclusion, such as a protein  
962 aggregate or nanoscale droplet, can deform, or reconfigure under an applied bias, thereby  
963 modulating ionic transport. It was demonstrated that introducing SiO<sub>2</sub> nanoparticles  
964 into a conical nanopore led to elastic deformation-mediated memristive hysteresis, arising  
965 from the coupled motion of the particle and the surrounding ionic flow.<sup>140</sup> Although the  
966 nanoparticle itself may be mechanically rigid, its mobility within the fluid effectively  
967 creates a composite system in which a hard scaffold hosts a dynamically reconfigurable  
968 internal phase. This illustrates how embedding responsive nanoscale objects within  
969 otherwise rigid nanofluidic channels provides an additional route to memristive behavior,  
970 by coupling ionic transport to the history-dependent dynamics of an internal phase.

971 A deformable nanoscale vesicle can function as a plug that couples a nanopore  
972 conductance with memory. Yazbeck et al.<sup>138</sup> demonstrated that liposomes driven into a  
973 solid-state pore will irreversibly block ionic flow until a stimulus removes them (Figure  
974 10e). Under a modest electric field, a charged liposome is electrophoretically sucked  
975 into the pore and elastically deforms to seal it, achieving near-100% current blockade  
976 (Figure 10f). Noticeably, the occlusion remains even after the voltage is turned off,  
977 enabling a nonvolatile memory effect, because the soft vesicle wedges in place rather than



978 diffusing away. A brief pressure pulse can eject the vesicle, reopening the pore, which  
979 then persists until the next voltage stimulus. This nanoparticle-blockage gating is highly  
980 repeatable and tunable, effectively emulating a voltage-controlled ionic switch with  
981 volatile vs. nonvolatile memory determined by its softness. The key is that the inherent  
982 flexibility and surface adhesion give the system a built-in memory of its last blocked or  
983 unblocked state.<sup>141</sup>

984

#### 985 **4.6 Bio-hybrid systems**

986 Perhaps the most fascinating hybrids involve actual biological components  
987 integrated with artificial ones. An example is growing living neurons on a solid-state  
988 ionic device so that they form a closed-loop hybrid network. The ionic memristor might  
989 receive neurotransmitter from the neuron and feedback an ionic current that stimulates  
990 the neuron, making a neuron-artificial-synapse hybrid. Early work has interfaced  
991 neurons with iontronic devices where the device can release ions like  $K^+$  to trigger neural  
992 signals.<sup>126</sup> As we refine these interfaces, we may effectively bolt an artificial memristor  
993 in place of a missing synapse in a neural circuit, a true hard/soft hybrid synapse.

994

#### 995 **4.7 Summary of hybrid strategies**

996 Soft materials, particularly droplet interface bilayers and lipid membranes, offer  
997 exquisite biomimicry and dynamic behavior but are often fragile and difficult to scale.  
998 Hard materials, such as conical nanopores etched in silicon or polymer substrates, afford  
999 integration and reproducibility but can struggle to encode complex ionic histories.<sup>142</sup> To  
1000 bridge this divide, researchers are increasingly turning to hybrid systems, combinations  
1001 of soft ionic elements embedded within rigid scaffolds, that blend the best of both  
1002 approaches. This section illustrates the emerging strategy, highlighting devices where  
1003 ionic gels, polymer brushes, or embedded nanoparticles introduce memory functions  
1004 within hard geometries. These designs leverage multi-timescale ionic dynamics,  
1005 chemical specificity, and tunable conductance, while maintaining the mechanical  
1006 integrity and addressability needed for circuit integration. The interplay of materials in  
1007 such hybrids enables rich functionality: polymer brushes permit chemical learning, ionic  
1008 gels stabilize device geometry while encoding plasticity, and embedded particles offer  
1009 new routes to responsiveness.

1010 Overall, these hybrid architectures suggest a design paradigm where complexity is  
1011 compositional. Rather than seeking a single material solution, engineers are building  
1012 layered systems that mimic biological synapses as mechanically stable, yet chemically  
1013 and electrically dynamic. This modular approach is paving the way for scalable



1014 iontronic platforms that retain the nuance of soft matter while embracing the precision of  
1015 microfabrication. As the field advances, these hybrids are poised not just to supplement  
1016 but to define future nanofluidic computing systems, embodying a pragmatic, multifaceted  
1017 strategy for combining softness with scale.

1018

## 1019 **5. From devices to ionic circuits**

1020 This section makes the system-level progression explicit, moving from single  
1021 memristive junctions to coupled logic elements and then to small iontronic networks so  
1022 the boundary between device physics and circuit-level function remains clear. Connecting  
1023 multiple nanofluidic memristors into circuits is a necessary step beyond single-device  
1024 phenomena, because networked ionic memory elements can display collective dynamics  
1025 and computational capability that are not accessible in isolated devices.

1026 Beyond digital logic, ion-driven circuits are being explored in which coordinated  
1027 ionic dynamics naturally emerge. Conical nanopore memristors integrated into  
1028 nonlinear oscillator circuits have been shown to exhibit alternating chaotic and periodic  
1029 oscillations reminiscent of neural network dynamics (Figure 11a).<sup>143</sup> Coupling three  
1030 such ionic conductors demonstrated purely ionic XOR and NAND logic gates to a neural  
1031 network,<sup>94,101</sup> and thus the potential to realize a complete set of logic operations using  
1032 only memristors and simple electrical components (Figure 11b). Here, ionic currents in  
1033 one element entrain or modulate others, with the electrolyte itself serving as the  
1034 communication medium. Mutual electrolyte coupling thus allows one memristor to  
1035 modulate another state, analogous to synaptic gating in neural networks. Even in  
1036 passive structures, similar coupling effects arise, as ordered nanopore arrays exhibit pore-  
1037 pore transport interference due to overlapping diffusion layers and shared ion depletion  
1038 zones. In other words, ionic transport through one pore can modify local concentration  
1039 and electric field profiles sufficiently to gate the conductance of neighboring pores.  
1040 Collective effects are enhanced by close proximity or shared reservoirs and can be  
1041 exploited for computation.<sup>90</sup>

1042 A landmark demonstration involved an ionic logic gate formed by two memristive  
1043 nanopores coupled through a resistor (Figure 11c).<sup>23</sup> Here, each nanopore modulated  
1044 the voltage experienced by the other, enabling mutual gating and conditional switching  
1045 analogous to electronic logic. The circuit realized a material implication gate, a Boolean  
1046 primitive from which all other logic gates can be derived. This result showed  
1047 unequivocally that computation can be implemented in ionic circuits using ions in  
1048 solution without electronic carriers. Despite operating on second-long timescales, the  
1049 demonstration established that basic computing primitives can be realized solely with

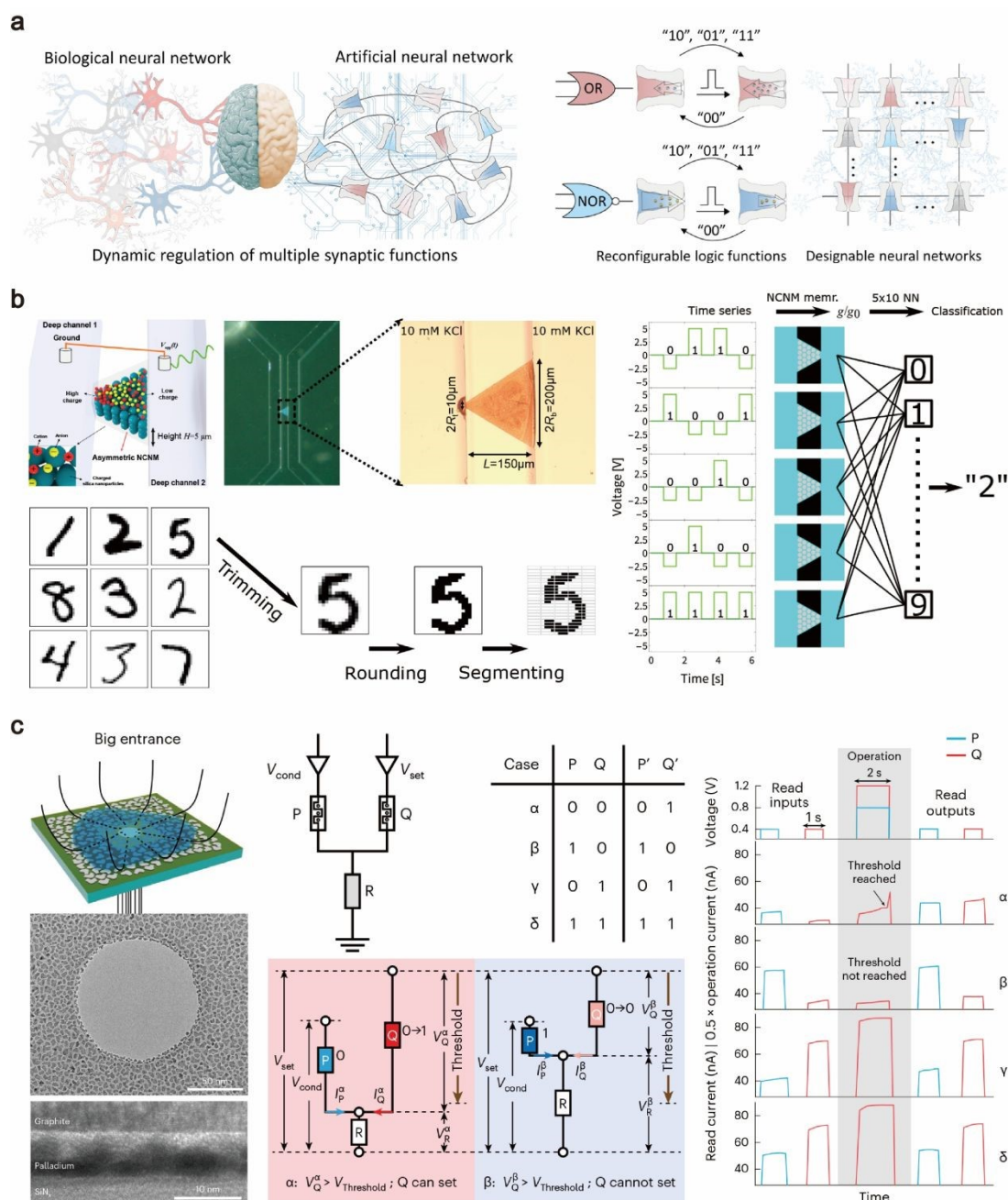


**Figure 11. Iontronic circuits and learning architectures.** **a**, Single-pore nanofluidic logic memristors leverage ion enrichment/depletion states that coevolve with chemical cues and voltage history to implement reconfigurable synaptic functions and logic, while programmable series/parallel interconnects scale these elements into multi-memristor assemblies and small neural networks. Adapted with permission from ref. 143. Copyright 2024 American Chemical Society. **b**, Tapered microchannels embedding a colloidal nanochannel-network membrane generate volatile yet reproducible conductance dynamics through transient salt concentration polarization, such that handwritten digits encoded as input time series are mapped onto channel responses and classified with a simple readout layer. Adapted with permission from ref. 101. Copyright 2024 Creative Commons CC BY 4.0. **c**, Circuit-scale nanofluidic logic using mechano-ionic memristive switches. Highly asymmetric channels are designed for in-memory processing and can be assembled into logic circuits composed of two interactive devices and an ohmic resistor. Adapted with permission from ref. 23. Copyright 2024 Creative Commons CC BY.

1050 nanofluidic memristors. Importantly, the two memristors in the IMP gate were not



1051 isolated but interacted through the shared circuit, allowing each device to influence the  
1052 state of the other.<sup>23</sup> Electrolyte-coupled interactions mark recurrent, state-dependent  
1053 dynamics even in simple two-element networks.

1054 Another striking manifestation is in chemical reaction-mediated memristors: in  
1055 single nanopores, cyclical precipitation and dissolution of ionic solids can produce self-  
1056 oscillating currents.<sup>119,121</sup> If multiple memristive pores governed by such in-pore  
1057 reactions were coupled, their oscillations could synchronize in a manner analogous to  
1058 coupled chemical oscillators. Networked nanofluidic memristors can thus exhibit new  
1059 dynamical modes, from sustained oscillations to chaotic switching, expanding the  
1060 computational repertoire of iontronic circuits.

1061 Theoretical models support the promise of small ionic memristor networks for  
1062 neuromorphic function. Brownian dynamics simulations by Noh *et al.*<sup>111</sup> showed that  
1063 just a handful of coupled nanofluidic memristors can reproduce neuron-like spiking  
1064 behavior. In their model, quasi-2D slit nanopores with memristive conductance were  
1065 connected in a circuit analog of an integrate-and-fire neuron, and the collective ionic  
1066 dynamics generated action potential-like voltage spikes.<sup>112</sup> There is also work  
1067 demonstrated an all-ionic leaky integrate-and-fire oscillator using conical nanopore  
1068 memristors and a resistor, which could fire repetitive spikes analogous to neural  
1069 oscillations.<sup>144</sup> Notably, these designs achieved neuron functionality with far fewer  
1070 components than an equivalent electronic circuit: a direct outcome of the rich physics  
1071 within each ionic memristor like electric double-layer rearrangement, ionic adsorption, or  
1072 concentration polarization. These theoretical findings suggest that ionic memristor  
1073 networks could inherently perform neuromorphic tasks such as pattern generation and  
1074 potentially even learning with minimal circuitry.

1075 The prospect of ionic memory circuits also opens intriguing possibilities for bio-  
1076 interfacing. Because they use the same carriers as biology, arrays of ionic memristors  
1077 might seamlessly interface with living neural tissue. One could imagine an implantable  
1078 iontronic chip where each memristor responds to local biochemical signals and drives an  
1079 electronic feedback to neurons, effectively communicating in the native ionic language  
1080 in the brain.<sup>145,146</sup> Such hybrid soft-hard systems would blur the boundary between  
1081 computing devices and biology, leveraging the biocompatibility and soft mechanics of  
1082 fluidic components.

1083 Assessing the potential and limitations of multi-memristor nanofluidic circuits  
1084 makes it clear that the field remains at a very early stage. The integration scale today is  
1085 on the order of only 2-3 devices working in concert, compared to the billions of transistors  
1086 in modern electronic chips, effectively the iontronic analogue of early electronic



1087 computer prototypes from the 1940s. Scaling these systems to large, reliable circuits is  
1088 challenging, as ionic devices are orders of magnitude slower than semiconductor switches  
1089 and long-distance ionic transport is limited by diffusion and fluidic resistance. The  
1090 requirement for specific liquid environments or isolation further complicates large-scale  
1091 integration of nanofluidic memristors.

1092 Concerns also remain regarding manufacturability and uniformity, as nanofluidic  
1093 elements are likely to show greater device-to-device variability in geometry or surface  
1094 chemistry than semiconductor transistors. Nonetheless, a tangible path forward is  
1095 emerging: modern micro- and nanofabrication techniques enable the creation of  
1096 nanochannel and nanopore arrays with high precision, and recent studies have begun to  
1097 exploit these capabilities. For example, some of the memristive nanopore devices were  
1098 fabricated in a scalable way on silicon nitride chips, yielding dozens of working devices  
1099 that could potentially be addressed in parallel.<sup>119</sup> Likewise, two-dimensional  
1100 nanochannel memristors have been demonstrated on-chip, showing that multiple fluidic  
1101 memories can coexist and even be tuned individually by adjusting their local electrolyte  
1102 conditions.<sup>106</sup> As a result, one can envision a future ionic integrated circuit comprising  
1103 many memristors arranged in a network, analogous to a crossbar of artificial synapses.  
1104 In practice, large-scale iontronic processors are therefore expected to adopt hybrid  
1105 architectures, in which electrodes and wiring are used to interconnect and control arrays  
1106 of fluidic devices organized into modular units. Signal readout and interfacing present  
1107 an additional challenge, as ionic currents must be converted to electronic signals at some  
1108 stage. Ultimately, although scaling iontronic circuits to very large-scale integration  
1109 (VLSI) complexity is an ambitious goal, the rewards are considerable. Large networks  
1110 of ionic memristors would operate in regimes of ultra-low power and inherent parallelism,  
1111 potentially achieving brain-like efficiencies. They could be directly merged with  
1112 chemical and biological processes, enabling forms of soft computing in environments  
1113 where silicon chips falter. In the coming years, it is anticipated that the field will  
1114 transition from one-off device physics demonstrations to developing the design principles  
1115 and architectures for multi-memristor ionic circuits. By analogy with the evolution of  
1116 electronic computing, rudimentary iontronic gates and synapses may become the  
1117 foundational building blocks of future ion-based intelligent machines.

1118  
1119

## 1120 **6. Prospects and challenges**

1121 Nanofluidic memristors have proven their ability to emulate synapses and neural  
1122 circuits in concept, but transforming these laboratory devices into practical, large-scale



1123 neuromorphic systems comes with significant challenges. In this section, we outline the  
1124 key hurdles and prospects for the field, including device integration, scalability and  
1125 switching speed. Each of these factors could limit performance or reliability if not  
1126 addressed, yet each also offers opportunities for innovation. Whereas many of the  
1127 challenges for ionic memristors are shared with those faced by traditional electronics,  
1128 there are also issues unique to iontronics, such as water drying and slow ionic mobility.  
1129 The prospects, on the other hand, include leveraging the intrinsic advantages of ionic  
1130 systems such as super-efficient energy usage and inherent biocompatibility to create  
1131 computing platforms that could profoundly impact both technology and bioengineering.

### 1132 1133 **6.1 Thermal management**

1134 Thermal management is an inevitable issue in integrated circuits.<sup>147</sup> While ionic  
1135 memristors operate at extremely low energy per event, often in the femtojoule to picojoule  
1136 range, the challenge of thermal management becomes significant when scaling to large  
1137 arrays or increasing switching speed. Efforts to accelerate switching by increasing ion  
1138 concentrations or bias voltages can introduce ohmic heating.<sup>148-150</sup> Heat accumulation  
1139 should be mitigated as it can lead to evaporation, bubble formation, ion mobility drift,  
1140 and degradation of soft materials like lipid bilayers or polymer brushes. In this regard,  
1141 nanoscale channels offer limited paths for heat dissipation. Solutions include using  
1142 thermally conductive substrates, pulsed operation to allow for passive cooling, or  
1143 microfluidic circulation of electrolytes. Designs inspired by the brain, i.e., short sparse  
1144 spikes and distributed computation, help minimize local heating. The goal can be cold  
1145 computing that functions at room temperature without active cooling. The brain  
1146 remains a blueprint with minimal energy per event, distributed load, and graceful  
1147 operation. Achieving this in engineered iontronics requires both material innovation  
1148 and rethinking how we compute.

### 1149 1150 **6.2 Ionic fatigue**

1151 Like metals under repeated stress, ionic memristors face degradation from cyclic ion  
1152 migration and associated chemical or mechanical changes, a phenomenon termed ionic  
1153 fatigue. This can manifest as reduced hysteresis, drift in resistance states, or complete  
1154 failure due to fouling, delamination, or irreversible reactions. For example, side  
1155 reactions, such as unintended water electrolysis, can alter pH and surface charge,  
1156 degrading materials like polyelectrolytes or brushes over time. Ion depletion or  
1157 irreversible trapping, especially in systems relying on finite ionic species, can exhaust  
1158 switching capacity. Mechanical effects like swelling, drying, or interfacial stress can

1159 also fracture gels, rupture membranes, or wear down soft layers.

1160 Mitigating fatigue demands chemically stable architectures, minimizing reactive  
1161 species, and confining operation to regimes that avoid extreme ionic or pH excursions.  
1162 Some soft materials offer self-healing like hydrogels with dynamic bonds that can restore  
1163 structure and conductivity after damage.<sup>151</sup> Another strategy is to reserve volatile  
1164 switching for frequent activity while limiting non-volatile writes, analogous to dynamic  
1165 RAM refresh or memory consolidation in the brain.

1166 Still, more complex architectures, especially those involving redox-active  
1167 components or porous frameworks, may face increased susceptibility. As in batteries,  
1168 long-term retention may come at the cost of reversibility or responsiveness. Balancing  
1169 endurance with plasticity thus remains an open design challenge.

1170 Meanwhile, several devices already exhibit excellent endurance. Zhang et al.<sup>107</sup>  
1171 report ionic liquid system remaining stable over many cycles, likely due to its non-volatile  
1172 medium and reversible interfacial motion.<sup>107</sup> A molecular brush-confined device also  
1173 maintained performance through extensive cycling, owing to robust covalent attachment  
1174 and non-consumptive ion interactions.<sup>136</sup> With careful chemistry, mechanical  
1175 robustness, and thoughtful operation, future ionic devices could achieve lifetimes rivaling  
1176 solid-state transistors while retaining the unique dynamics of soft, ion-driven systems.

1177

### 1178 **6.3 Mechanical stability**

1179 Mechanical fragility is a key challenge for nanofluidic memristors, especially those  
1180 incorporating soft matter such as lipid bilayers, hydrogels, or droplets. These  
1181 components are vulnerable to deformation, drying, and rupture under environmental  
1182 stress, limiting device durability. Long-term deformation, such as hydrogel creep or  
1183 nanopore etching, can shift device baselines, necessitating recalibration. Emulsion-  
1184 based systems offer one route to enhanced mechanical stability through droplet  
1185 miniaturization and self-stabilization. Equally important is packaging: maintaining  
1186 hydration and shielding devices from contamination can dramatically extend operational  
1187 lifetimes. Hybrid strategies like polymer-stabilized bilayers, hydrogel encapsulation,  
1188 and soft-hard integration offer enhanced mechanical integrity. As fabrication  
1189 techniques mature, ionic devices are expected to become as mechanically reliable as  
1190 conventional electronic components.

1191

### 1192 **6.4 Device integration scalability**

1193 Scaling nanofluidic memristors from lab prototypes to large-scale systems remains  
1194 a core challenge. Unlike electronics, where lithography processes enable to integrate



1195 billions of transistors, ionic systems require managing liquids, interfaces, and ion  
 1196 transport across many channels, thereby posing distinct architectural and fabrication  
 1197 hurdles. Device arrays are feasible via microfabrication, since nanopores or

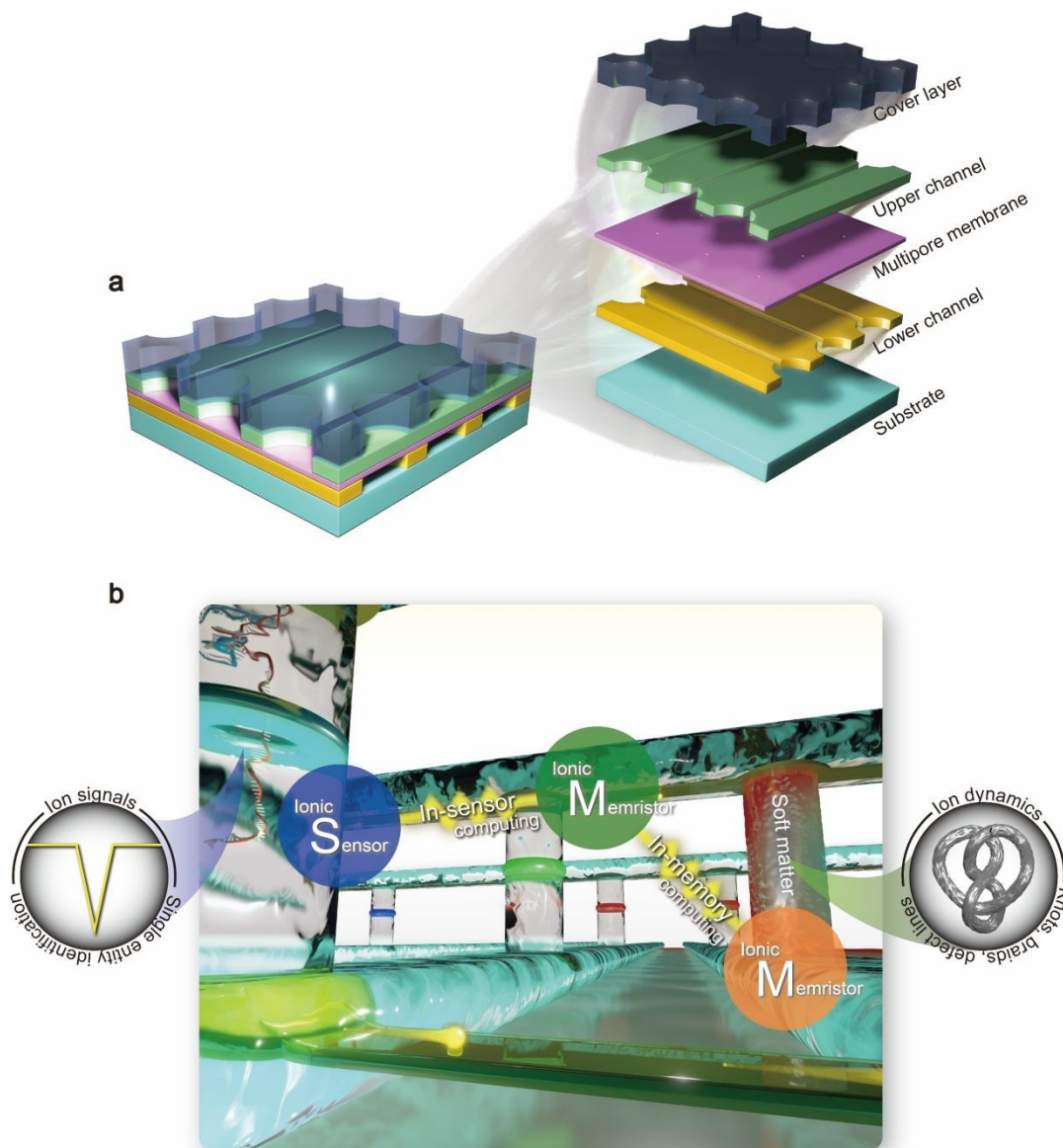


**Figure 12. Crossbar nanopore junction system.** **a**, Schematic of a crossbar architecture in which row and column fluidic channels are patterned on opposite sides of a multipore membrane, so that each channel intersection defines an individually addressable nanopore junction. Selecting a specific row-column pair localizes the applied bias and ionic flux to the corresponding junction, enabling dense, addressable ionic memristor arrays in a layout analogous to crossbar RRAM. Expanded view of the stacked implementation (cover layer, upper channel layer, multipore membrane, lower channel layer, and substrate) illustrates a manufacturable route to scaling nanopore-junction devices with simplified interconnect routing and on-chip integration. **b**, Conceptual nanopore-junction architecture for in-sensor and in-memory computing. Each addressable junction senses ionic events while nearby adaptive conductance stores local context, enabling in-sensor classification and in-memory computing with analogue ionic weights.



1198 nanochannels can now be defined with sub-100 nm precision. Early demonstrations of  
1199 multi-memristor layouts suggest scalable ionic circuits are within reach.<sup>106</sup> Further  
1200 refinements can pursue crossbar nanopore junction architectures as an analogue of the  
1201 resistive random access memory (RRAM) configurations that could enable dense,  
1202 addressable ionic memristor arrays (Figure 12a). Key to this is integrating electrode  
1203 networks for local gating, and optimizing designs for functional scalability, where few  
1204 devices can perform complex logic.

1205 A complementary route to scalability would be to view integration not only as adding  
1206 more devices, but as increasing the function per junction. For example, an addressable  
1207 array can operate as a co-integrated sensor/memory fabric, where each junction performs  
1208 nanopore sensing<sup>152-154</sup> while neighboring junctions store and update conductance states  
1209 that retain local context. This architecture naturally supports in-sensor computing,  
1210 where raw translocation pulses are classified directly at the sensing site, or in-memory  
1211 computing, where the adaptive ionic conductance acts as an analog weight so that  
1212 computation proceeds where the state is stored rather than shuttling signals across slow  
1213 diffusive ionic paths. Ionic polymers would provide a practical materials bridge for this  
1214 co-integration, where polymer brushes, gels, and other confined polyelectrolytes add  
1215 tunable chemical selectivity and multi-timescale internal state variables that stabilize  
1216 memory while remaining compatible with hard nanofabricated nanopores and channels.  
1217 Further advances in the state engineering may also be achievable by exploiting soft  
1218 matter<sup>67</sup> in which information is stored not only in ion concentrations but also in  
1219 reconfigurable spatial patterns, such as arrays of line defects as well as knotted and  
1220 braided filamentary structures, that create a large accessible space of stable configurations  
1221 and transitions for robust,<sup>155,156</sup> low-power physical information processing. In this  
1222 view, scalable iontronic systems will likely emerge as modular networks of  
1223 sensor/memristor nodes, coupled by short-range ionic dynamics for rich analog  
1224 processing and by electronic interconnects for long-range communication (Figure 12b).

1225 At the system level, the most credible near-term architecture is an ion-electron co-  
1226 processor. Ionic junctions are well suited to local state evolution, analogue weighting,  
1227 and chemically coupled adaptation, whereas electronic amplifiers, multiplexers, and  
1228 CMOS circuitry remain superior for addressing, signal conditioning, and long-range  
1229 communication. The central engineering task is therefore not to replace electronics  
1230 outright, but to build low-leakage interfaces that preserve slow ionic state dynamics while  
1231 enabling fast and stable readout. This same logic extends to neural interfaces, where  
1232 soft conductive composites and hydrogel-based conductors can reduce mechanical  
1233 mismatch with tissue while providing reliable ion-electron transduction.



1234 To approach brain-like computation with many interacting ionic weights, multiple  
1235 ionic memristors should be organized as a cross-bar nanopore-junction array in which  
1236 orthogonal fluidic or electronically addressed word lines and bit lines intersect at  
1237 individually defined nanopore junctions. Each cross-point then functions as a local  
1238 ionic synapse, where the applied row/column bias sets the transmembrane field across  
1239 that nanopore, the junction conductance stores the synaptic weight, and the summed  
1240 current collected along a shared line naturally implements the fan-in operation required  
1241 for analogue vector-matrix multiplication. In this architecture, short-range ionic  
1242 coupling can support local state adaptation and history-dependent learning, whereas  
1243 electronic selectors, amplifiers, or gate electrodes should handle addressing, isolation,  
1244 and long-range communication so that write/read operations remain stable despite the  
1245 slower relaxation of ions. A practical brain-inspired implementation is therefore not a  
1246 purely ionic network, but a hierarchical ion-electron system in which dense crossbar  
1247 nanopore junctions provide massively parallel adaptive weighting while surrounding  
1248 circuitry orchestrates timing, multiplexing, and error control.

1249

1250

### 1251 **6.5 Switching speed**

1252 The rate at which ionic memristors change state is constrained by the inherent  
1253 slowness of ion transport compared to electrons. While ionic memristors will not rival  
1254 the GHz speed of electronic transistors, their efficiency and analog capabilities position  
1255 them for applications where millisecond precision and energy-saving characteristics  
1256 outweigh clock frequency.

1257 Typical ionic devices switch at rates from hertz to kilohertz, with some reports of  
1258 nanopore-based memristors reaching 100 kHz. Such speeds, though modest, are  
1259 sufficient for many sensory and learning tasks. Further speed enhancement may be  
1260 possible by device miniaturization through shorter channels for smaller droplets to reduce  
1261 ion transit times. Pulsed or high-field operation may also transiently accelerate  
1262 switching, albeit with trade-offs in energy efficiency and stability. Volatility also shapes  
1263 speed. Fast, volatile devices offer quick response but poor retention, while stable, non-  
1264 volatile ones tend to switch slowly. Adjusting volatility or pairing ionic elements with  
1265 electronic drivers may optimize speed for specific tasks. Parallelism provides a system-  
1266 level workaround. Massive arrays of slower devices operating concurrently, similar to  
1267 the brain architecture, can deliver high throughput despite modest individual speeds. This  
1268 model suits neuromorphic inference at biologically relevant timescales.

1269



**Table 4.** Benchmark ranges across ionic and electronic memristive platforms.

<i>Platform</i>	<i>Energy per event</i>	<i>Switching time</i>	<i>Retention time</i>	<i>Scalability</i>
Soft fluidics	10 aJ - pJ	ms - s	ms - hours	Low to moderate
Hard fluidics	fJ - pJ	$\mu$ s - ms	s - hours	Moderate
Soft/hard hybrid fluidics	10 aJ - pJ	$\mu$ s - ms	ms - days	Moderate to high
Electronic memristors (RRAM/CMOS)	pJ - nJ	ns - $\mu$ s	days - years	Very high

## 1270 7. Conclusions

1271 Table 4 shows the emerging landscape of memristive memory into a single cross-  
 1272 platform benchmark. By placing soft, solid-state nanofluidic and hybrid ionic systems  
 1273 alongside conventional electronic memristors, it makes the governing trade-offs  
 1274 transparent across write energy, switching time, retention, on/off ratio and scalability.  
 1275 Soft ionic platforms occupy the corner of highest physicochemical richness, lowest  
 1276 energy cost and closest compatibility with biological media. Solid-state nanofluidic and  
 1277 hybrid architectures, in contrast, sacrifice some of that freedom to gain reproducible  
 1278 geometry, addressability and routes to manufacturable integration. Electronic  
 1279 memristors remain unrivalled in raw switching speed and industrial maturity,<sup>157-160</sup> yet  
 1280 their internal state is typically less entangled with chemistry, hydration and multiscale  
 1281 relaxation; features that give ionic platforms distinctive leverage for adaptive, life-  
 1282 adjacent computing.

1283 Seen in this way, fluidic and solid-state memristors are better understood as points  
 1284 along a continuum than as competing categories. Soft fluidics operate in the most  
 1285 biomimetic regime, where memory is inseparable from chemical environment and  
 1286 mechanical compliance, although this same coupling can amplify drift and slow dynamics  
 1287 as systems scale. Hard nanofluidic devices move closer to the engineering logic of  
 1288 semiconductor hardware by fixing geometry and compressing the active volume, while  
 1289 preserving the central premise of ionic intelligence: information is stored and processed  
 1290 in liquid-phase ionic distributions rather than in electronic carriers within solids. Hybrid  
 1291 devices offer the most practical bridge between these regimes, combining wafer-  
 1292 compatible scaffolds with fluid-like internal state variables and thereby providing a

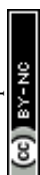


1293 credible route towards large-scale ion-electron co-integration. Framed in this way,  
1294 benchmarking is not a matter of deciding which platform wins, but of mapping  
1295 complementary operating regimes and identifying the design opportunities that arise  
1296 when computation is allowed to be both electrical and chemical.

1297 Nanofluidic memristors embody a convergence of chemistry, biology, and electronics,  
1298 defining a new class of devices where ions, not electrons, serve as the fundamental  
1299 carriers of information. Throughout this review, we have seen how harnessing ion  
1300 transport in confined fluids enables rich, synapse-like behaviors, i.e., history-dependent  
1301 conductance, short- and long-term plasticity, and the integration of electrical and  
1302 chemical signaling within a single device. By operating with ions rather than electrons,  
1303 these memristors mimic the signaling mechanisms of biological neural networks, offering  
1304 prospects for brain-like energy efficiency and inherent biocompatibility. Proof-of-  
1305 concept devices already exhibit a diverse array of functions, from droplet-based synapses  
1306 capable of learning and forgetting, to solid-state nanopores executing logic with liquid  
1307 blister memories, to polymer brush-lined nanochannels that transduce chemical cues into  
1308 electrical responses. These advances point toward an emerging iontronics, where  
1309 information is processed through flowing electrolytes, rather than within rigid  
1310 semiconductor lattices.

1311 Yet, realizing the full promise of ionic memristors for artificial intelligence  
1312 applications will require continued innovation to overcome the challenges. Thermal  
1313 management should ensure that these devices, often operating in aqueous environments,  
1314 remain cool and stable even as we scale up integration. Materials and designs need to  
1315 be refined to prevent ionic fatigue so that devices can learn and re-learn over billions of  
1316 cycles without degrading. The delicate soft components of many ionic devices require  
1317 reinforcement through hybrid architectures and packaging to guarantee mechanical  
1318 stability in real-world operating conditions. Perhaps most critically, methods to  
1319 integrate large arrays of ionic memristors, bridging the gap from single demonstrators to  
1320 dense networks, will determine whether ionic computing can move from a laboratory to  
1321 practical deployment.

1322 A balanced assessment also requires identifying the regimes in which each platform  
1323 is likely to thrive, and those in which its limitations become fundamental. Soft devices  
1324 are unparalleled in biocompatibility, compliance and chemically rich state dynamics, but  
1325 remain susceptible to dehydration, drift and limited clock speed. Solid-state nanofluidic  
1326 devices offer tighter control over geometry and stronger prospects for large-scale  
1327 fabrication, although their memory can be diminished at high ionic strength when double-  
1328 layer contrast is screened. Hybrid architectures widen the design window by combining



1329 robust scaffolds with adaptive ionic materials, but they introduce their own interfacial  
1330 challenges, including delamination, solvent loss and packaging complexity. These  
1331 boundaries are not weaknesses to be hidden, but design constraints that should inform  
1332 platform choice for neural interfaces, soft robotics, sensing and on-chip analogue learning.

1333 In terms of performance, ionic memristors should not be erected to rival the gigahertz  
1334 switching of transistors as they do not need to. Their comparative advantage lies in  
1335 energy efficiency and rich functionality rather than raw speed. As multiple studies have  
1336 highlighted, these fluidic devices can operate at femtojoule or picojoule energy scales per  
1337 event, approaching the unmatched efficiency of the human brain. Furthermore, they  
1338 inherently support analog storage and computation within the same medium, eliminating  
1339 the artificial separation of memory and processing that plagues von Neumann electronic  
1340 architectures. For AI tasks like pattern recognition, sensory processing, and adaptive  
1341 control, ionic memristor networks are particularly well suited. Indeed, as we build chips  
1342 with thousands of ionic synapses operating in parallel, we may find that despite slower  
1343 individual devices, the overall system throughput for AI computations is competitive with  
1344 or even superior to conventional approaches, all while consuming orders of magnitude  
1345 less power.

1346 The road ahead for nanofluidic memristors will likely see increased synergy with  
1347 other emerging technologies. We anticipate hybrid platforms where ionic memristor  
1348 cores interface with CMOS control circuits, bridging the best of both worlds, the ion-  
1349 electron hybrid computers that use electrons for communication and ions for computation.  
1350 On the algorithmic front, researchers will explore how to exploit the multivariate nature  
1351 of ionic signals to implement novel forms of computation that have no easy electronic  
1352 analog.

1353 Nanofluidic memristors bring us a significant step closer to the vision of brain-like  
1354 artificial intelligence hardware: systems that are not only low-power and highly parallel,  
1355 but also adaptive, self-organizing, and intimately linked to the chemical and ionic  
1356 processes of life. As these devices mature, we foresee them becoming central  
1357 components in next-generation AI as in-memory analog computing units on chips, soft  
1358 neuromorphic robots, brain-interface prosthetics, and beyond. Ionic intelligence  
1359 remains in its infancy, yet current progress outlines a compelling trajectory toward a new  
1360 computing paradigm rooted in ion and fluid physics, with the potential to seamlessly  
1361 bridge artificial systems and biological function.

1362 Over the next decade, progress will likely be shaped by four priorities. First, multi-  
1363 ion and multi-channel devices should move beyond single-species memory to access the  
1364 richer, state-dependent dynamics that support neuron-like behavior. Second, scalable



1365 ion-electron co-integration will be essential, with dense ionic arrays coupled to CMOS  
1366 backplanes that provide addressing, low-noise current-to-voltage conversion, and high-  
1367 bandwidth readout and control, approach already established in CMOS-integrated  
1368 nanopore front ends and in analyses of bandwidth/noise constraints in ionic recordings.<sup>161</sup>  
1369 Third, new materials platforms, including soft conductive composites and chemically  
1370 programmable interfaces, should improve stability without sacrificing the chemically  
1371 coupled functionality that makes iontronic state variables distinctive. Fourth, the field  
1372 needs shared benchmarking standards for endurance, retention, environmental robustness  
1373 and energy per update, enabling meaningful comparisons across platforms and  
1374 accelerating translation. Progress along these axes will determine whether ionic  
1375 intelligence remains an intriguing laboratory concept or matures into a practical hardware  
1376 platform, especially as mixed ionic-electronic transducers provide a direct bridge from  
1377 ionic state variables to electronic signals suitable for long-range routing and CMOS-  
1378 compatible processing.<sup>162,163</sup> If successful, nanofluidic memristors could become  
1379 primary members of the future integrated circuits family, powering a revolution in  
1380 computing as profound as the advent of the semiconductor era, but this time driven by the  
1381 dance of ions in nanoconfinements.

1382



1384 **Acknowledgments**

1385 A part of this work was supported by the Japan Society for the Promotion of Science (JSPS) KAKENHI  
1386 Grant Number 25K01639, 24K01511, and Japan Agency for Medical Research and Development (AMED)  
1387 25fk0534001h001.

1388

1389 **REFERENCES**

1390

- 1391 1. C. -J. Wu, B. Acun, R. Raghavendra and K. Hazelwood, Beyond efficiency: scaling AI  
1392 sustainably. *IEEE Micron* 2024, **44**, 37-46.
- 1393 2. R. Istrate, V. Tulus, R. N. Grass, L. Vanbever, W. J. Stark and G. Guillen-Gosalbez, The  
1394 environmental sustainability of digital content consumption. *Nat. Commun.* 2024, **15**,  
1395 3724.
- 1396 3. Z. Li, H. Luo, Y. Jiang, H. Liu, L. Xu, K. Cao, H. Wu, P. Gao and H. Liu, Comprehensive  
1397 review and future prospects on chip-scale thermal management: core of data center's  
1398 thermal management. *Appl. Therm. Eng.* 2024, **251**, 123612.
- 1399 4. Boosting AI with neuromorphic computing. *Nat. Comp. Sci.* 2025, **5**, 1-2.
- 1400 5. A. L. Hodgkin and A. F. Huxley, A quantitative description of membrane current and its  
1401 application to conduction and excitation in nerve. *J. Physiol.* 1952, **117**, 500-544.
- 1402 6. T. J. Sejnowski, C. Koch and P. Churchland, Computational neuroscience. *Science* 1988,  
1403 **241**, 1299-1306.
- 1404 7. J. B. Aimone and O. Parekh, The brain's unique take on algorithms. *Nat. Commun.* 2023,  
1405 **14**, 4910.
- 1406 8. E. R. Kandel, J. D. Koester, S. H. Mack and S. A. Siegelbaum, Principles of neural  
1407 science, sixth edition. 2021, McGraw Hill/ Medical.
- 1408 9. Y. He, M. Tsutsui, Y. Zhou and X. -S. Miao, Solid-state nanopore systems: from materials  
1409 to applications. *NPG Asia Mater.* 2021, **13**, 48.
- 1410 10. T. Emmerich, N. Ronceray, K. V. Agrawal, S. Garaj, M. Kumar, A. Noy and A. Radenovic,  
1411 Nanofluidics. *Nat. Rev. Methods Prim.* 2024, **4**, 69.
- 1412 11. V. A. Baulin, A. Giacometti, D. A. Fedosov, S. Ebbens, N. R. Varela-Rosales, N. Feliu,  
1413 M. Chowdhury, M. Hu, R. Fuchslin, M. Dijkstra, M. Mussel, R. van Roij, D. Xie, V. Tzanov,  
1414 M. Zu, S. Hidalgo-Caballero, Y. Yuan, L. Cocconi, C. -M. Ghim, C. Cottin-Bizonne, M. C.  
1415 Miguel, M. J. Esplandiu, J. Simmchen, W. J. Parak, M. Werner, G. Gompfer and M. M.  
1416 Hanczyc, Intelligent soft matter: towards embodied intelligence. *Soft Matter* 2025, **21**,



- 1417 4129.
- 1418 12. S. A. Sarles, J. S. Najem and A. S. Mohamed, Voltage-responsive biomimetic  
1419 membranes and ion channels for neuromorphic computing. *npj Unconv. Comp.* 2025, **2**,  
1420 26.
- 1421 13. C. S. Law, J. Wang, K. Nielsch, A. D. Abell, J. Bisquert and A. Santos, Recent advances  
1422 in fluidic neuromorphic computing. *Appl. Phys. Rev.* 2025, **12**, 021309.
- 1423 14. J. Luo, A. Remy and Y. Zhang, Iontronic devices from biological nanopores to artificial  
1424 systems: emerging applications and future perspectives. *Chem. Rev.* 2025, **125**, 11840-  
1425 11877.
- 1426 15. Y. van de Burgt, E. Lubberman, E. J. Fuller, S. T. Keene, G. C. Faria, S. Agarwal, M. J.  
1427 Marinella, A. A. Talin and A. Salleo, A non-volatile organic electrochemical device as a  
1428 low-voltage artificial synapse. *Nat. Mater.* 2018, **17**, 414-418.
- 1429 16. W. Wang, Y. Ma and Y. Liang, Field-effect nanofluidic memristor. *Phys. Fluid.* 2025, **37**,  
1430 082013.
- 1431 17. Y. Hoh and A. Smolyanitsky, Synaptic-like plasticity in 2D nanofluidic memristor from  
1432 competitive bicationic transport. *Sci. Adv.* 2024, **10**, adr1531.
- 1433 18. K. Liu, Y. Wang, M. Sun, J. Lu, D. Shi and Y. Xie, Resistance-restorable nanofluidic  
1434 memristor and neuromorphic chip. *Nano Lett.* 2025, **25**, 6530-6538.
- 1435 19. P. Ramirez, V. Gomez, J. Cervera, S. Mafe and J. Bisquert, Synaptical Tunability of  
1436 Multipore Nanofluidic Memristors. *J. Phys. Chem. Lett.* 2023, **14**, 10930-10934.
- 1437 20. R. Song, P. Wang, H. Zeng, S. Zhang, N. Wu, Y. Liu, P. Zhang, G. Xue, J. Tong, B. Li,  
1438 H. Ye, K. Liu, W. Wang and L. Wang, Nanofluidic memristive transition and synaptic  
1439 emulation in atomically thin pores. *Nano Lett.* 2025, **25**, 5646-5655.
- 1440 21. Y. -T. Xu, S. -Y. Yu, Z. Li, B. -H. Kou, J. -X. Pang, W. -W. Zhao, H. -Y. Chen and J. -J.  
1441 Xu, A nanofluidic spiking synapse. *Proc. Natl. Acad. Sci.* 2024, **121**, e2403143121.
- 1442 22. B. Xie, T. Xiong, G. Guo and P. Yu, Bioinspired ion-shuttling memristor with both  
1443 neuromorphic functions and ion selectivity. *Proc. Natl. Acad. Sci.* 2025, **122**,  
1444 e2417040122.
- 1445 23. T. Emmerich, Y. Teng, N. Ronceray, E. Lopriore, R. Chiesa, A. Chernev, V. Artemov, M.  
1446 Di Ventra, A. Kis and A. Radenovic, Nanofluidic logic with mechano-ionic memristive  
1447 switches. *Nat. Electron.* 2024, **7**, 271-278.
- 1448 24. E. Axpe, G. Orive, K. Franze and E. A. Appel, Towards brain-tissue-like biomaterials.  
1449 *Nat. Commun.* 2020, **11**, 3423.
- 1450 25. E. K. Pillai and K. Franze, Mechanics in the nervous system: From development to  
1451 disease. *Neuron* 2024, **112**, 342-361.
- 1452 26. E. Kreysing, H. O. B. Gautier, S. Mukherjee, K. A. Mooslehner, L. Muresan, D. Haarhoff,



- 1453 X. Zhao, A. K. Winkel, T. Boric, S. Vasquez-Sepulveda, N. Gampel, A. Dimitracopoulos,  
1454 E. K. Pillai, R. Humphrey, R. T. Karadottir and K. Franze, Environmental stiffness  
1455 regulates neuronal maturation via Piezo1-mediated transthyretin activity. *Nat. Commun.*  
1456 2025, **16**, 9842.
- 1457 27. Q. -Y. Zhang, Y. -Y. Zhang, J. Xie, C. -X. Li, W. -Y. Chen, B. -L. Liu, X. -A. Wu, S. -N. Li,  
1458 B. Huo, L. -H. Jiang and H. -C. Zhao, Stiff substrates enhance cultured neuronal network  
1459 activity. *Sci. Rep.* 2014, **4**, 6215.
- 1460 28. O. H. S. Ollila, M. Louhivuori, S. J. Marrink and I. Vattulainen, Protein shape change has  
1461 a major effect on the gating energy of a mechanosensitive channel. *Biophys. J.* 2011,  
1462 **100**, 1651.
- 1463 29. E. Flood, C. Boiteux, B. Lev, I. Vorobyov and T. W. Allen, Atomistic simulations of  
1464 membrane ion channel conduction, gating, and modulation. *Chem. Rev.* 2019, **119**,  
1465 7737-7832.
- 1466 30. Structural and functional plasticity of dendritic spines-root or result of behavior? *Gen.*  
1467 *Brain Behav.* 2016, **16**, 101-117.
- 1468 31. I. Levental and E. Lyman, Regulation of membrane protein structure and function by their  
1469 paralipidomes. *Nat. Rev. Mol. Cell Biol.* 2022, **24**, 107-122.
- 1470 32. S. B. Laughlin, R. R. de Ruyter van Steveninck and J. C. Anderson, The metabolic cost  
1471 of neural information. *Nat. Neurosci.* 1998, **1**, 36-41.
- 1472 33. A. Mehonic and A. J. Kenyon, Brain-inspired computing needs a master plan. *Nature*  
1473 2022, **604**, 255-260.
- 1474 34. C. Maffeo, S. Bhattacharya, J. Yoo, D. Wells and A. Aksimentiev, Modelling and  
1475 simulation of ion channels. *Chem. Rev.* 2012, **112**, 6250-6284.
- 1476 35. L. Chua, Memristor, Hodgkin-Huxley, and edge of chaos. *Nanotechnology* 2012, **24**,  
1477 383001.
- 1478 36. D. Deamer, M. Akeson and D. Branton, Three decades of nanopore sequencing. *Nat.*  
1479 *Biotechnol.* 2016, **34**, 518-524.
- 1480 37. Y. -L. Yung, Z. -L. Hu, S. Zhang, Y. Qing, A. Fragasso, G. Maglia, A. Meller, H. Bayley,  
1481 C. Dekker and Y. -T. Long, Nanopore-based technologies beyond DNA sequencing. *Nat.*  
1482 *Nanotechnol.* 2022, **17**, 1136-1146.
- 1483 38. A. Dorey and S. Howorka, Nanopore DNA sequencing technologies and their  
1484 applications towards single-molecule proteomics. *Nat. Chem.* 2024, **16**, 314-334.
- 1485 39. J. Ritmejeris, X. Chen and C. Dekker, Single-molecule protein sequencing with  
1486 nanopores. *Nat. Rev. Bioeng.* 2025, **3**, 303-316.
- 1487 40. B. Xie, T. Xiong, G. Guo and P. Yu, Bioinspired ion-shuttering memristor with both  
1488 neuromorphic functions and ion selectivity. *Proc. Natl. Acad. Sci.* 2025, **122**,



- 1489 e2417040122.
- 1490 41. G. Paulo, K. Sun, G. D. Muccio, A. Gubbiotti, B. M. D. Rocca, J. Geng, G. Maglia, M.  
1491 Chinappi and A. Giacomello, Hydrophobically gated memristive nanopores for  
1492 neuromorphic applications. *Nat. Commun.* 2023, **14**, 8390.
- 1493 42. S. Howorka, Building membrane nanopores. *Nat. Nanotechnol.* 2017, **12**, 619-630.
- 1494 43. K. Shimizu, B. Mijiddori, M. Usami, I. Mizoguchi, S. Yoshida, S. Akayama, Y. Hamada,  
1495 A. Ohyama, K. Usui, I. Kawamura and R. Kawano, De novo design of a nanopore for  
1496 single-molecule detection that incorporates a  $\beta$ -hairpin peptides. *Nat. Nanotechnol.* 2022,  
1497 **17**, 67-75.
- 1498 44. S. F. Mayer, M. F. Mitsione, P. Robin, L. van den Heuvel, N. Ronceray, M. J. Marcaida,  
1499 L. A. Abirata, L. F. Krapp, J. S. Anton, S. Soussou, J. Jeanneret-Grosjean, A. Fulciniti,  
1500 A. Moller, S. Vacle, L. Feletti, H. Brinkerhoff, A. H. Laszlo, J. H. Gundlach, T. Emmerich,  
1501 M. D. Peraro and A. Radenovic, Lumen charge governs gated ion transport in  $\beta$ -barrel  
1502 nanopores. *Nat. Nanotechnol.* 2025, <https://doi.org/10.1038/s41565-025-02052-6>.
- 1503 45. Kamsma, T. M., Klop, M. S., Boon, W. Q., Spitoni, C., Rueckauer, B. & van Roij, R.  
1504 Chemically regulated conical channel synapse for neuromorphic and sensing  
1505 applications. *Phys. Rev. Res.* 2025, **7**, 013328.
- 1506 46. M. M. Makhoul-Mansour and E. C. Freeman, Droplet-based membranous soft materials.  
1507 *Langmuir* 2021, **37**, 3231–3247.
- 1508 47. E. B. Stephenson, J. L. Korner and K. S. Elvira, Challenges and opportunities in achieving  
1509 the full potential of droplet interface bilayers. *Nat. Chem.* 2022, **14**, 862–870.
- 1510 48. Z. Li, S. Myers, J. Xiao, Y. Li, N. Noy, A. Leuski and A. Noy, Neuromorphic ionic  
1511 computing in droplet interface synapses. *Sci. Adv.* 2025, **11**, adv603.
- 1512 49. R. L. Sacci, H. L. Scott, Z. Liu and D. Bolmatov, Disentangling memristive and  
1513 memcapacitive effects in droplet interface bilayers using dynamic impedance  
1514 spectroscopy. *Adv. Electron. Mater.* 2022, **8**, 2200121.
- 1515 50. J. S. Najem, Md S. Hasan, R. S. Williams, R. J. Weiss, G. S. Rose, G. J. Taylor, S. A.  
1516 Sarles and C. P. Collier, Dynamical nonlinear memory capacitance in biomimetic  
1517 membranes. *Nat. Commun.* 2019, **10**, 3239.
- 1518 51. M. M. Mansour, J. J. Maraj, R. J. Pyron, F. N. Barrera and S. A. Sarles, Biomolecular  
1519 neuristors from functionalized lipid membranes. *Adv. Funct. Mater.* 2024, **34**, 2409296.
- 1520 52. J. S. Najem, G. J. Taylor, R. J. Weiss, Md S. Hasan, G. Rose, C. D. Schurman, A.  
1521 Belianinov, C. P. Collier and S. A. Sarles, Memristive ion channel-doped biomembranes  
1522 as synaptic mimics. *ACS Nano* 2018, **12**, 4702-4711.
- 1523 53. S. Haylock, M. S. Friddin, J. W. Hindley, E. Rodriguez, K. Charalambous, P. J. Booth, L,  
1524 M, C, Barter and O. Ces, Membrane protein mediated bilayer communication in networks



- 1525 of droplet interface bilayers. *Commun. Chem.* 2020, **3**, 77.
- 1526 54. E. J. Challita, J. S. Najem, R. Monroe, D. J. Leo and E. C. Freeman, Encapsulating  
1527 networks of droplet interface bilayers in a thermoreversible organogel. *Sci. Rep.* 2015, **8**,  
1528 6494.
- 1529 55. Y. Ma, Y. Niu, R. Pei, W. Wang, B. Wei and Y. Xie, Reconfigurable neuromorphic  
1530 computing by a microdroplet. *Cell Rep. Phys. Sci.* 2024, **5**, 102202.
- 1531 56. E. D. Lullo and A. R. Kriegstein, The use of brain organoids to investigate neural  
1532 development and disease. *Nat. Rev. Neurosci.* 2017, **18**, 573-584.
- 1533 57. I. Chiaradia and M. A. Lancaster, Brain organoids for the study of human neurobiology  
1534 at the interface of in vitro and in vivo. *Nat. Neurosci.* 2020, **23**, 1496-1508.
- 1535 58. Y. Samei, I. Cheung, P. Papavasileiou, C. K. Franz and J. D. Finan, Elastic and  
1536 viscoelastic properties of human cortical organoids. *Acta Biomater.* 2026, **209**, 481-492.
- 1537 59. D. -M. A. E. Din, L. Moenkemoeller, A. Loeffler, F. Habibollahi, J. Schenkman, A. Mitra,  
1538 T. van der Molen, L. Ding, J. Laird, M. Schenke, E. C. Johnson, B. J. Kagan, T. Hartung  
1539 and L. Smirnova, Human neural organoid microphysiological systems show the building  
1540 blocks necessary for basic learning and memory. *Commun. Biol.* 2025, **8**, 1237.
- 1541 60. H. Cai, Z. Ao, C. Tian, Z. Wu, H. Liu, J. Tchieu, M. Gu, K. Mackie and F. Guo, Brain  
1542 organoid reservoir computing for artificial intelligence. *Nat. Electron.* 2023, **6**, 1032-1039.
- 1543 61. H. Ledford, Neurons in a dish learn to play Pong – what's next? *Nature* 2022, **610**, 433.
- 1544 62. B. J. Kagan, A. C. Kitchen, N. T. Tran, F. Habibollahi, M. Khajehnejad, B. J. Parker, A.  
1545 Bhat, B. Rollo, A. Razi and K. J. Friston, In vitro neurons learn and exhibit sentience  
1546 when embodied in a simulated game-world. *Neuron* 2022, **110**, 3952-3969.
- 1547 63. M. U. Khan, B. Hassan, A. Alazzam, S. Eissa and B. Mohammad, Brain inspired iontronic  
1548 fluidic memristive and memcapacitive device for self-powered electronics. *Microsys.*  
1549 *Nanoeng.* 2025, **11**, 37.
- 1550 64. Y. Talavera and B. Ulmann, Brain organoid computing – an overview. arXiv:2503.19770.
- 1551 65. Y. Zhou, L. Li, Z. Han. Q. Li, J. He and Q. Wang, Self-healing polymers for electronics  
1552 and energy devices. *Chem. Rev.* 2023, **123**, 558-612.
- 1553 66. Z. Li, J. Fu, X. Zhou, S. Gui, L. Wei, H. Yang, H. Li and X. Guo, Ionic conduction in  
1554 polymer-based solid electrolytes. *Adv. Sci.* 2023, **10**, 2201718.
- 1555 67. V. A. Baulin, A. Giacometti, D. A. Fedosov, S. Ebbens, N. R. Varela-Rosakes, N. Feliu,  
1556 M. Chowdhury, M. Hu, R. Fuchslin, M. Dijkstra, M. Mussel, R. van Rooij, D. Xie, V. Tzanov,  
1557 M. Zu, S. Hidalgo-Caballero, Y. Yuan, L. Cocconi, C. -M. Ghim, C. Cottin-Bizonne, M. C.  
1558 Miguel, M. J. Esplandiu, J. Simmchen, W. J. Parak, M. Werner, G. Gompfer and M. M.  
1559 Hanczyc, Intelligent soft matter: towards embodied intelligence. *Soft Matter* 2025, **21**,  
1560 4129.



- 1561 68. Zhong, L., Zhu, Q., Wang, X., Huang, G., Liu, J., Liu, H. and Wang, Q. When  
1562 nanocellulose meets liquid metal: a review of the synergistic frontier for flexible  
1563 electronics. *Cellulose* 2025, **32**, 9787-9818.
- 1564 69. J. Xu, Z. Luo, L. Chen, X. Zhou, H. Zhang, Y. Zheng and L. Wei, Recent advances in  
1565 flexible memristors for advanced computing and sensing. *Mater. Horiz.* 2024, **11**, 4015-  
1566 4036.
- 1567 70. H. Yoo, Y. H. Lee, M. -G. Lee and J. -Y. Sun, Gel-based ionic circuits. *Chem. Rev.* 2025,  
1568 **125**, 8956.
- 1569 71. I. A. Aziz and D. Mecerreyes, Ionic polymers for bioelectronics. *Prog. Poly. Sci.* 2025,  
1570 **167**, 101994.
- 1571 72. A. Melianas, T. J. Quill, G. LeCroy, Y. Tuchman, H. V. Loo, S. T. Keene, A. Giovannitti,  
1572 H. R. Lee, I. P. Maria, I. McCulloch and A. Salleo, Temperature-resilient solid-state  
1573 organic artificial synapses for neuromorphic computing. *Sci. Adv.* 2020, **6**, abb2958.
- 1574 73. J. Shi, Y. Lin, Z. Wang, X. Shuan, T. Tao, X. Zhao, H. Xu and Y. Liu, Adaptive processing  
1575 enabled by sodium alginate based complementary memristor for neuromorphic sensory  
1576 system. *Adv. Mater.* 2024, **36**, 2314156.
- 1577 74. C. Zhao, J. Hou, M. Hill, B. Freeman, H., Wang and H. Zhang, Enhanced gating effects  
1578 in responsive sub-nanofluidic ion channels. *Acc. Mater. Res.* 2023, **4**, 786-797.
- 1579 75. D. Vokoun, S. Samal and I. Stachiv, Impact of initial cyclic loading on mechanical  
1580 properties and performance of Nafion. *Sensors* 2023, **23**, 1488.
- 1581 76. Y. -Y. Zhao, W. -J. Sun, J. Wang, J. -H. He, H. Li, Q. -F. Xu, N. -J. Li, D. -Y. Chen and J.  
1582 -M. Lu, All-inorganic ionic polymer-based memristor for high-performance and flexible  
1583 artificial synapse. *Adv. Funct. Mater.* 2020, **30**, 2004245.
- 1584 77. M. -K. Song, S. D. Namgung, D. Choi, H. Kim, H. Seo, M. Ju, Y. H. Lee, T. Sung, Y. -S.  
1585 Lee, K. T. Nam and J. -Y. Kwon, Proton-enabled activation of peptide materials for  
1586 biological bimodal memory. *Nat. Commun.* 2020, **11**, 5896.
- 1587 78. Z. Lv, S. Zhu, Y. Wang, Y. Ren, M. Luo, H. Wang, G. Zhang, Y. Zhai, S. Zhao, Y. Zhou,  
1588 M. Jiang, Y. -B. Leng and S. -T. Han, Development of bio-voltage operated humidity-  
1589 sensory neurons comprising self-assembled peptide memristors. *Adv. Mater.* 2024, **36**,  
1590 e2405145.
- 1591 79. M. Zwolak, Johan Lagerqvist and M. Di Ventra, Quantized ionic conductance in  
1592 nanopores. *Phys. Rev. Lett.* 2009, **103**, 128102.
- 1593 80. J. Feng, K. Liu, M. Graf, D. Dumcenco, A. Kis, M. Di Ventra and A. Radenovic,  
1594 Observation of ionic Coulomb blockade in nanopores. *Nat. Mater.* 2016, **15**, 850-855.
- 1595 81. X. -Y. Huang, Y. Cui, C. Ying, J. Tian and Z. Liu, Scaling behavior and conductance  
1596 mechanisms of ion transport in atomically thin graphene nano/subnanopores. *Nano Lett.*



- 1597 2025, **25**, 1722-1728.
- 1598 82. B. C. Bocquet, A. T. Bui, D. Toquer, A. Michaelides, N. Kavokine, S. J. Cox and L.  
1599 Bocquet, Momentum tunnelling between nanoscale liquid flows. *Nat. Nanotechnol.* 2025,  
1600 **20**, 397-403.
- 1601 83. E. Rigo, Z. Dong, J. H. Park, E. Kennedy, M. Hokmabadi, L. Almonte-Garcia, L. Ding, N.  
1602 Aluru and G. Timp, Measurements of the size and correlations between ions using an  
1603 electrolytic point contact. *Nat. Commun.* 2019, **10**, 2382.
- 1604 84. M. Tsutsui, W. -L. Hsu, K. Yokota, I. W. Leong, H. Daiguji and T. Kawai, Scalability of  
1605 nanopore osmotic energy conversion. *Exploration* 2024, **4**, 20220110.
- 1606 85. J. -Y. Jung, P. Joshi, L. Petrossian, T. J. Thornton and J. D. Posner, Electromigration  
1607 current rectification in a cylindrical nanopore due to asymmetric concentration  
1608 polarization. *Anal. Chem.* 2009, **81**, 3128-3133.
- 1609 86. Z. Liu, L. Ma, H. Zhang, J. Zhuang, J. Man, Z. S. Siwy and Y. Qiu, Dynamic response of  
1610 ionic current in conical nanopores. *ACS Appl. Mater. Interf.* 2024, **16**, 30496-30505.
- 1611 87. Y. Bu, Z. Ahmed and L. Yobas, A nanofluidic memristor based on ion concentration  
1612 polarization. *Analyst* 2019, **144**, 7168.
- 1613 88. M. Jahangeer, J. Guo, Z. Qin, C. Li, W. Liu, C. Zhao, W. Zhou, H. Mou, R. Wu, C. Shen,  
1614 L. Fu, B. Li, M. Junaid, H. Yao, Q. Wang and G. Du, Memory effects with broken  
1615 symmetry in nanofluidic memristor for neuromorphic computing. *Adv. Funct. Mater.* 2025,  
1616 <https://doi.org/10.1002/adfm.202525932>.
- 1617 89. J. Bisquert, M. Sanchez-Mateu, A. Bou, C. S. Law and A. Santos, Synaptic response of  
1618 fluidic nanopores: the connection of potentiation with hysteresis. *Chem. Phys. Chem.*  
1619 2024, **25**, e202400265.
- 1620 90. Z. S. Siwy, Ion-current rectification in nanopores and nanotubes with broken symmetry.  
1621 *Adv. Funct. Mater.* 2006, **16**, 735-746.
- 1622 91. H. Daiguji, Ion transport in nanofluidic channels. *Chem. Soc. Rev.* 2010, **39**, 901-911.
- 1623 92. R. Yang, Y. Balogun, S. Ake, D. Baram, W. Brown and G. Wang, Negative differential  
1624 resistance in conical nanopore iontronic memristors. *J. Am. Chem. Soc.* 2024, **146**,  
1625 13183-13190.
- 1626 93. I. -W. Leong, M. Tsutsui, S. Murayama, T. Hayashida, Y. He and M. Taniguchi, Quasi-  
1627 stable salt gradient and resistive switching in solid-state nanopores. *ACS Appl. Mater.*  
1628 *Interf.* 2020, **12**, 52175-52181.
- 1629 94. N. C. X. Stuhlmuller, R. van Roij and M. Dijkstra, Microfluidic memristive oscillators as  
1630 universal logic gates for neuromorphic computing. *Soft Matter*. 2025, **21**, 6707.
- 1631 95. T. M. Kamsma, W. Q. Boon, T. ter Rele, C. Spitoni and R. van Roij, Iontronic  
1632 neuromorphic signaling with conical microfluidic memristors. *Phys. Rev. Lett.* 2023, **130**,



- 1633 268401.
- 1634 96. Han, W. and Chen., X. Nano-electrokinetic ion enrichment of highly viscous fluids in  
1635 micro-nanochannel. *Chem. Eng. Proc. Pro. Intens.* 2019, **143**,107626.
- 1636 97. Han, W. and Chen, X. Nano-electrokinetic ion enrichment in a micro-nanofluidic  
1637 preconcentrator with nanochannel's Cantor fractal wall structure. *Appl. Nanosci.* 2020,  
1638 **10**, 95-105.
- 1639 98. Han, W. and Chen. X. A novel micro-nanofluidic preconcentrator with Koch fractal  
1640 nanochannel surface. *J. Dispers. Sci. Technol.* 2021, **42**, 1060-1072.
- 1641 99. Han, W. and Chen, X. A novel design of nanochannel structure in a micro-nanofluidic  
1642 preconcentrator for electrokinetic ion enrichment. *J. Braz. Soc. Mech. Sci. Eng.* 2020, **42**,  
1643 1-9.
- 1644 100. Han, W. and Chen, X. A review: Applications of ion transport in micro-nanofluidic  
1645 systems based on ion concentration polarization. *J. Chem. Technol. Biotechnol.* 2020,  
1646 **95**, 1622-1631.
- 1647 101. T. M. Kamsma, J. Kim, K. Kim, W. Q. Boon, C. Spitoni, J. Park and R. van Rooij,  
1648 Brain-inspired computing with fluidic iontronic nanochannels. *Proc. Natl. Acad. Sci.* 2024,  
1649 **121**, e2320242121.
- 1650 102. R. Qiao and N. R. Aluru, Scaling of electrokinetic transport in nanometer channels.  
1651 *Langmuir* 2005, **21**, 8972-8977.
- 1652 103. K. Gopinadhan, S. Hu, A. Esfandiari, M. Lozada-Hidalgo, F. C. Wang, Q. Yang, A.  
1653 V. Tyurnina, A. Keerthi, B. Radha and A. K. Geim, Complete steric exclusion of ions and  
1654 proton transport through confined monolayer water. *Science* 2019, **363**, 145-148.
- 1655 104. P. Robin, N. Kavokine and L. Bocquet, Modeling of emergent memory and voltage  
1656 spiking in ionic transport through angstrom-scale slits. *Science* 2021, **373**, 687-691.
- 1657 105. P. Robin, T. Emmerich, A. Ismail, A. Nigues, Y. You, G. -H. Nam, A. Keerthi, A. Siria,  
1658 A. K. Geim, B. Radha and L. Bocquet, Long-term memory and synapse-like dynamics in  
1659 two-dimensional nanofluidic channels. *Science* 2023, **379**, 161-167.
- 1660 106. A. Ismail, G. -H. Nam, A. Lokhandwala, S. V. Pandey, K. V. Saurav, Y. You, H.  
1661 Jyothilal, S. Goutham, R. Sajja, A. Keerthi and B. Radha, Programmable memristors with  
1662 two-dimensional nanofluidic channels. *Nat. Commun.* 2025, **16**, 7008.
- 1663 107. P. Zhang, M. Xia, F. Zhuge, Y. Zhou, Z. Wang, B. Dong, Y. Fu, K., Yang, Y. Li, Y.  
1664 He, R. H. Scheicher and X. S. Miao, Nanochannel-based transport in an interfacial  
1665 memristor can emulate the analog weight modulation of synapses. *Nano Lett.* 2019, **19**,  
1666 4279-4286.
- 1667 108. K. Chen, M. Tsutsui, F. Zhuge, Y. Zhou, Y. Fu, Y. He and X. Miao, Nanochannel-  
1668 based interfacial memristor: Electrokinetic analysis of the frequency characteristics. *Adv.*



- 1669 *Electron. Mater.* 2021, **16**, 2000848.
- 1670 109. M. Niu, Y. Chen, F. Chen, C. Zhao, Y. Yang, Y. Xu and J. Feng, Light-driven ion  
1671 transport through single-heterojunction nanopores. *Nano Lett.* 2023, **23**, 1010-1016.
- 1672 110. J. Wang, Y. Jiang, T. Xiong, J. Ly, X. He and P. Yu, Optically modulated nanofluidic  
1673 ionic transistor for neuromorphic functions. *Angew. Chem.* 2025, **64**, e202418949.
- 1674 111. Z. Li, Y. Lin, X. Shan, Z. Wang, X. Zhao, Y. Tao, H. Xu and Y. Liu, Optogenetics-  
1675 inspired nanofluidic artificial dendrite with spatiotemporal integration functions. *Adv.*  
1676 *Mater.* 2025, **37**, 2502438.
- 1677 112. Y. Noh and A. Smolyanitsky, Synaptic-like plasticity in 2D nanofluidic memristor  
1678 from competitive bicationic transport. *Sci. Adv.* 2024, **10**, adr1531.
- 1679 113. A. Douaki, S. Weng, G. Lanzavecchia, A. Sapunova, A. Stuber, G. Nanni, N.  
1680 Nakatsuka, M. Tsutsui, K. Yokota, R. Krahne and D. Garoli, Molecular plasmonic  
1681 nanopore for opto-thermal gating. *Adv. Opt. Mater.* 2025, **13**, 2402189.
- 1682 114. E. C. Yusko, Y. N. Billeh and M. Mayer, Current oscillations generated by precipitate  
1683 formation in the mixing zone between two solutions inside a nanopore. *J. Phys.: Condens.*  
1684 *Matter.* 2010, **22**, 454127.
- 1685 115. B. Vilozny, P. Actis, R. A. Segar and N. Pourmand, Dynamic control of  
1686 nanoprecipitation in a nanopipette. *Nat. Nanotechnol.* 2011, **5**, 3191-3197.
- 1687 116. F. M. Maddar, D. Perry and P. R. Unwin, Confined crystallization of organic  
1688 materials in nanopipettes: Tracking the early stages of crystal growth and making seed  
1689 for unusual polymorphs. *Cryst. Growth Des.* 2017, **17**, 6565-6571.
- 1690 117. Z. S. Siwy, M. R. Powell, E. Kalman, R. D. Astumian and R. S. Eisenberg, Negative  
1691 incremental resistance induced by calcium in asymmetric nanopores. *Nano Lett.* 2006,  
1692 **6**, 473-477.
- 1693 118. Z. Liu, H. Zhang, D. Liu, T. Sui and Y. Qiu, Modulation of memristive characteristics  
1694 by dynamic nanoprecipitation inside conical nanopores. *Small Methods* 2025, **9**, e01205.
- 1695 119. A. D. Cho, A. Wawrzekiewicz-Jalowicka, C. E. P. Dewi, S. Tang, D. Cain, E. Cao,  
1696 C. Martens, T. E. Schaffer, J. Cervera, P. Ramirez, S. Mafe and Z. S. Siwy, Nanopores  
1697 with ionic memory in oscillating ion current signals. *J. Am. Chem. Soc.* 2025, **147**, 47559-  
1698 47572.
- 1699 120. M. Tsutsui, W. -L. Hsu, C. Hsu, D. Garoli, S. Weng, H. Daiguji and T. Kawai,  
1700 Transmembrane voltage-gated nanopores controlled by electrically tunable in-pore  
1701 chemistry. *Nat. Commun.* 2025, **16**, 1089.
- 1702 121. Tsutsui, M., Hsu, W. -L., Garoli, D., Douaki, A., Komoto, Y., Daiguji, H. and Kawai,  
1703 T. Chemistry driven autonomous nanopore membranes. *Nat. Commun.* 2026, **17**, 1496.
- 1704 122. Wang, W., Weng, S., Douaki, A., Lanzavecchia, G., Zou, Y., Ma, Q., Jin, H., Krahne,



- 1705 R., Jin, S., Tsutsui, M. & Garoli, D. Plasminic nanopore to monitor in-pore chemistry.  
1706 *Chem. Commun.* 2026, **62**, 3536-3540.
- 1707 123. L. Wang, H. Zhang, Z. Yang, J. Zhou, L. Wen, L. Li and L. Jiang, Fabrication of  
1708 hydrogel-coated single conical nanochannels exhibiting controllable ion rectification  
1709 characteristics. *Phys. Chem. Chem. Phys.* 2015, **17**, 6367.
- 1710 124. Z. Zhang, B. Sabbagh, Y. Chen and G. Yossifon, Geometrically scalable iontronic  
1711 memristors: Employing bipolar polyelectrolyte gels for neuromorphic systems. *ACS Nano*  
1712 2024, **18**, 15025-15034.
- 1713 125. H. Yoo, Y. H. Lee, M. -G. Lee and J. -Y. Sun, Gel-based ionic circuits. *Chem. Soc.*  
1714 *Rev.* 2025, **125**, 8956-9011.
- 1715 126. M. -A. Oh, C. I. Shin, M. Kim, J. Kim, C. M. Kang, S. H. Han, J. -Y. Sun, S. S. Oh,  
1716 Y. -R. Kim and T. D. Chung, Inverted ion current rectification-based chemical delivery  
1717 probes for stimulation of neurons. *ACS Appl. Mater. Interf.* 2021, **13**, 26748-26758.
- 1718 127. Y. Wu, S. Joseph and N. R. Aluru, Effect of cross-linking on the diffusion of water,  
1719 ions, and small molecules in hydrogels. *J. Phys. Chem. B* 2009, **113**, 3512-3520.
- 1720 128. R. Islam, H. Li, P. -Y. Chen, W. Wan, H. -Y. Chen, B. Gao, H. Wu, S. Yu, K.  
1721 Saraswat and H. -S. P. Wong, Device and materials requirements for neuromorphic  
1722 computing. *J. Phys. D: Appl. Phys.* 2019, **52**, 113001.
- 1723 129. B. Yameen, M. Ali, R. Neumann, W. Ensinger, W. Knoll and O. Azzaroni, Single  
1724 conical nanopores displaying pH-tunable rectifying characteristics. Manipulating ionic  
1725 transport with zwitterionic polymer brushes. *J. Am. Chem. Soc.* 2009, **131**, 2070-2071.
- 1726 130. W. Guo, H. Xia, L. Cao, F. Xia, S. Wang, G. Zhang, Y. Song, Y. Wang, L. Jiang and  
1727 D. Zhu, Integrating ionic gate and rectifier within one solid-state nanopore via  
1728 modification with dual-responsive copolymer brushes. *Adv. Funct. Mater.* 2010, **20**, 3561-  
1729 3567.
- 1730 131. M. Geoghegan, Weak polyelectrolyte brushes. *Soft Matter* 2022, **18**, 2500-2511.
- 1731 132. F. S. Samghabadi, S. R. Bajgiran, M. V. Orellana, J. C. Conrad and A. B. Marciel,  
1732 Charge state of weak polyelectrolyte brushes determines salt-dependent swelling and  
1733 hysteretic behavior. *ACS Macro Lett.* 2024, **13**, 1570-1576.
- 1734 133. J. Yu, J. Mao, G. Yuan, S. Satija, Z. Jiang, W. Chen and M. Tirrell, Structure of  
1735 polyelectrolyte brushes in the presence of multivalent counterions. *Macromolecules* 2016,  
1736 **49**, 5609-5617.
- 1737 134. F. Wu, P. Yu and L. Mao, Neurotronics: Communicating with brain through  
1738 chemically intelligent materials. *Innovation Mater.* 2023, **1**, 100007.
- 1739 135. T. Xiong, C. Li, X. He, B. Xie, J. Zong, Y. Jiang, W. Ma, F. Wu, J. Fei, P. Yu and L.  
1740 Mao, Neuromorphic functions with a polyelectrolyte-confined fluidic memristor. *Science*



- 1741 2023, **379**, 156-161.
- 1742 136. T. Xiong, X. He, B. Xie, G. Guo, Y. Zhao, Y. Liu, C. Pan, Y. Jiang, W. Ma, F. Wu, P.  
1743 Yu and L. Mao, A nanofluidic oscillating neuron. *Nat. Commun.* 2025, **17**, 238.
- 1744 137. Stuber, A., Douaki, A., Hengsteler, J., Buckingham, D., Momotenko, D., Garoli, D.  
1745 & Nakatsuka, N. Aptamer conformational dynamics modulate neurotransmitter sensing  
1746 in nanopores. *ACS Nano* 2023, **17**, 19168-19179.
- 1747 138. B. Schlicht and M. Zagnoni, Droplet-interface-bilayer assays in microfluidic passive  
1748 network. *Sci. Rep.* 2015, **5**, 9951.
- 1749 139. G. Villar, A. D. Graham and H. Bayley, A tissue-like printed material. *Science* 2013,  
1750 **340**, 48-52.
- 1751 140. X. Zhou, Y. Zong, Y. Wang, M. Sun, D. Shi, W. Wang, G. Du and Y. Xie, Nanofluidic  
1752 memristor based on the elastic deformation of nanopores with nanoparticle adsorption.  
1753 *Natl. Sci. Rev.* 2024, **11**, nwad216.
- 1754 141. R. Yazbeck, Y. Xu, T. Porter and C. Duan, Nanoparticle-blockage-enabled rapid  
1755 and reversible nanopore gating with tunable memory. *Proc. Natl. Acad. Sci.* 2022, **119**,  
1756 e2200845119.
- 1757 142. Lanzavecchia, G., Sapunova, A., Douaki, A., Weng, S., Momotenko, D., Paulo, G.,  
1758 Giacomello, A., Krahe, R. & Garoli, D. Tailored fabrication of 3D nanopores made of  
1759 dielectric oxides for multiple nanoscale applications. *Nano Lett.* 2024, **24**, 10098.
- 1760 143. Y. Ling, L. Yu, Z. Guo, F. Bian, Y. Wang, X. Wang, Y. Hou and X. Hou, Single-pore  
1761 nanofluidic logic memristor with reconfigurable synaptic functions and designable  
1762 combinations. *J. Am. Chem. Soc.* 2024, **146**, 14558-14565.
- 1763 144. J. Bisquert, Iontronic nanopore model for artificial neurons: The requisites of spiking.  
1764 *J. Phys. Chem. Lett.* 2023, **14**, 9027-9033.
- 1765 145. Kamsma, T., Gu, Y., Spitoni, C., Dijkstra, M., Xie, Y. and van Roij, R. Energy-  
1766 efficient time series processing in real-time with fluidic iontronic memristor circuits.  
1767 *Faraday Disc.* DOI: 10.1039/D5FD00168D
- 1768 146. Barnabelli, A., Kamsma, T. M., Boon, W. Q. and van Roij, R. Pressure-gated  
1769 microfluidic memristor for pulsatile information processing. *Phys. Rev. Appl.* 2024, **22**,  
1770 054057.
- 1771 147. R. Kong, H. Zhang, M. Tang, H. Zou, C. Tian and T. Ding, Enhancing data center  
1772 cooling efficiency and ability: A comprehensive review of direct liquid cooling  
1773 technologies. *Energy* 2024, **308**, 132846.
- 1774 148. D. P. Chen, R. S. Eisenberg, J. W. Jerome and C. W. Shu, Hydrodynamic model of  
1775 temperature change in open ionic channels. *Biophys. J.* 1995, **69**, 2304-2322.
- 1776 149. M. Tsutsui, A. Arima, K. Yokota, Y. Baba and T. Kawai, Ionic heat dissipation in



- 1777 solid-state pores. *Sci. Adv.* 2022, **8**, abl7002.
- 1778 150. M. Tsutsui, K. Yokota, W. -L. Hsu, D. Garoli, H. Daiguji and T. Kawai, Peltier cooling  
1779 for thermal management in nanofluidic devices. *Device* 2024, **2**, 100188.
- 1780 151. S. -H. Shin, W. Lee, S. -M. Kim, M. Lee, J. M. Koo, S. Y. Hwang, D. X. Oh and J.  
1781 Park, Ion-conductive self-healing hydrogels based on an interpenetrating polymer  
1782 network for a multimodal sensor. *Chem. Eng.* 2019, **371**, 452-460.
- 1783 152. Y. Wu and J. J. Gooding, The application of single molecule nanopore sensing for  
1784 quantitative analysis. *Chem. Soc. Rev.* 2022, **51**, 3862-3885.
- 1785 153. R. Ren, S. Cai, X. Fang, X. Wang, Z. Zhang, M. Damiani, C. Hudlerova, A. Rosa, J.  
1786 Hope, N. J. Cook, P. Gorelkin, A. Erofeev, P. Novak, A. Badhan, M. Crone, P. Freemont,  
1787 G. P. Taylor, L. Tang, C. Edwards, A. Shevchuk, P. Cherepanov, Z. Luo, W. Tan, Y.  
1788 Korchev, A. P. Ivanov and J. B. Edel, Multiplexed detection of viral antigen and RNA  
1789 using nanopore sensing and encoded molecular probes. *Nat. Commun.* 2023, **14**, 7362.
- 1790 154. M. Tsutsui, M. Wada, A. Arima, Y. Tsunekawa, T. Sasaki, K. Sakamoto, K. Yokota,  
1791 Y. Baba, T. Kawai and T. Okada, Identifying viral vector characteristics by nanopore  
1792 sensing. *ACS Nano* 2024, **18**, 15695-15704.
- 1793 155. I. I. Smalyukh, Review: knots and other new topological effects in liquid crystals and  
1794 colloids. *Rep. Prog. Phys.* 2020, **83**, 106601.
- 1795 156. D. Hall, J. -S. B. Tai, L. H. Kauffman and I. I. Smalyukh, Fusion and fission of  
1796 particle-like chiral nematic vortex knots. *Nat. Phys.* 2026, **22**, 103-111.
- 1797 157. Wang, Q., Luo, R., Wang, Y., Fang, W., Jiang, L., Liu, Y., Wang, R., Dai, L., Zhao,  
1798 J., Bi, J., Liu, Z., Zhao, L., Jiang, Z., Song, Z., Schwarzkopf, J., Schroeder, T., Wu, S.,  
1799 Ye, Z. -G., Ren, W., Song, S. and Niu, G. Set/reset bilaterally controllable resistance  
1800 switching Ga-doped Ge<sub>2</sub>Sb<sub>2</sub>Te<sub>5</sub> long-term electronic synapses for neuromorphic  
1801 computing. *Adv. Funct. Mater.* 2023, **33**, 2213296.
- 1802 158. Wu, E., Wang, Y., Huo, S., Xu, J., Sheng, M., Liu, H., Zhong, L., Gao, J., Xie, Y.  
1803 and Pan, C. Universal core-shell nanowire memristor platform with quasi-2D filament  
1804 confinement for scalable neuromorphic applications. *Adv. Funct. Mater.* 2026, **36**,  
1805 e18764.
- 1806 159. Thakkar, P., Gosai, J., Gogoi, H. J. and Solanki, A. From fundamentals to frontiers:  
1807 a review of memristor mechanisms, modeling and emerging applications. *J. Mater. Chem.*  
1808 *C* 2024, **12**, 1583-1608.
- 1809 160. Huang, W., Xia, X., Zhu, C., Steichen, P., Quan, W., Mao, W., Yang, J., Chu, L. and  
1810 Li, X. Memristive artificial synapses for neuromorphic computing. *Nano- Micro Lett.* 2021,  
1811 **13**, 85.
- 1812 161. Rosenstein, J. K., Wanunu, M., Merchant, C. A., Drndic, M. and Shepard, K. L.



- 1813 Integrated nanopore sensing platform with sub-microsecond temporal resolution. *Nat.*  
1814 *Methods* 2012, **18**, 487-492.
- 1815 162. Rivnay, J., Inal, S., Salleo, A., Owens, R. M., Berggren, M. and Malliaras, G. G.  
1816 Organic electrochemical transistors. 2018, *Nat. Rev. Mater.* **3**, 17086.
- 1817 163. Paulsen, B. D., Tybrandt, K., Stavrinidou, E. and Rivnay, J. Organic mixed ionic–  
1818 electronic conductors. *Nat. Mater.* 2020, **19**, 13–26.
- 1819  
1820  
1821



#### Data Availability Statement:

This Review article does not report new experimental or computational data. Data sharing is not applicable to this work. Any data discussed or re-plotted in figures are available in the cited primary literature.

